ISAS - INTERNATIONAL SCHOOL
FOR ADVANCED STUDIES

Doping States in Cuprate Oxide Superconductors

Thesis submitted for the degree of
"Doctor Philosophiæ"

Condensed Matter Sector

CANDIDATE:
José Lorenzana

SUPERVISOR:
Prof. Yu Lu

Academic Year 1991/92

TRIESTE

SISSA - SCUOLA
INTERNAZIONALE
SUPERIORE
STUDI AVANZATI
TRIESTE
Strada Costiera 11

Doping States in Cuprate Oxide Superconductors

Thesis submitted for the degree of

"Doctor Philosophiæ"

Condensed Matter Sector

CANDIDATE:

José Lorenzana

SUPERVISOR:

Prof. Yu Lu

Academic Year 1991/92

This is indeed a mistery, remarked Watson,
what do you imagine that it means?

- I have no data yet, replied Sherlock Holmes. It is a capital mistake to make theories before one has enough data. Insensibly, one starts twisting the data to fit the theory, instead of making the theory fit the facts.

Conan Doyle

Table of Contents

Acknowledgements

Trieste is a crossroads of theoreticians and experimentalists of all nationalities and this gave me the opportunity to benefit from discussions and interactions with many of them. Many people all around the world contributed to the development of the the ideas presented in this thesis and the list here is by no means exhaustive. Dr. C. Taliani and Dr. G. Ruani explained to me patiently the secrets of their fascinating photoinduced experiments. I also got valuable insight on the optical experiments from Prof. D. Mihailović and Dr. G. A. Thomas. I also benefited a lot from a short collaboration with Dr. M. Charalambous. I am greatly in debted to Dr. A. R. Bishop and Dr. K. Yonemitsu who introduced me to the nuclear physics's RPA technique. I was very much influenced by discussions with Dr. P. Littlewood and Dr. C. Varma on the marginal Fermi liquid ideas. I got deep and stimulating critical views from Profs. E. Tosatti and G. A. Sawatzky and appreciated fruitful discussions with Profs. J. Ranninger, A. Parola and Dr. M. Steiner. I wish to express my gratitude to Profs. B. Alascio, C. A. Balseiro and the group of Bariloche for their encouragement and valuable discussions in the early stages of this work. My colleague M. Fabrizio was always ready to help me when things become really hard (calculus, change of units and all that stuff). I am very grateful to my friend and advisor Prof. Yu Lu. The trust and respect he put in me grew in the invaluable tool of creativity: self-confidence. The numerical work was performed at CINECA. Jorge Kohanoff, Clarisa Siperman and Vibeke Clausen helped me with the English in an early version of some chapters. My house mates Paolo Catelan and Gisselle Carphio supported me in the hard times of the writing, my family give me long distance support from Argentina and many friends contributed to make my stay in Trieste very pleasant.

Chapter 1

Introduction

Five years ago, a few months after Bednorz and Müller's[1] remarkable discovery of ceramic compounds superconducting at unexpected high temperatures, Carlos Balseiro and Blas Alascio suggested me to study the electronic structure of these new materials. By that time I was an undergraduate student at Bariloche and the local theory group was exploring a superconducting mechanism involving charge transfer excitons, a subject which we were very much encouraged to think about. For the time when I was doing very simple minded Hartree-Fock calculations, many people all around the world were diagonalizing all possible models in small clusters with the hope to find one model showing tendency to Cooper pair formation. Blas showed me one of these calculations and told me his thought that the binding found was a "simple Hartree-Fock effect" in the sense that the Hartree-Fock approximation could give a similar result. What this innocent comment triggered, is the outcome of this thesis. He was not only right but, unexpectedly, the binding in Hartree-Fock, a very small quantity resulting as difference of extensive energies, was in almost perfect agreement with the exact result. This was surprising (not for Blas) since the binding energy was supposed to be an effect of correlations, something which Hartree-

Fock is not supposed to deal with. So we turn the statement "this is not an effect of correlations" the other way around to say: maybe particles like to be close (correlated) to take advantage of this Hartree-Fock effect. In fact, in such a small cluster particles were obliged to be close to each other any way. The underneath assumption in the exact small cluster calculations was that if one would have a collection of such clusters and allow the particles to jump from one cluster to another they will choose to be in the same cluster if there were pairing tendencies. The same reasoning was possible with the Hartree-Fock calculation but even more, being a much simpler technique it was possible to make the calculation in a very large cluster rather than on many small clusters, and in a spatial dependent way so that if particles wanted to be in the same spatial region they could do so. It was natural then to ask what would happen if instead of adding two particles we put only one. By that time, people doing all kind of spectroscopies, were beginning to talk about gap states appearing upon doping in the presence of strong correlations. So I played with the spatial dependent Hartree-Fock ideas a bit and in Trieste, under the supervision of Yu Lu, such first attempts of studying strong correlations and self-trapping gave rise to Chapters 3 and 4. As the time went on, the model considered appeared too simplistic but it provided an excellent test ground for the methods and ideas that produced the exciting results of Chapters 5 and 6. The agreement between exact diagonalization results and the inhomogeneous Hartree-Fock convinced us that the technique was accurate enough to try a more detailed comparison with experiments. At the same time it was clear that the dynamical effects were not included in the calculation and I began to think in terms of a time-dependent Hartree-Fock approach which, in the small amplitude of oscillation limit, was nothing more than the random phase approximation (RPA). The photodoping

experiments of Taliani's[2] and other groups[3, 4] made it clear that the lattice effects were certainly present. Magnetism and consequences of a non-infinite Cu Coulomb repulsion was another main question. With all this in mind I switched from the simpler model of Chapters 3 and 4 to the full p-d model. By that time I met Alan Bishop. He was playing with similar ideas and had similar projects. Moreover, his group had began to adapt the real space RPA techniques developed by the nuclear physics community to treat this kind of problems. We began a collaboration and since Alan put priority on lattice effects, which were calling increasing attention of the high Tc community, Chapter 6 was produced before Chapter 5. Whereas for the polarons of the simplified model the physical idea of the self-trapping preceded the results, for the polarons in the p-d model I first got the results and then understood them (similar results were simultaneously obtained by Kenji Yonemitsu). At a first look they seemed ordinary small ferromagnetic polarons. However, a closer examination shows something strange. First the magnetic moment at the center of the polaron is very much reduced and there are two close levels in the gap. For some parameters the magnetic moment was zero and the two levels in the gap became degenerate. This was not what one would expect for a naive magnetic polaron. It is curious to see how similar reasoning that worked for the electronic polarons of the simplified model, would explain this effect. The key issue is the competition between the two giant forces of the Cu-O planes: the strong Cu on-site repulsion, that makes the system insulating, and the strong covalency, that makes the layers so rigid (in the simplified model the game is played between the nearest neighbour repulsion and covalency). People tend to assign the large distance between the two Hubbard bands only to the on-site Coulomb repulsion. A simple example shows that this is not the case. Solving the unrestricted Hartree-Fock

equations for a Hubbard molecule with two atoms and two electrons gives a transition between a magnetic "insulator" and a nonmagnetic "metal" for an on-site repulsion U equal to twice the interatomic hopping integral t. Whereas the atomic magnetic moment vanishes as $m^2 = \frac{1}{4}[1 - (\frac{2t}{U})^2]$, the distance between the Hubbard "bands" does not go to zero but is equal to U independently of t up to the transition and afterwards they become the bonding and antibonding orbitals of the uncorrelated molecule. The splitting, close to the transition, is mainly due to the strong covalent repulsion of the levels and not to the distance between the renormalized atomic $\uparrow$, $\downarrow$ levels. The latter is only $2mU$. Only for very large U can the splitting be considered only due to the distance between the on-site renormalized levels. The consequences of the strong covalency in the p-d model manifest dramatically away from half-filling where magnetic moments tend locally to collapse by increasing doping (Chapter 5) or locally increased covalency. This last effect is achieved by relaxing the lattice around the polarons (Chapter 6). Kenji made an adiabatic RPA calculation over these states that explained nicely some of the features of the photoinduced experiment at phonon frequencies[2, 4, 5].

Further insight came by calculating the random phase approximation fluctuations in the simplified model. The interesting thing was that by varying a parameter favoring self-trapping it was possible to pass from an extended state to a polaronic state. The transition was signaled by RPA modes going to zero. Here, apart from the photoinduced experiments, I got very much influenced by the optical experiments of the group led by Uchida[6], the Bell group[5] and the Rome[7, 8] group. They showed that what, for strong doping becomes a mysterious mid-infrared band in the optical spectra, corresponded, for very small doping, to a transition in the gap. I thought that the analogous soft modes of the

simplified model had a good chance of giving that behaviour in the p-d model. Moreover, Uchida's experiments looked very much like a softening of the mode with doping and a subsequent transition of the electronic ground state. The final agreement between theory and experiment was better than I expected and the physics turned out to be more complex. The softening came out not only because of the delocalization of the added particles, as in the simpler model, but mainly due to the delocalization of the Cu spins which showed that doping was triggering a transition from a strange polaronic liquid to a more conventional metal. How these soft modes influence the Fermi liquid behaviour and, maybe, produce superconductivity is something to look at in the future with more refined techniques. At this point the techniques used here reach their limits.

The landscape of the Hartree-Fock states is enormously complex. There are too many degrees of freedom. First it is not clear what parameters to put in the Hamiltonian and even if one gets the right parameters there is a tremendous richness of nearby mean field states. As time goes people will learn to travel along these landscapes at high speed and it will not be anymore a craftsman's work. I spent the last four years touring in this labyrinth with the hope that there was something interesting to discover. I think, finally I arrive to a nice point and it was worth the effort.

Chapter 2

The Model

On modeling and studying a real material we have to face two difficult decisions: which model to use and which technique to use. For cuprates the preferences range from taking a very simple model and applying a very accurate (exact) and complicated technique like the Bethe's ansatz applied to the $1D$, supersymmetric $t-j$ model, to a more naive technique (like LDA) for a very complicated Hamiltonian. From both extremes there is something to learn (although the first case is closer to statistical mechanics than to condensed matter physics). Here we hope we have reached a balance with a model realistic enough and a technique accurate enough to allow detailed comparison with experiments and at the same time to keep the physics tractable.

A prototype hamiltonian to describe the superconducting cuprate oxides is the p-d model. This model has been proposed in the early time of the high temperature superconducting studies for the $La_{2-x}Sr_xCuO_4$, and applies to all Cu-O based compounds. It has been later generalized to the three-dimensional Bi-O compounds[9]. In the case of $La_{2-x}Sr_xCuO_4$ it takes into account the following:

- The compound is quasi-two-dimensional.

- The La valence states are far above the Fermi energy[10].
- The main states near the Fermi energy[10] are the $d_{x^2-y^2}$ orbitals of Cu and the p_x,p_y orbitals of O directed towards Cu. Their energies are close to each other, producing a bonding and anti-bonding bands. They are the ones that mix the most.
- The on-site correlations are large[10].
- As suggested by many authors we include also the interatomic repulsion[11, 12, 13]. We expect it to be important because we know that the carrier density is small[14] and, as a consequence, the screening length is large. On the other hand, if the Cu-O bond were ionic, this term would not play any important role, but we know this is not the case.

Both density functional calculations and experiments suggest that lattice effects are important. At least close to the stoichiometric compositions, where the compound is insulating, lattice effects are unavoidable since the carriers are not very mobile and then self-trapping by the lattice is warrant. However, since the major source of trapping proves to be the electronic background some time the lattice can be neglected and one can still get quite good agreement with experiment at large enough energies. The lattice displacements that disturb most the electronic system are O moving toward Cu. We include the corresponding phonons in the Hamiltonian. This is known as a 2-d, 3-band extended Peierls-Hubbard model in the jargon on the subject. The Hamiltonian reads,

$$\begin{aligned} H &= \sum_{i\neq j,\sigma} t_{ij}(\{u_k\})c^\dagger_{i\sigma}c_{j\sigma} + \sum_{i,\sigma} e_i(\{u_k\})c^\dagger_{i\sigma}c_{i\sigma} + \sum_i U_i c^\dagger_{i\uparrow}c^\dagger_{i\downarrow}c_{i\downarrow}c_{i\uparrow} \\ &+ \sum_{\langle i\neq j\rangle,\sigma,\sigma'} U_{ij}c^\dagger_{i\sigma}c^\dagger_{j\sigma'}c_{j\sigma'}c_{i\sigma} + \sum_l \frac{1}{2M_l}p_l^2 + \sum_{k,l}\frac{1}{2}K_{kl}u_k u_l \ , \end{aligned} \tag{2.1}$$

where the operator $c^\dagger_{i\sigma}$ creates a *hole* of spin σ at site i in the Cu $d_{x^2-y^2}$ or the O $p_{x,y}$ orbital. We assume that the parameters for the one-fermion operators, the hopping integrals $t_{ij}(\{u_k\})$ between sites i and j and site-diagonal energies $e_i(\{u_k\})$ at site i, depend

linearly on lattice displacements u_k with coefficients $\bar{g}^k_{ij}$ and $\bar{g}^k_{ii}$, respectively,

$$t_{ij}(\{u_k\}) = t^0_{ij} + \sum_k \bar{g}^k_{ij} u_k \quad , \tag{2.2}$$

$$e_i(\{u_k\}) = e^0_i + \sum_k \bar{g}^k_{ii} u_k \quad . \tag{2.3}$$

Holes repel each other with strength U_i on site i and strength U_{ij} between different sites i and j. Displacements of atoms and their conjugate momenta are denoted by u_l and p_l, respectively. The quantity M_l stands for the ionic mass at site l and K_{kl} for the phenomenological spring constant between ions at sites k and l. The symbol $\langle i \neq j \rangle$ under the summation symbol means that a pair (i, j) is counted only once.

We consider the nearest-neighbor Cu-O (t_{pd}) and O-O ($-t_{pp}$) hoppings for t^0_{ij}, Cu-site (ϵ_d) and O-site (ϵ_p) energies for e^0_i, with $2\Delta = \epsilon_p - \epsilon_d$, Cu-site ($U_d$) and O-site ($U_p$) repulsions for U_i, and the nearest-neighbor Cu-O repulsion (U_{pd}) for U_{ij}. For the lattice part, we study only the displacements of planar O atoms along the Cu-O bonds. (We take the Cu atoms to be fixed, for simplicity.) Furthermore, we assume that only diagonal components of the spring-constant matrix are finite, $K_{kl} = \delta_{k,l} K$. For the electron-lattice coupling, we assume that the nearest-neighbor Cu-O hopping is modified by the O-atom displacement, u_k, linearly with coefficient α, $t_{ij}(\{u_k\}) = t_{pd} - \alpha u_k$ if the Cu-O bond becomes longer with positive u_k, or $t_{pd} + \alpha u_k$ if the bond becomes shorter. The Cu-site energy is assumed to be modulated by the displacements of the four surrounding O atoms, u_k, linearly with coefficient β, $e_i(\{u_k\}) = \epsilon_d + \beta \sum_k (\pm u_k)$, where the sign takes "+" if the bond becomes longer with positive u_k, or "−" if the bond becomes shorter. The electronic parameters in the Hamiltonian can be taken from the experiments[15] or LDA[16, 17] calculations. As a reference parameter set, we use $t_{pd} = 1$, $t_{pp} = 0.4$, $2\Delta = 2.2$, $U_d = 5$, $U_p = 2.1$, and $U_{pd} = .4$, which are almost in proportion to the values $t_{pd} = 1.47$eV,

$t_{pp} = 0.61\text{eV}$, $2\Delta = 3.29\text{eV}$, $U_d = 7.42\text{eV}$, $U_p = 3.09\text{eV}$, and $U_{pd} = .41\text{eV}$ derived from the constrained-density-functional approach[18, 17]. Dimensionless electron-lattice coupling strengths are defined by $\lambda_\alpha = \alpha^2/(Kt_{pd})$ and $\lambda_\beta = \beta^2/(Kt_{pd})$. It is easily shown that, within the mean-field theory, two parameter sets differing only by $\bar{g}^k_{ij} = s\bar{g'}^k_{ij}$ ($\alpha = s\alpha'$, $\beta = s\beta'$) and $K_{kl} = s^2K'_{kl}$ (thus $\lambda_\alpha = \lambda'_\alpha$, $\lambda_\beta = \lambda'_\beta$, s: real number) give the same HF configuration for charge and spin densities and the lattice displacements related by $\langle u_k\rangle = s^{-1}\langle u'_k\rangle$. For the lattice a good procedure is to fit the displacement obtained with "LDA + U" calculations[19]. When we study lattice fluctuation (in the RPA), we use $K = 32$, which gives a dispersionless bare O phonon frequency of 104meV (840cm^{-1}) if this value is interpreted as $K = 32 \times 1.3\text{eV/Å}^{-2}$. This value is also consistent with "LDA+U" calculations[19].

Different limits of this model are studied in this work. For $\lambda_\alpha = \lambda_\beta = 0$ we recover the standard p-d model for the electronic part,

$$\begin{aligned} H &= \sum_{i\neq j,\sigma} t^0_{ij} c^\dagger_{i\sigma} c_{j\sigma} + \sum_{i,\sigma} e^0_i c^\dagger_{i\sigma} c_{i\sigma} + \sum_i U_i c^\dagger_{i\uparrow} c^\dagger_{i\downarrow} c_{i\downarrow} c_{i\uparrow} \\ &+ \sum_{\langle i\neq j\rangle,\sigma,\sigma'} U_{ij} c^\dagger_{i\sigma} c^\dagger_{j\sigma'} c_{j\sigma'} c_{i\sigma} \ . \end{aligned} \tag{2.4}$$

If we further restrict it to 1D and take the limit $U_p, U_d \longrightarrow \infty$, charge and spin degrees of freedom decouple, and the former are described by a spinless fermion hamiltonian [20, 13],

$$H = \sum_i [(-1)^i \Delta C^\dagger_i C_i + t(C^\dagger_i C_{i+1} + h.c.) + U_{pd} n_i n_{i+1}] \ . \tag{2.5}$$

By doing this we lose all relevant information about the spin degrees of freedom (which are described by a Heisenberg model) but we gain simplicity on the charge degrees of freedom. We know that U_d is very large. Naively, one could expect the results to be insensitive to the value of U_p because the double occupancy on O is rare. However, we shall see later

(Sec. 3.7) that this is not the case.

The spinless model (2.5) will be studied in Chapter 3 and its 2D generalization in Chapter 4. The full p-d model (2.4) in 2D case will be investigated in Chapter 5. Finally Chapter 6 is devoted to the full Hamiltonian (2.1) where the lattice effects are included explicitly.

Chapter 3

Electronic polarons in a one dimensional spinless model

Since many of the techniques emploied in this work were, and still are, in a primitive stage of development we found very useful to test them in a simplified spinless model. Moreover this model contains most of the essential physics of charge transfer process in the p-d model without complications that arise from the magnetic degrees of freedom or charge fluctuations due to the finiteness of U_d. The model is given by the Hamiltonian Eq. (2.5). This one-dimensional spinless fermion model was used in connection with modeling high temperature superconductors[21, 20, 13], and one-dimensional charge transfer systems[22]. The model has the advantage for our propose that it supports non trivial self-trapped states[21] at the mean field level and is simple enough to allow exact diagonalization on relatively large chains[23]. We first show that the nearest-neighbour Coulomb repulsion can generate charge transfer polaron and exciton states. The importance of charge transfer excitations in HTSC has been stressed by theorists[11]-[13] and experimentalists[24]-[29]. Structure related to charge transfer excitations in the Cu-O planes has been identified in optical measurements[27]-[29].

We first obtain homogeneous (HHF) and inhomogeneous (IHF) Hartree-Fock solutions (Sec. 3.1) and compute the ground state energy (Sec. 3.4) as well as static correlation functions (Sec. 3.5). These are compared with exact diagonalization results obtained with the Lanczos method[30]. The IHF approach gives better results for the ground state energy and describes short distance correlation functions better than its homogeneous counterpart.

An intuitive approach to the dynamics of the system is to try to solve the time dependent Schröedinger equation in the Hartree-Fock approximation. In this way one can look for a solution in which the polaron with its self-trapping potential moves self-consistently. But a time dependent Hartree-Fock in the small amplitude of oscillation limit is nothing more than the random phase approximation (RPA). In other words, one has to look for the linear modes or the one loop corrections around the localized solution. In the limit in which the polaron is large with respect to the lattice space one can pass to the continuum limit and one of the modes becomes a Goldstone mode. A similar problem has been faced for the polyacetylene[31].

RPA fluctuations are added through the matrix form of RPA used in nuclear physics problems[32]. This allows us to compute dynamical correlation functions (Sec. 3.6) that compare well with exact diagonalization results reported in the literature[13]. For both strong and weak coupling limits the correlation energy in RPA agrees quite well with the exact result. A related approach that amounts to treating the electron-hole pairs as bosons (quasi-boson approximation) overestimates the correlation energy by a factor of 2 in weak coupling due to double counting.

The Hartree-Fock self-trapped solution appears above a critical value of the interaction.

The transition is sharp at the mean field level and is signaled by an RPA mode with frequency approaching zero. Above the transition the homogeneous Hartree-Fock solution has unstable RPA modes with imaginary frequencies. The general formalism is described in the Appendix A. The range of validity of the approximations involved is discussed in section 3.3

3.1 Hartree-Fock results

3.1.1 Uniform case

The spinless Hamiltonian is,

$$H = \sum_i [(-1)^i \Delta C_i^\dagger C_i + t(C_i^\dagger C_{i+1} + h.c.) + U_{pd} n_i n_{i+1}] \,. \tag{3.1}$$

At half filling the charge distribution is uniform and the mean field equations can be solved in reciprocal space. There are two bands separated by a gap and the chemical potential is in the middle of the gap. The effect of U_{pd}, Eq. (A.25) is to increase the gap and to renormalize the bandwidth. The most naive approach away from half filling is to assume that the charge goes to a uniform plane wave state. In Fig. 3.1 we show the chemical potential as a function of doping in the uniform Hartree-Fock approximation for different values of U_{pd}/t. We see that the compressibility is negative for small enough doping. This means that the uniform Hartee-Fock ground state is unstable and, hence, something better should be tried. There are several candidates such as phase separation, superconductivity or, as we shall see, a polaronic phase. Since we are in the unstable phase, no precise statement can be made. The instability can be traced back to the behavior of the renormalized Hartree-Fock diagonal energies. Let us give an heuristic argument in the strong coupling limit. The effective levels for a chain of Cu and O at half-filling vs. the

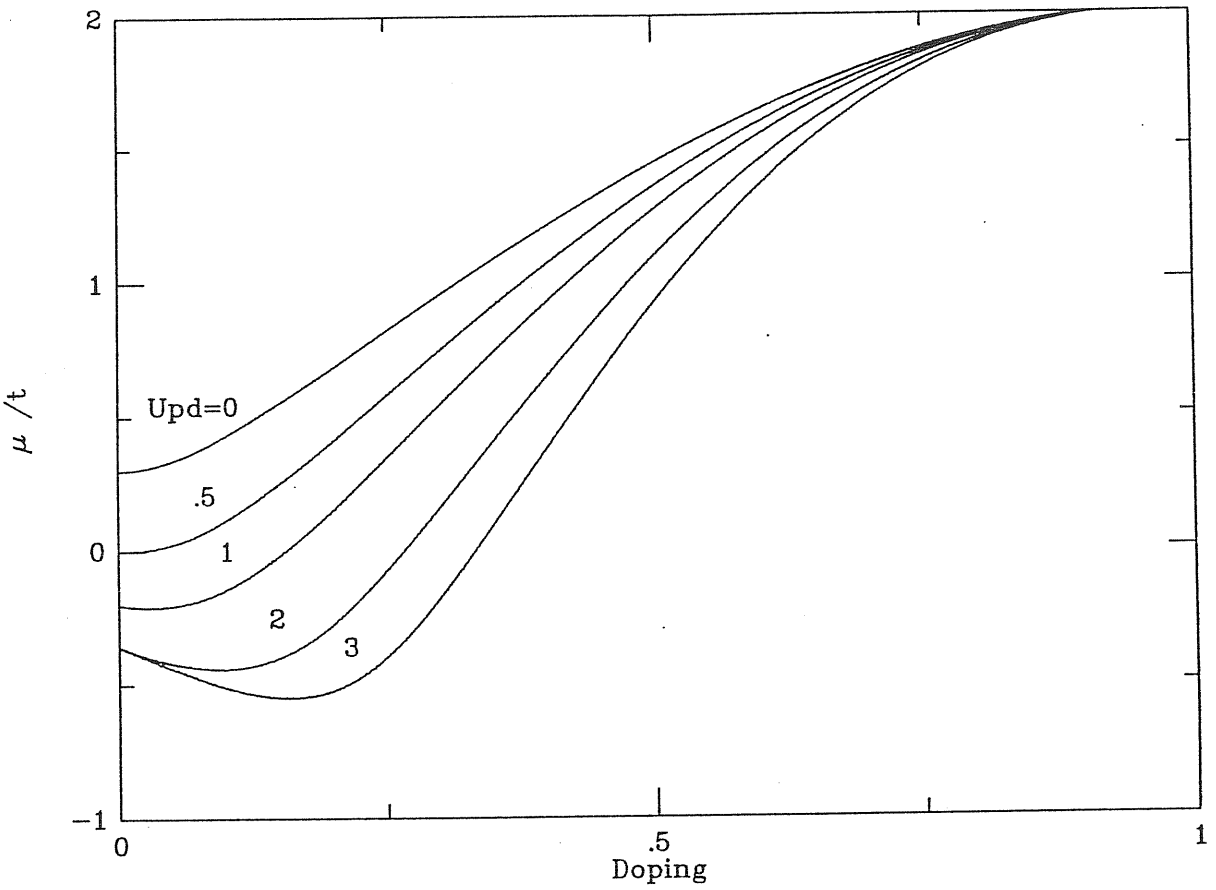

Figure 3.1: Chemical potential as a function of doping in 1D for $\Delta = .3$. We subtracted the corresponding value of $2U_{pd}$ to each curve in order to make them all fall on the same scale.

site are schematically shown in Fig. 3.2(a). In the Hartree approximation the diagonal energies of the orbitals renormalize as:

$$\tilde{\epsilon}_d = \epsilon_d + 2n_O U_{pd}, \tag{3.2}$$

$$\tilde{\epsilon}_p = \epsilon_p + 2n_{Cu} U_{pd}. \tag{3.3}$$

At half-filling and for small t, $n_{Cu} \sim 1$ and $n_o \sim 0$, then

$$\tilde{\epsilon}_d \sim \epsilon_d, \tag{3.4}$$

and

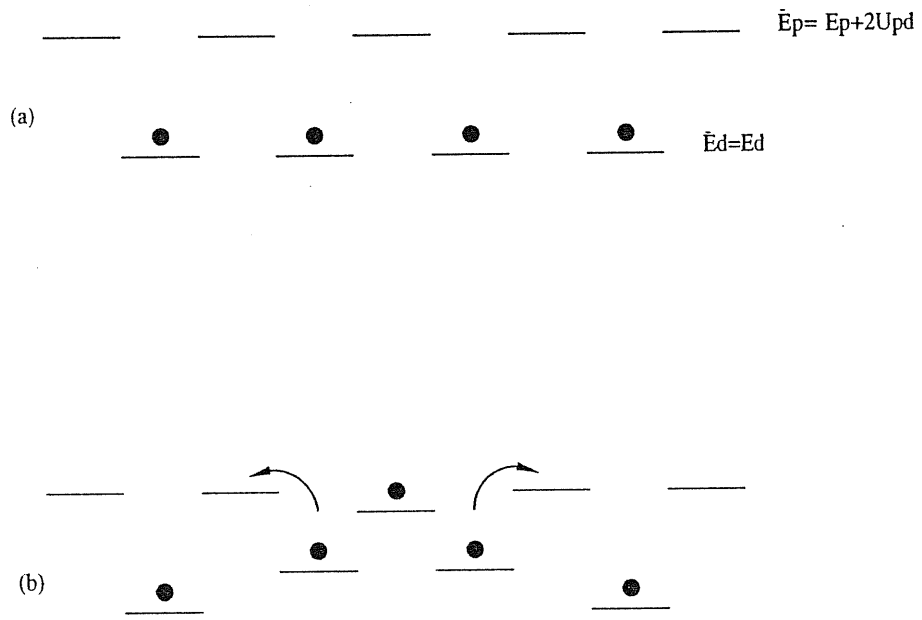

Figure 3.2: Schematic plot of the renormalized energy levels in real space. A dot represents an occupied site. (a)Ground state at half filling, (b) One particle added. Arrows indicate increased charge transfer.

$$\tilde{\epsilon}_p \sim \epsilon_p + 2U_{pd}. \tag{3.5}$$

When we add holes they go mainly to O sites raising the Cu level. These will increase the mixing of Cu and O and will imply a transfer of charge from Cu to O. The net effect will be that n_{Cu} decreases, and the O level renormalizes to lower energies. This means that we are putting charge in a level whose energy is decreasing. Therefore, the chemical potential decreases with doping and the compressibility turns out to be negative.

3.1.2 Non-uniform case

Let us now suppose that instead of putting the charge in a Bloch state we localize it on an O site (Fig. 3.2(b)). The energies of the neighbouring Cu will strongly renormalize and then, there will be charge transfer towards the O. The net effect will be that the O level

will locally renormalize to lower energies. This will create a potential in which the hole can be self-trapped.

In Fig. 3.3 we show the example of one hole added to the stoichiometric case. This

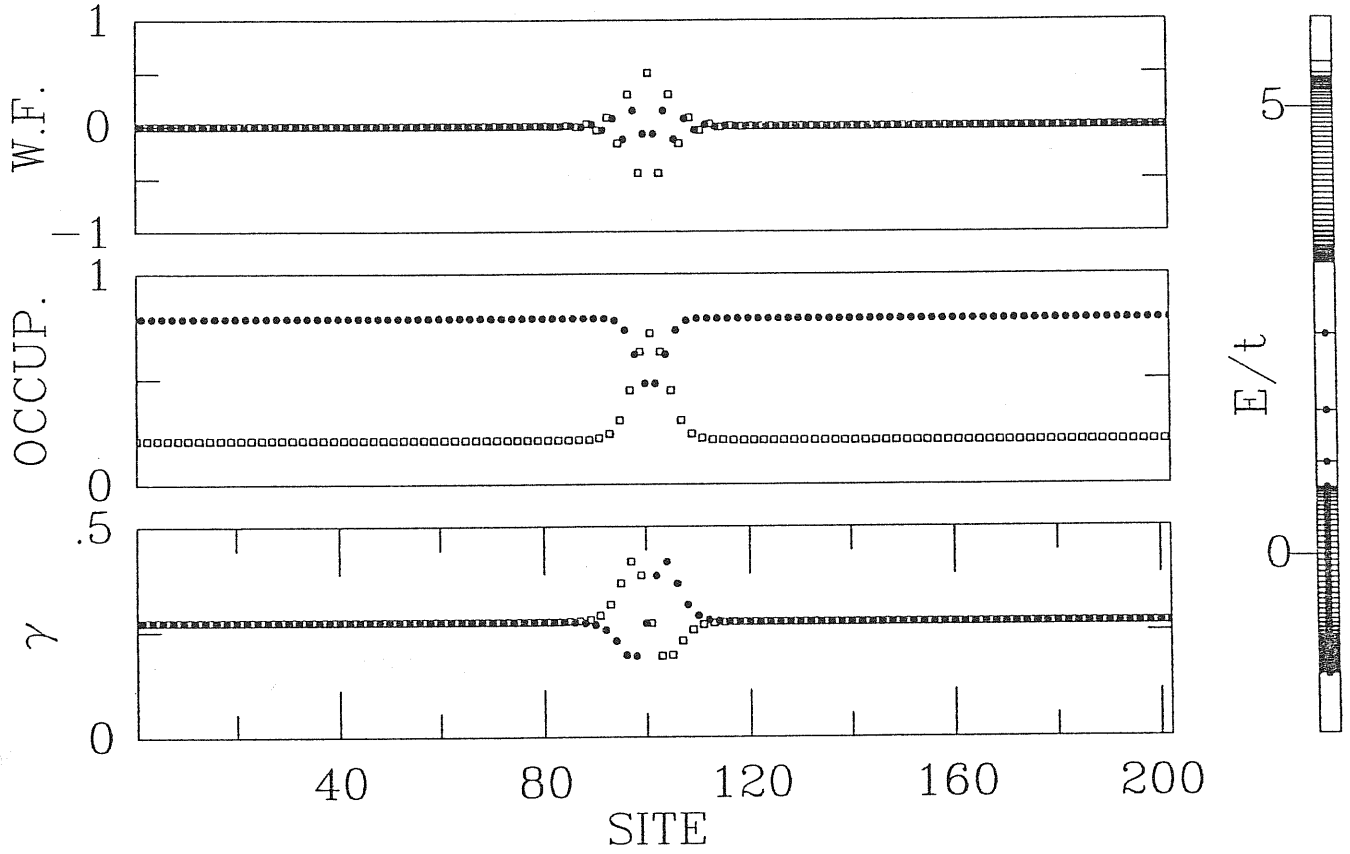

Figure 3.3: One particle added to the half filling case for $\Delta = .1$, $U_{pd} = 2$. We show the one particle wave function (W.F.) of the polaron state, the site occupation, and the γ as a function of the site. Solid circles correspond to Cu and squares correspond to O except for γ in which they differentiate even and odd bonds. The plot on the right is the single particle energy levels; note the states in the gap. A dot represents an occupied level.

effect can be studied in a wide region of parameter space performing the unrestricted Hartree-Fock approximation (Sec. A). In a simplified view, we can think of the particles of the O band as moving in a potential generated by the charge distribution on the Cu site and vice versa (Eqs. (3.2),(3.3)). Therefore, in Fig. 3.3 the plot of the charge distribution

represents, in a different scale, the distribution of site energies in which the particles move. The depletion in the Cu charge pulls down a state from the O band and the bump in the O charge pulls up states from the Cu band. The polaron wave function carries some features of the bottom Bloch state of the O band. The amplitude is larger on O sites and it changes sign from one O site to the next. Note that the polaron forms an "impurity"-like state. In all cases we found that the self-trapped solution has lower energy than the uniform one.

Our problem presents a neat analogy with 1D problems studied in the past[31]. In this context a related problem has been studied by Hubbard[33]. He showed that for the case $\Delta = 0$ and $t << U_{pd}$ (strong coupling), one hole added to the system dissociates into a soliton (kink-like) pair, each one with charge $e/2$. When $\Delta \neq 0$ the free soliton pair is not stable because the charge between the two solitons is located "in the wrong place".

In our case we can think of the polaron as a bound state of the pair. For $\Delta = 0$ the ground state is degenerate. Similar to Hubbard's[33] results we found kink-like solutions. In a kink-like solution half of the chain has the charge displaced towards the Cu sites, and the other half vice versa. Furthermore, in the continuum limit the unrestricted Hartree-Fock equations can be mapped into a problem closely related to that of the polyacetylene[31]. In this limit the polaron solution dissociates as a free soliton pair. Fig. 3.4 shows the weak coupling version of Hubbard's strong coupling result. We see that the localized wave function has equal weight on Cu and O sites as required from symmetry considerations. It has similar oscillating behavior to the polaron case. It is interesting to note the behavior of γ (see Appendix A). There is a constant part and a oscillating part. The later is clearly dominated by the localized states. In Eq. (A.28) the sum over the extended states has a smooth behavior and the sum over the localized states provides

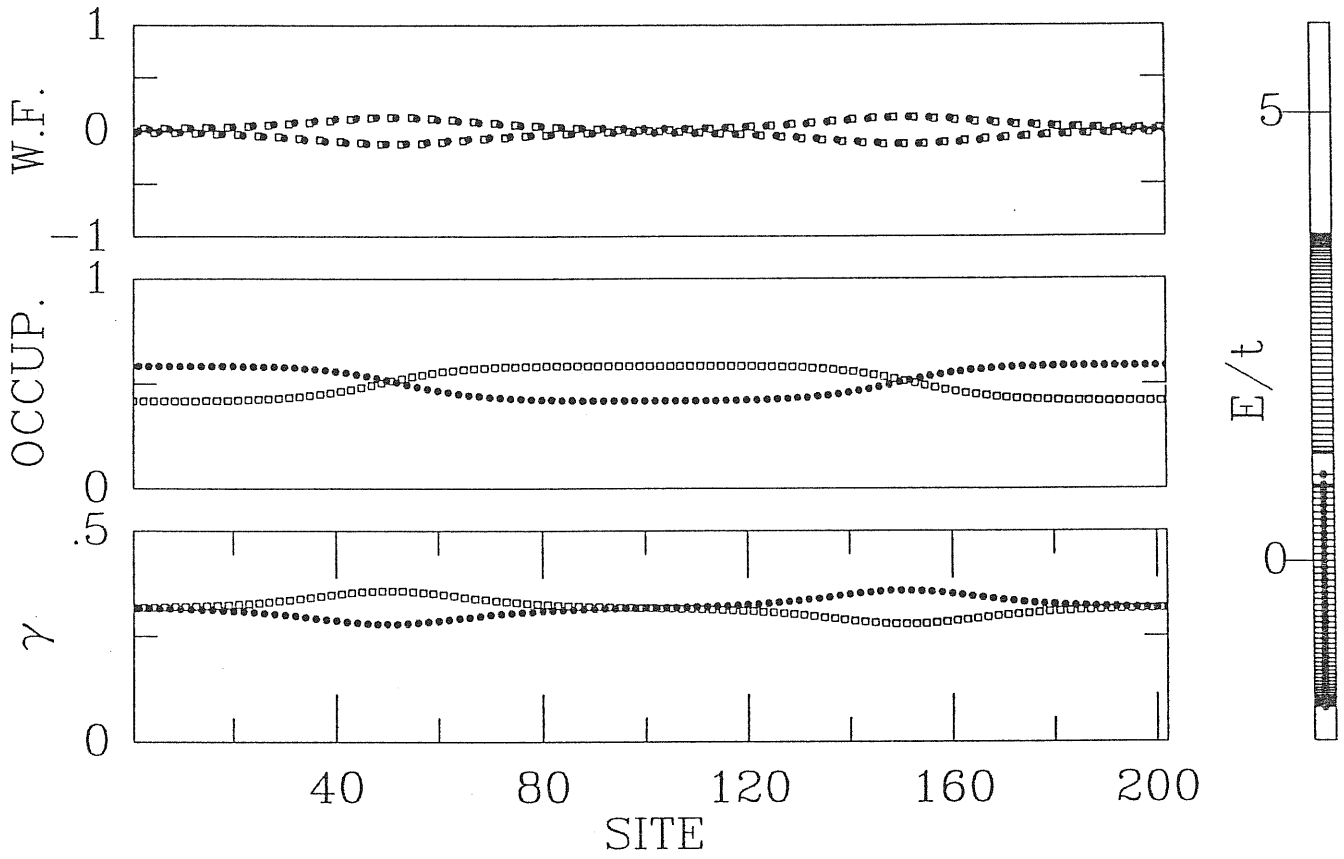

Figure 3.4: One particle added to the half filling case for $\Delta = 0$, $U_{pd} = 1$. We show the one particle wave function (W.F.) of the polaron state, the site occupation, and the γ as a function of the site. Solid circles correspond to Cu and squares correspond to O except for γ in which they differentiate even and odd bonds. The plot on the right is the single particle energy levels; note the states in the gap. A dot represents an occupied level.

the oscillating part. We can now consider the problem of phase separation. If there is a phase separation one would expect that for more than one particle added, the system will nucleate a hole-rich phase. Due to the short-range character of the interactions it is enough to consider the two-polaron case. We generated a configuration with two particles close to each other and iterated up until convergence. We found that the energy decreases monotonically and the system converges to a situation in which the polarons are well far apart (Fig. 3.5). Hence, in this approach there is no phase separation.

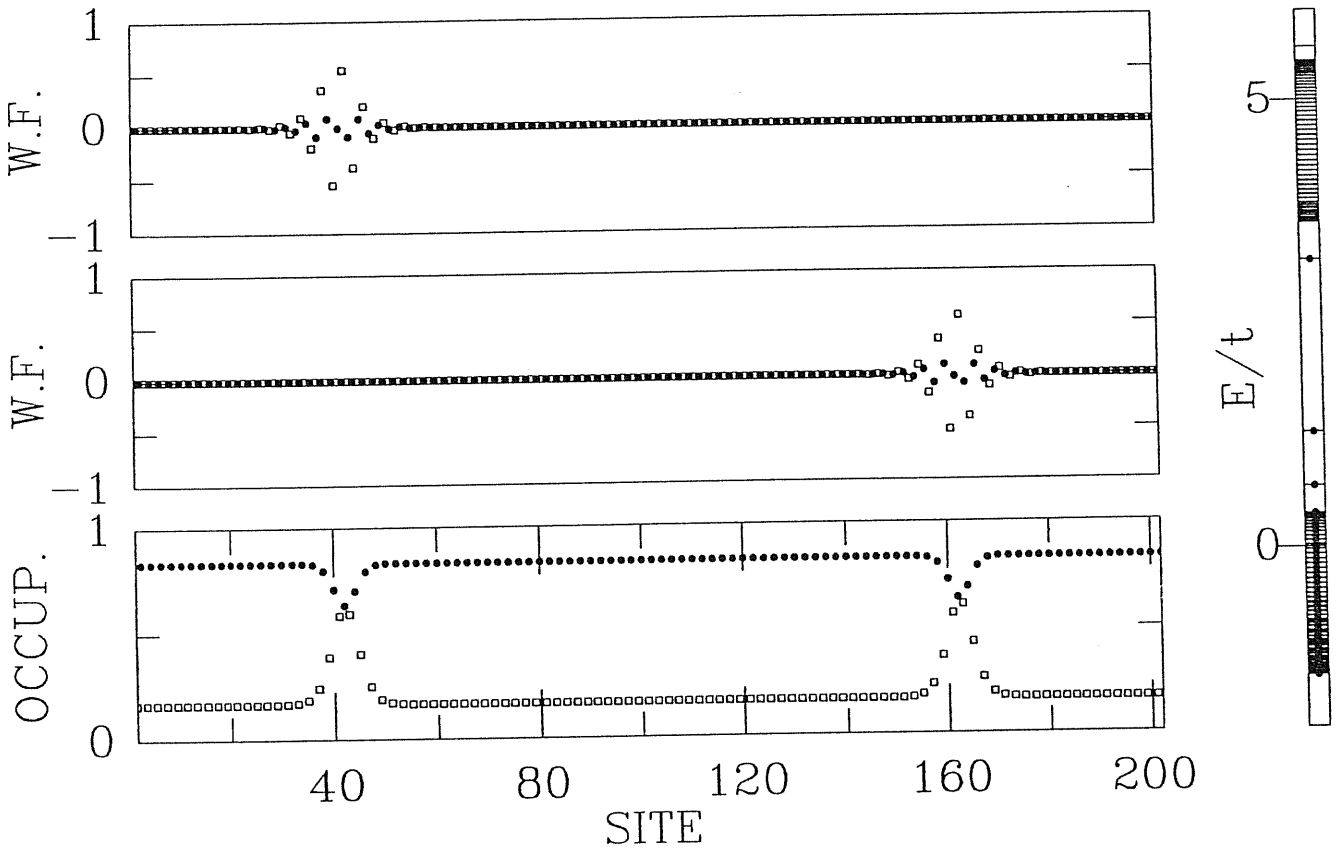

Figure 3.5: Two particles added to the half filling case for $\Delta = .3$, $U_{pd} = 2$. We show the one particle wave function (W.F.) of the two-polaron state and the site occupation. Solid circles correspond to Cu and squares correspond to O. The plot on the right is the single particle energy levels. A dot represents an occupied level.

We can also study excitonic states. In such state we consider the stoichiometric case leaving the top state of the lower band empty, and the bottom state of the upper band occupied. In Fig. 3.6 we show such an example.

We note that the charge gap for these excitations is smaller than the uniform Hartree-Fock gap. For equal parameters the exciton is more localized than the polaron state because the self-trapping potential is deeper. This can be understood by comparing the distribution of charge in the Cu for the two cases. For the polaron case the self-trapping potential is generated by a relatively small lack of charge on Cu, which has been trans-

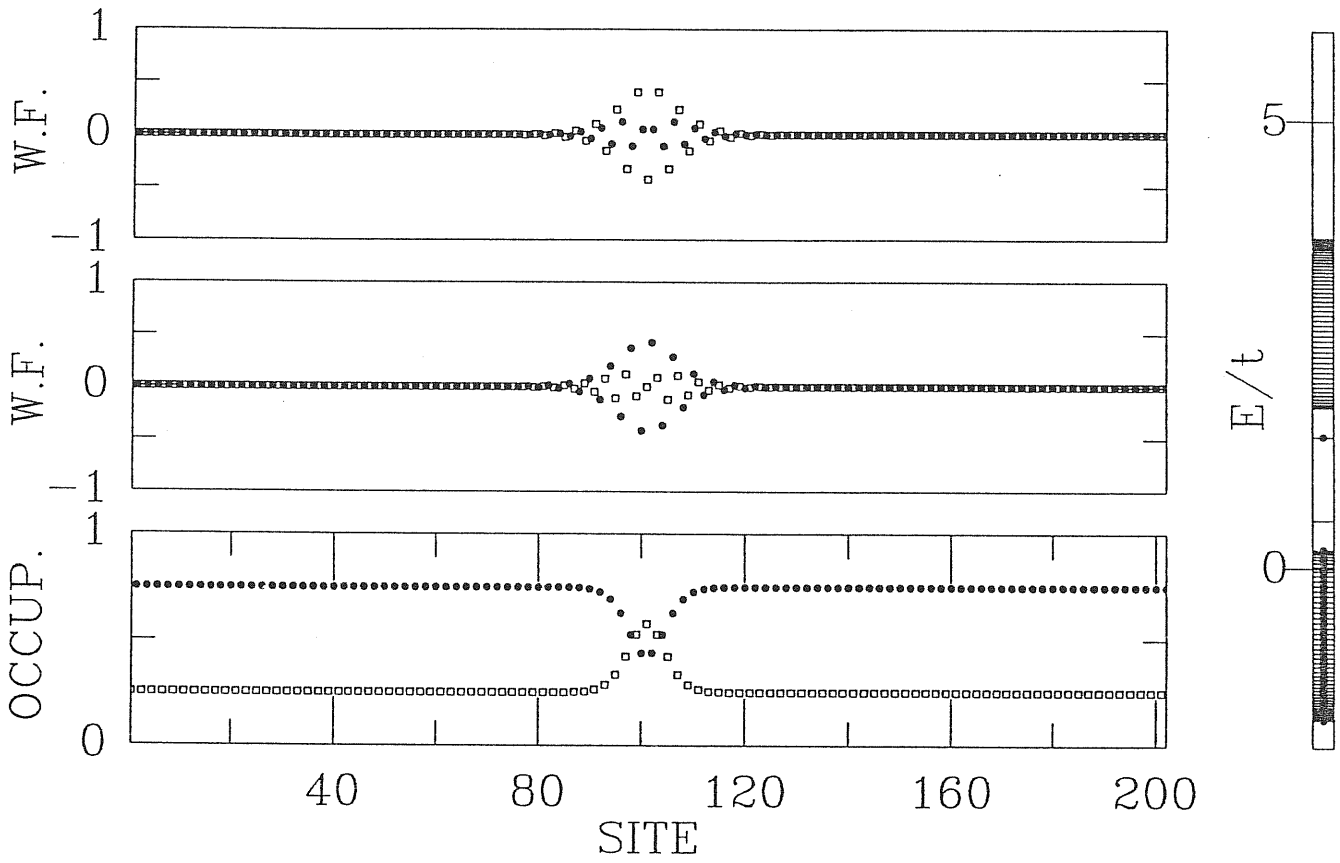

Figure 3.6: Exciton state for $\Delta = .3$, $U_{pd} = 1$. We show the one particle wave function (W.F.) of the two localized states and the site occupation. Solid circles correspond to Cu and squares correspond to O. The plot on the right are the single particle energy levels. A dot represents an occupied level.

ferred to O (see Fig. 3.3), while for the exciton case, there is a whole particle missing which generates the self-trapping potential. For the same reason the exciton spectrum is symmetric. In the limit $\Delta = 0$ the exciton solution dissociates into a free kink- antikink pair.

3.2 Transition between the polaron state and the extended state

As explained in the previous section when one particle is added to the system, it self-traps[21] at the HF level and forms a polaron-like state. In Fig. 3.7 we show the HF charge distribution for different values of U_{pd} for a chain of $N = 10$ unit cells. The polaron is small for large U_{pd}.

As U_{pd} decreases it extends more and more, up to a critical value of the interaction

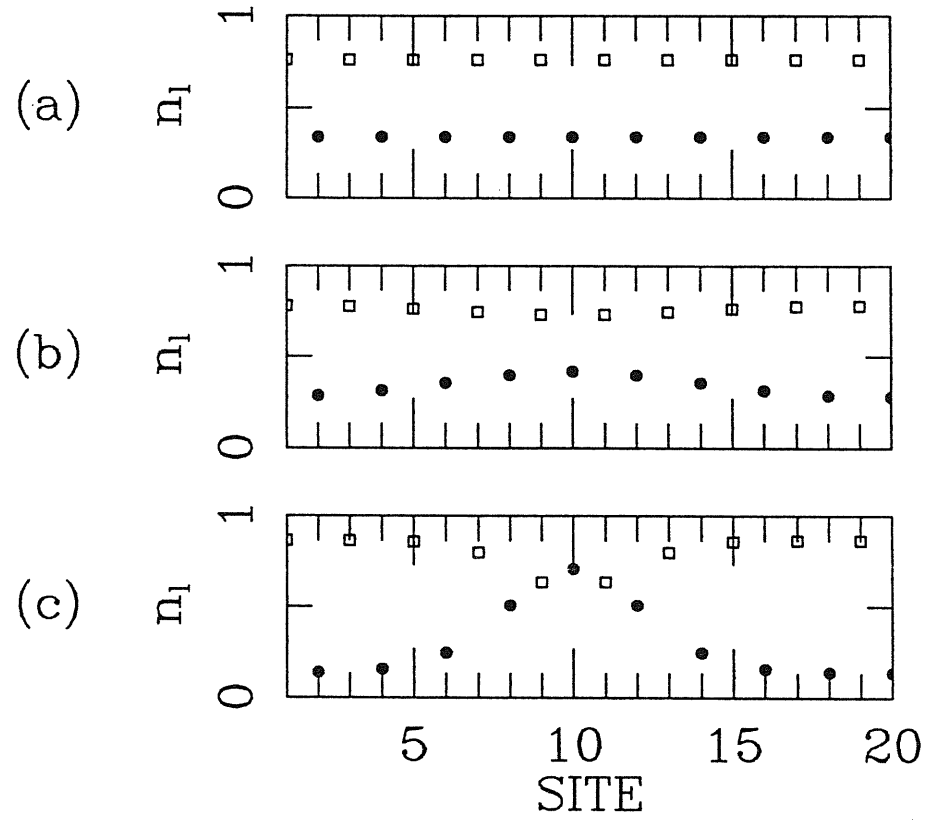

Figure 3.7: Site occupation for one particle added to the half filling case, (a) $N = 10$, $\Delta = 0.3$, $U_{pd} = U_{pd}^c - \eta$;(b) $U_{pd} = U_{pd}^c + \eta$; and (c) $U_{pd} = 2.5$. η is a small number with which the equations can be solved without convergence problems. Solid circles correspond to the even sites and squares correspond to the odd sites.

($U_{pd}^c = 1.58$ for $\Delta = 0.3$) when it reaches the size of the box[Fig. 3.7(b)]. At this point the HF ground state changes and it becomes homogeneous [Fig. 3.7(a)]. Below this value the HF state is translationally invariant. This "phase transition" is an artifact of the HF approximation. No sharp transition occurs in the exact results and one has to think in terms of a smooth, although possibly rapid, crossover. At the RPA level (for the formalism see Appendix A) the transition is signaled by the softening of the corresponding modes (Fig. 3.8). On the uniform side, the modes can be labeled by the momentum q transfered in the scattering process. Except for the modes with $q = 0, \pi$, all the other modes are doubly degenerate due to the symmetry $q \rightarrow -q$.

The normal modes around the mean field state are characterized by the so-called transition densities $< RPA|n_l|\lambda >$. They determine the dynamic components of the expectation value of n_l in a wave packet formed by the ground state and small admixtures of excited states: viz,

$$
\begin{aligned}
&|\Psi(t) >= |RPA > + \sum_{\lambda>0} c_\lambda e^{-i\omega_\lambda t}|\lambda >, \\
&< \Psi(t)|n_l|\Psi(t) >= n_l^0 + \delta n_l(t), \\
&n_l^o =< RPA|n_l|RPA >, \\
&\delta n_l(t) = \sum_{\lambda>0} c_\lambda < RPA|n_l|\lambda > e^{-i\omega_\lambda t} + h.c. + \mathcal{O}(c_\lambda^2).
\end{aligned}
\tag{3.6}
$$

Similar expressions can be written for the off-diagonal elements of the one-body density matrix. In general they are computed by expressing the one-body operators in terms of

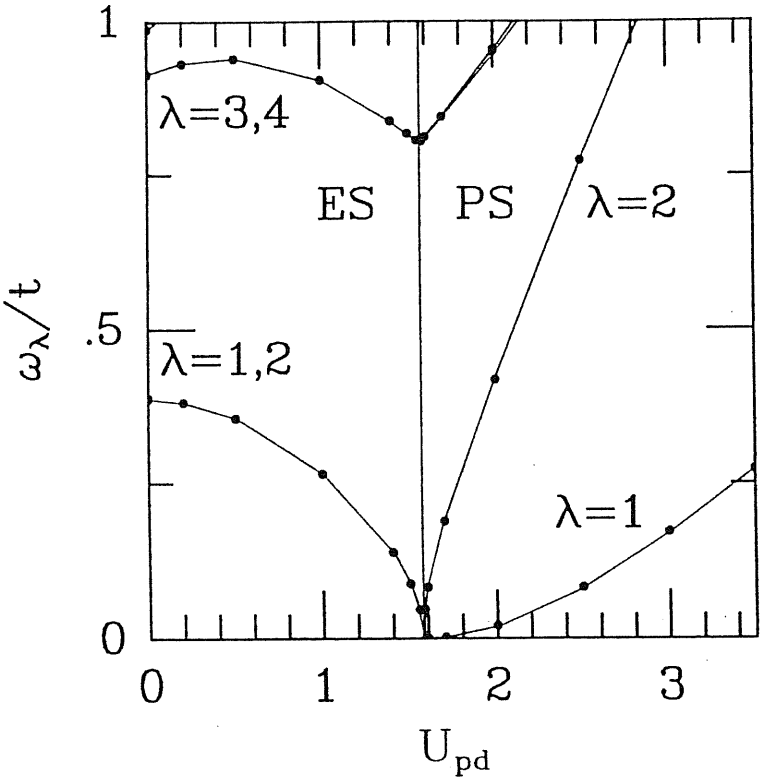

Figure 3.8: The lowest RPA frequencies as a function of the interaction U_{pd} for one particle added to half filling, $N = 10$ and $\Delta = 0.3$. The vertical line indicates the transition between the extended state (ES) and polaron state (PS).

the particle hole operators, through Eq. (A.12), and using the relations of Eq. (A.19). In our case, the transition densities can be taken as real. Note that in the last expression of Eq. (3.6) the vanishing of a frequency means the conversion of a dynamic distortion of the density into a static distortion. In Fig. 3.9 (a) we show the transition density for the mode that goes to zero frequency. The distortion is of the charge transfer (CT) type at short distances, i.e. the charge increases on even atoms and decreases on odd atoms, or vice versa, in a time dependent wave packet as above discussed. At long distances the charge flows from one half of the chain to the other, preempting the polaron effect. Due

to the fact that even sites have more weight in the upper band which is partially filled, the amplitude is larger at those sites indicating on more probability for the charge to flow. Comparison with Fig. 3.7(a) and (b) makes evident the "freezing" of this dynamical fluctuation.

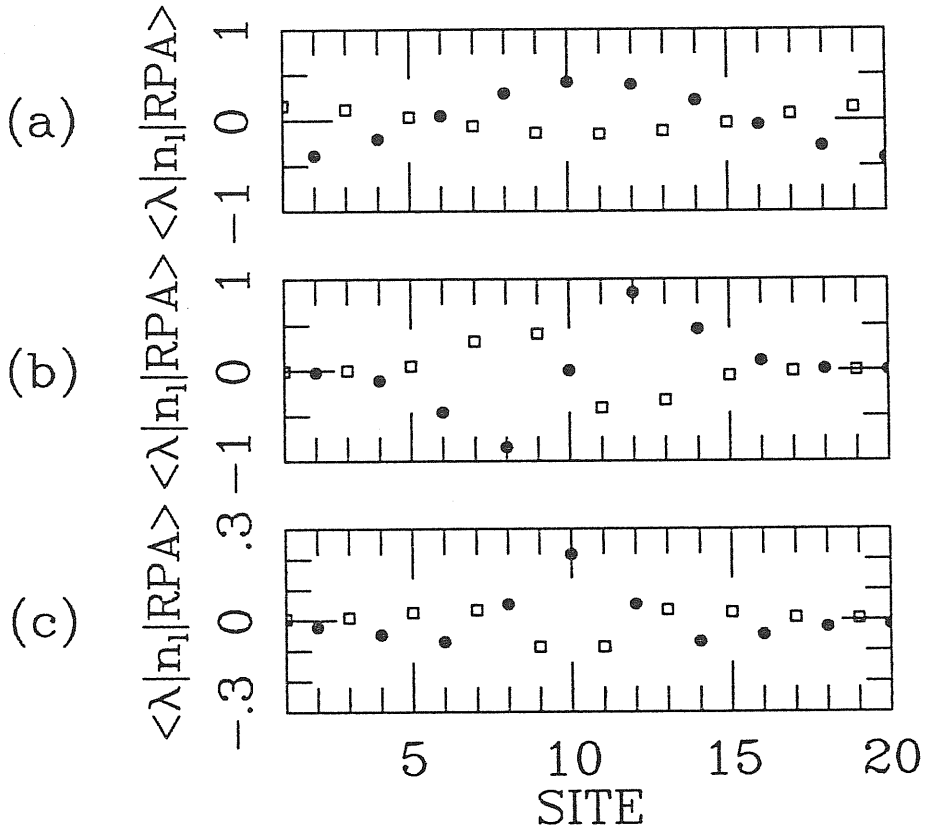

Figure 3.9: Transition densities for one particle added to the half filling case, $N = 10$, $\Delta = 0.3$ and different values of U_{pd}. (a) $\lambda = 1$, $U_{pd} = U_{pd}^c - \eta$. η is a small number with which the equations can be solved without convergence problems. The $\lambda = 2$ case is similar but with nodes on sites where the $\lambda = 1$ case shows maxima. (b) $U_{pd} = 2.5$ and $\lambda = 1$ (oscillation in the pinning potential). (c) $U_{pd} = 2.5$, $\lambda = 2$ (amplitude mode). Solid circles correspond to the even sites and squares correspond to the odd sites.

Above the transition the inhomogeneous mean field state breaks the translational symmetry of the lattice. If this were a continuous symmetry the Goldston theorem would guarantee the existence of a zero energy mode related to the translational motion of the

polaron that restores the symmetry. Here, because of the discrete character of the broken symmetry, the polaron is pinned to the lattice and at this level of approximation there is no translational motion but oscillation in the pinning potential. So this mode [Fig. 3.9(b)] has a finite frequency except right at the transition. Real translational motion can be thought as tunneling between different pinning centers.

Below the transition the lower energy modes are collective. Their frequencies are separated appreciably from the Hartree-Fock single particle excitations. Above the transition they become localized whereas the high energy modes remain extended and have a single particle-hole character.

It is interesting to follow how the modes change at the transition. The two degenerate CT modes split. One becomes the translational mode [Fig. 3.9 (b)], the other conserves its shape but localizes and becomes an amplitude mode [Fig. 3.9 (c)]. When the transition is approached from above, the latter mode is the one that becomes soft.

3.3 Range of validity of the approximations

As discussed in the Appendix A, the RPA is good if the number of electron-hole excitations over the mean field state is small. In principle this can be true even in the strong coupling limit provided the ground state is close to a Slater determinant. This approximation breaks down in regions of parameter space very close to changes in the mean field state. Generally, in the vicinity of such pseudo phase transitions the system is very anharmonic and the fluctuations are too large.

At the present level of approximation another constraint arises from the lack of translational motion. One is neglecting the fact that the self-trapped state (which we will call a "polaron", in analogy with self-trapping in the presence of electron-phonon intereaction)

will tunnel from a given localized state after some time τ. This means that one expects the approximation to be valid for short times ($t < \tau$), large energies and frequencies ($\omega > 1/\tau$), and short wave lengths ($l < c\tau$ with c as some characteristic velocity of the order of the Fermi velocity). Note that $1/\tau$ is of the order of the polaron bandwidth. Its estimation is beyond the present approximation.

In the next sections the ground state energy, and static and dynamic correlation functions are investigated in the inhomogeneous Hartree-Fock plus random phase approximation approach.

3.4 Ground state energy

Here we compare the result of the different approximations for the ground state energy with exact diagonalization results performed in systems of the same size and the same boundary conditions. We compute the correlation energy $E_c^{N+i} = E^{N+i} - E_{HF}^{N+i}$. E^{N+i} is the ground state energy for the system with $N+i$ particles. For E_{HF}^{N+i} we take the lowest (generally inhomogeneous) HF state.

At half filling the HF ground state is homogeneous and the HF energy reproduces correctly the behavior of the ground state energy as a function of U_{pd} and slightly underestimates it due to the variational nature. In Fig. 3.10 we show the exact correlation energy per site as a function of U_{pd} and compare it with the quasi-boson QB (see Appendix A) and RPA results. In the small coupling regime the RPA gives the correct quadratic behavior as a function of U_{pd} whereas QB overshots it by a factor of 2, as explained in the Appendix A.

Away from half filling the behavior is different depending on how we approach the strong coupling limit. If $U_{pd}/t \to \infty$ and Δ is kept zero the added particle separates into

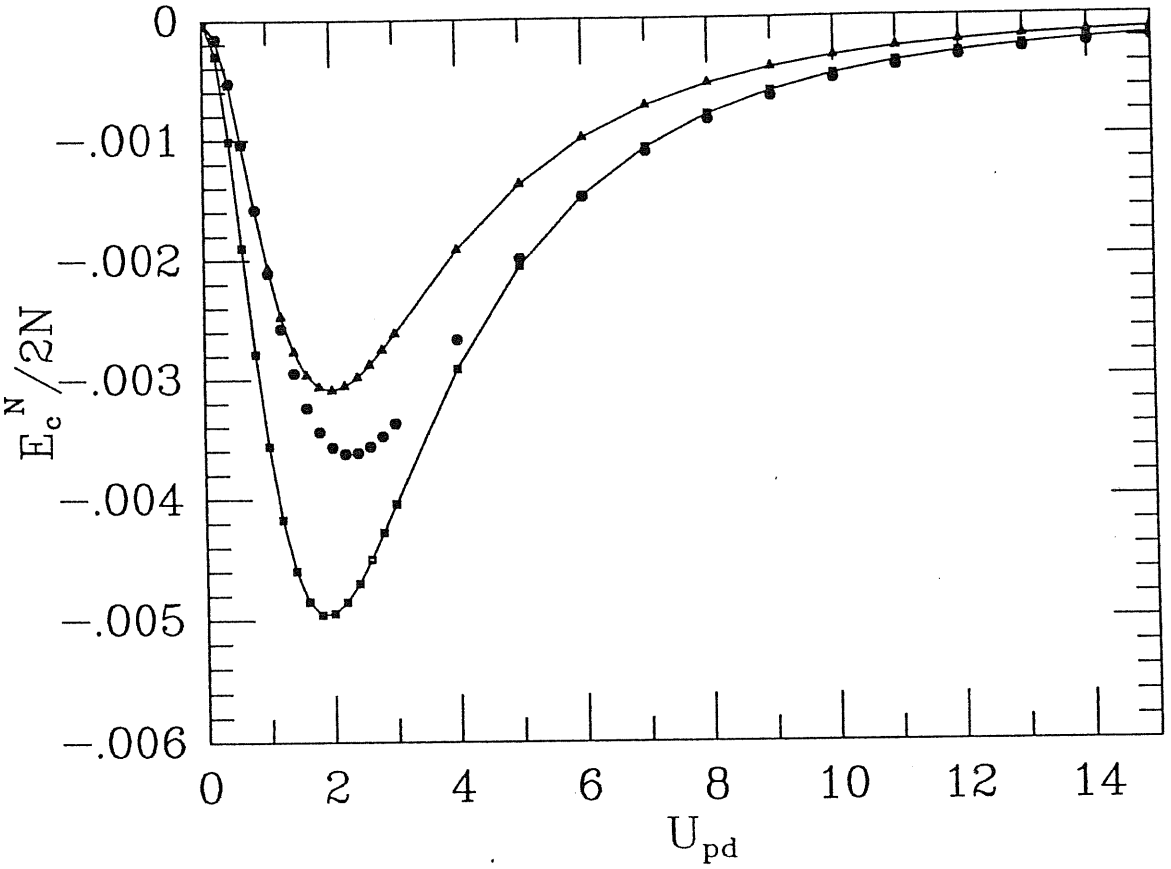

Figure 3.10: Correlation energy per site as a function of the interaction U_{pd} for $N = 10$ and $\Delta = 0.5$. Solid circles are the exact results, squares correspond to the QB and triangles to the RPA.

a kink-antikink soliton[33, 21] pair. If Δ is small, the solitons are weakly bound (in a small ring the effect can be negligible) and they can move with an effective band-width of the order t. This band motion of solitons is not included in our approach making the correlation energy underestimated than the true value. On the other hand, in the limit $U_{pd}/t, \Delta/t \to \infty$, keeping Δ/U_{pd} constant, the kink and antikink are tightly bound and the ground state is a polaron whose band-width goes to zero. We illustrate this behavior by showing the correlation energy required to add a polaron ($E_p^c = E_c^{N+1} - E_c^N$), (Fig. 3.11). We note that the homogeneous solutions for $U_{pd} > U_{pd}^c$ always have higher energy than

the corresponding inhomogeneous ones.

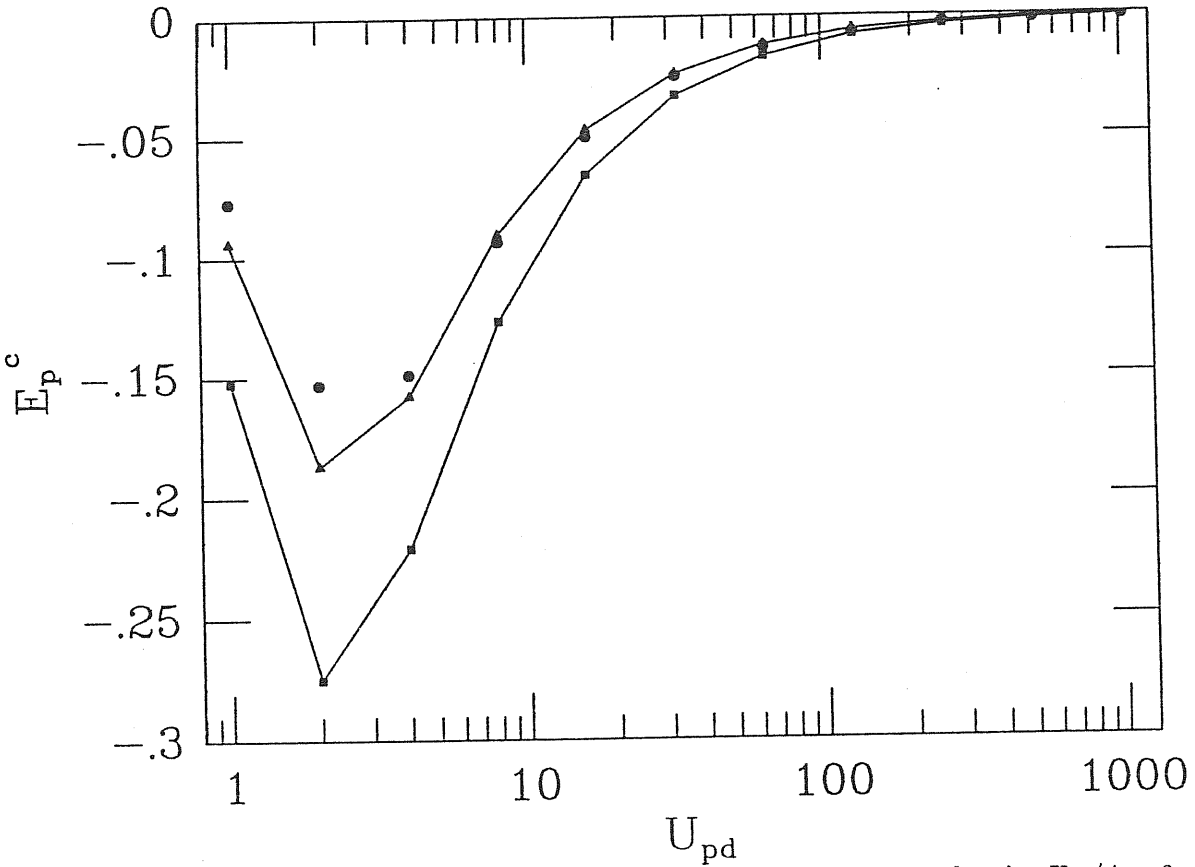

Figure 3.11: Correlation energy of a polaron as a function of the interaction U_{pd} keeping $U_{pd}/\Delta = 2$ for $N = 10$. Solid circles are the exact results, squares correspond to the QB and triangles to the RPA.

3.5 Static correlation functions

Here we compare static correlation function calculated in the IHF and HHF with exact digonalization results obtained with the Lanczos method[30]. Because the HF solution breaks the translational invariance the static correlation functions depend not only on the distance to the origin, but also on the position of the origin itself. We denote by $|HF, r_o>$ the HF state centered at r_o. There are N non-orthogonal HF wave functions with the same energy characterized by the position r_o of the center of the polaron state. The next level

of approximation would be to compute matrix elements of the Hamiltonian between the different IHF states and to construct Bloch states. A simpler approach is to completely neglect the overlap and to consider the different HF solutions as orthogonal degenerate states. Then, for example, the one-body density matrix can be calculated as a $T = 0$ thermodynamic average, that is:

$$[< c^{\dagger}_{r_o} c_r >] = \frac{1}{N} \sum_{s=0}^{N-1} < c^{\dagger}_{r_o+2s} c_{r+2s} > . \tag{3.7}$$

In Fig. 3.12 we show the off-diagonal part of the one-body density matrix for a single particle added to the system as a function of the distance from the origin at an even site, for $\Delta = 0.5$ and $U_{pd} = 3$.

The Fourier transform of such a quantity gives the momentum distribution function and the long distance behaviour is related to the Fermi level discontinuity Z. For the IHF state it decays exponentially, indicating at a fictitious insulating behavior ($Z = 0$). Such a long distance failure is beyond the range of applicability of the present calculation and should be cured in a polaron band approach as explained above. On the other hand, the HHF gives a better long distance behaviour but, as expected, overestimates the Z. At short distance this quantity shows only slight differences between the two approaches as one would expect, because the important correlations are due to local distortions of charge densities around the added particle. This is illustrated in the two-body correlation function that we plot in Fig. 3.13.

We see that IHF does better than its homogeneous counterpart at short distance, and, unexpectedly, at long distance as well. At short distances it takes into account the local distortion of the charge, but underestimates it.

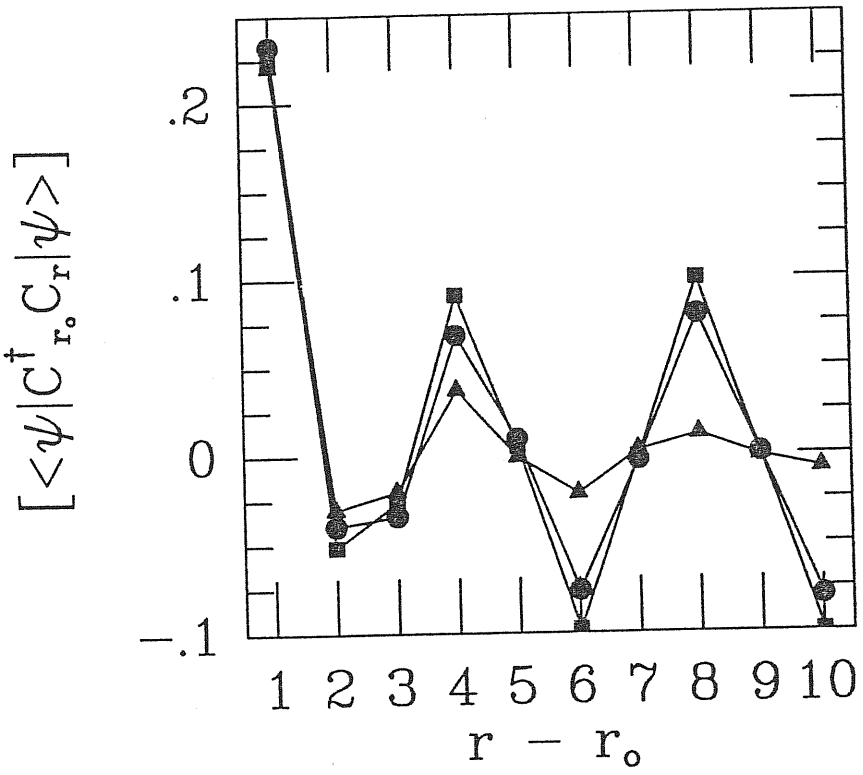

Figure 3.12: Off-diagonal part of the density matrix as a function of distance for one particle added to the half filling case, $N = 10$, $\Delta = 0.5$, $U_{pd} = 3$. r_o corresponds to an even site. Solid circles are the exact results, squares correspond to the HHF and triangles to the IHF.

3.6 Dynamic correlation functions

From the RPA eigenvectors it is easy to compute dynamical correlation functions of the form

$$C_{AB}(t - t') =< RPA|A(t)B(t')|RPA >, \tag{3.8}$$

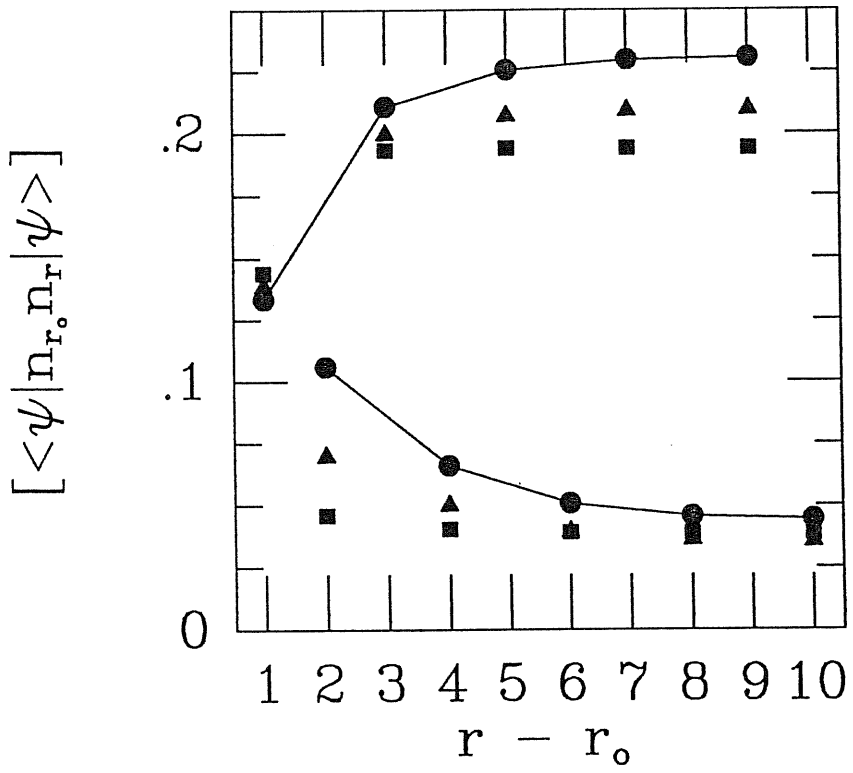

Figure 3.13: Charge-charge correlation function as a function of distance for one particle added to the half filling case, $N = 10$, $\Delta = 0.5$, $U_{pd} = 3$. Solid circles are the exact results, squares correspond to the HHF and triangles to the IHF.

where A and B are one-body operators. In fact the imaginary part of the Fourier transform admits the following spectral representation:

$$Im[C_{AB}(\omega)] = \sum_{\lambda>0} < RPA|A|\lambda >< \lambda|B|RPA > \delta(\omega - \omega_\lambda), \tag{3.9}$$

The matrix elements in Eq. (3.9) are given by the transition densities of Section 3.2.

At the RPA level there are single particle-hole excitations which have almost the same energy as the corresponding Hartree-Fock particle-hole excitations and collective excitations. At half filling one expects the correlation between particles and holes to produce an excitonic like peak below the smallest HF particle hole excitation which correspond to the

mean field gap. Such collective excitation can be seen in the current-current correlation function that gives the optical excitation spectra (Appendix B). In this case we use in Eq. (3.8) $A^\dagger = B = J$, where $J = -it\sum_l (c_l^\dagger c_{l+1} - c_{l+1}^\dagger c_l)$.

In Fig. 3.14 we show the imaginary part of the current-current correlation function for $N = 8$, $\Delta = 0.25$, $U_{pd} = 1$ and antiperiodic boundary conditions.

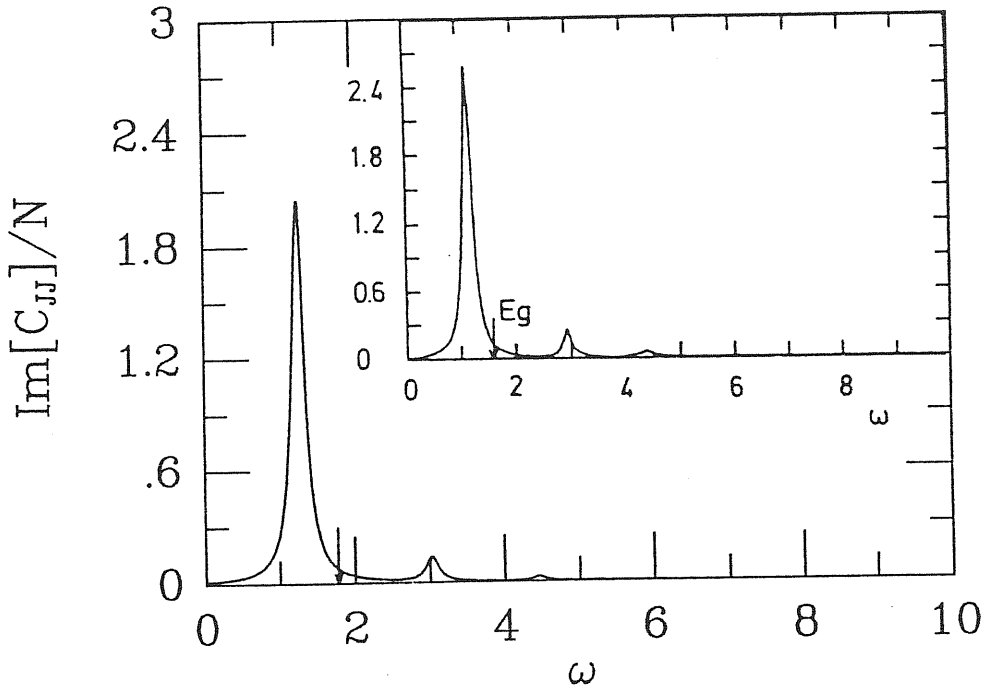

Figure 3.14: Imaginary part of the current-current correlation function in the RPA. We add a small imaginary part to the energy ($\eta = 0.1$) in order to broaden the delta functions. $N = 8$, $\Delta = 0.25$, $U_{pd} = 1$. The arrow indicates the value of the uniform HF gap. The inset shows the exact results of Ref [23] and the arrow indicates the value of the gap in the single particle spectral function.

The arrow indicates the position of the Hartree-Fock gap. The result compares very well with the exact solutions of Ref. [23]. In particular the position of the excitonic peak below the gap is very close to the exact value. This pole gives the energy to create an

exciton over the uniform state. The same excited state can be obtained in a rather different way as we have shown in 3.1.2. We can look for a site-dependent mean field solution in which the lowest state of the upper band is full and the highest state of the lower band is empty. Fig. 3.15 shows such an example.

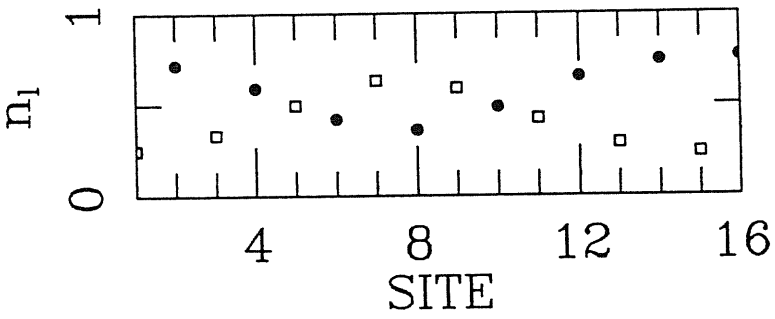

Figure 3.15: Site occupation for the exciton state. $N = 8$, $\Delta = 0.25$, $U_{pd} = 1$. Solid circles correspond to the even sites and squares correspond to the odd sites.

The energy difference $\epsilon_e = E^N_{exciton} - E^N$ gives the excitation energy in this approach and an interesting question is how it compares with the energy of the excitonic peak described above. In Fig. 3.16 we show the exciton creation energy for different values of Δ in the site-dependent HF and compare it with the RPA results and the exact diagonalization results of Ref. [13].

The pentagons indicate the value of the uniform Hartree-Fock gap. The agreement is quite good. One should keep in mind that the RPA is a linearized theory, in this case around the uniform mean field state. The above agreement suggests that the estimate of Fig. 3.15 is not too far from a linear excitation around the uniform state. Note however that the energy is not very sensitive to small errors due to non-linearities in the wave function.

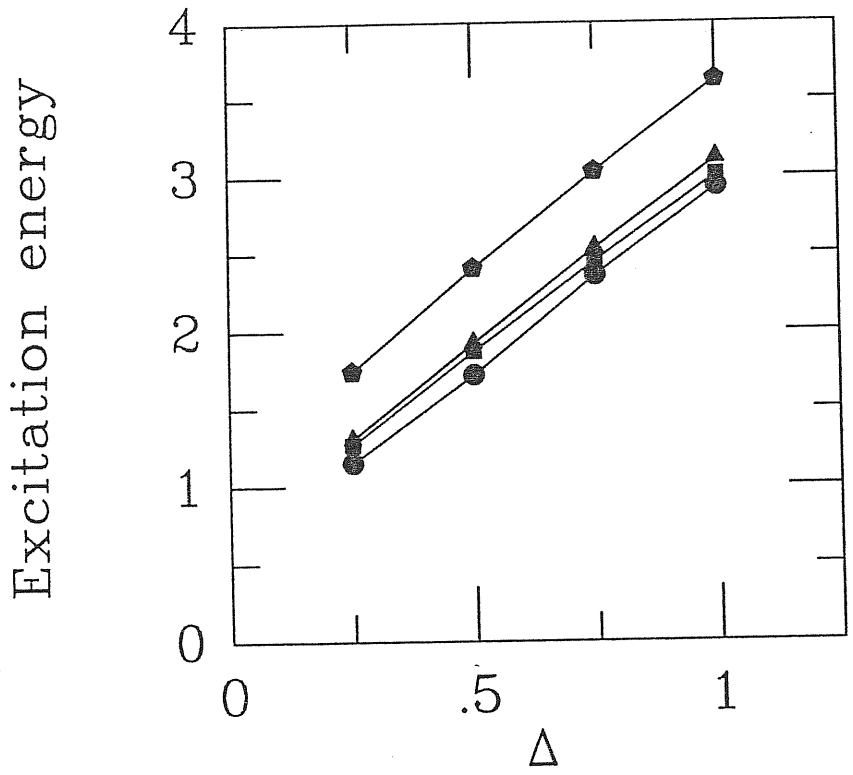

Figure 3.16: Excitation energy to create an exciton as a function of Δ. Solid circles are the exact results, squares correspond to the RPA and triangles to the IHF. For comparison we also plot the uniform Hartree-Fock gap (pentagons)

3.7 Conclusions

We see that one particle added to the half-filling case distorts the charge balance between Cu and O around it and forms a polaron of charge transfer origin. In this picture polarons will form a dispersive band growing with doping.

We found that the uniform HF state is unstable. Using a different formalism, Grilli[34] et al. found the same instability in the compressibility but they interpreted it as a phase separation. The difference is that they set the repulsion on the O equal to zero, while we set it equal to infinity. Since the polaron states are mainly due to O character, we

expect the result of Fig. 3.5 to be different in their case, so in principle the results are not contradictory to each other. The study of more realistic models in the next chapters will show that both situations are possible.

The p-d model has been studied in higher dimensions in the limit $t << \Delta << U_p, U_d$ by perturbation theory in the hopping, in connection with hole-doped CuO and BiO based HTSC[9], and electron doped CuO layers[35]. It has been shown that one particle added to the half-filling case produces charge transfer excitations around it in a way which resembles our results. When two particles are put close together low energy charge fluctuations are allowed which lower the energy and produce pairing. The same mechanism does not work in 1D. In the next chapter we will show how bipolaron states, relevant for the superconductivity, can be found in 2D.

We have calculated the ground state energies, static and dynamic correlation functions in the IHF + RPA approach. We have also shown how the transition between polaronic behaviour and band motion is signaled by collective modes that become soft.

The calculations were compared with exact diagonalization results. We showed that IHF describes short range correlations better in this strongly correlated model than the HHF. However, due to the fact that the first approach breaks translational invariance, all properties related to the metallic behaviour are not properly described at this level of approximation. This is not unexpected because the metallic regime is a long distance behaviour and hence it is out of the range of validity of the present level of approximation. In this sense this approach is complementary to other techniques like bosonization[36] or renormalization group that are expected to work in the opposite limit (long wavelength and low energies). A possible extension of the method would be to form polaron bands.

In principle this should give better long distance properties but requires additional approximations.

Another advantage of working with the stable IHF solutions instead of the HHF ones is that one can easily perform the matrix RPA on the basis of the IHF solutions and obtain the linear excitation spectra of the system. It allows computation of dynamical correlation functions that compare well with the exact ones. It can be performed in larger systems and faster than exact diagonalization methods but also, by plotting the site dependent IHF densities and RPA transition densities, one can visualize the physics involved.

Is interesting to note that the energy to crate an exciton is very close to the exact one in both the RPA and in a site dependent approach in which the occupations of the IHF orbitals are constrained to produce the excited state.

Finally we note that the technique is flexible enough to study different competing interactions[37, 38]. In this sense we will show in the next chapter that it provide a good understanding of strong correlations in realistic models.

Chapter 4

Pairing and phase separation in a two dimensional spinless model

Here we show that the polarons and excitons of charge-transfer origin in the 1D spinless model of the previous chapter can also occur in 2D.

We use a 2D spinless model which is expected to qualitatively describe the charge degrees of freedom of the p-d model in the limit of infinite on-site Coulomb repulsion on both Cu and O. The Cu-O repulsion U_{pd} is treated by an unrestricted Hartree-Fock scheme. We found that in addition to polarons and excitons, other nonlinear excitations like bipolarons and clustering of carriers (phase separation) arise as well. Since the energies of all these excitations are very close to each other at the mean field level, no definite statement can be made about the true ground state.

In search for the ground state of strongly correlated electron systems like the high temperature superconductors a variety of mean field phases have been proposed at half filling. Many of these phases turn out to be unstable upon doping[39]. As we have shown in the previous chapter in some cases the instability is signalled by a negative compressibility $\partial\mu/\partial x$, where μ is the chemical potential and x the doping. To find the true stable phase

is a delicate task. The Maxwell construction tells us that a phase separation is more favorable at the mean field level showing the tendency to clustering of the added charge carriers. However, even when one adds only one particle to the system there can be some kind of "phase separation" in the sense that one can find a mean field solution in which translational symmetry is broken and the added particle is localized in some region leaving the rest of the system unchanged. This is the mean field polaron of the previous chapter. The added particle disturbs the mean field order parameter to create a potential well in which it is self-trapped. Eventually the translational symmetry can be recovered by "moving" the polaron. Some examples of these localized states have been studied in the Hubbard model[40].

In the previous chapter we have studied the problem of a single particle added to the stoichiometric state in 1D by carrying out a site-dependent Hartree-Fock calculation. We have shown that it distorts the balance of charge between Cu and O forming a self-trapped polaron state or "charge-transfer bag". In this chapter we extend our studies to 2D. There are two reasons for doing this. Firstly, it is important to check if such nonlinear excitations can also arise in a 2D model and, secondly, the analytic[13, 9] and numerical[13] results suggest that the proposed charge-transfer-pairing mechanisms, at least in the strong coupling limit work only for dimensions greater than one. In the previous chapter we have shown that in 1D and in the limit of infinite on-site Coulomb repulsion on both Cu and O polarons repel each other. Here in 2D we find pairing of particles and other clustering effects suggesting a phase separation. However, configurations with different numbers of clustering have very close energies at the mean field level implying a highly frustrated state.

As we have shown in Chapter 2, there is a major simplification in 1D because in the limit of infinite on-site Coulomb repulsion on both Cu and O, the charge and spin degrees of freedom are decoupled from each other and the former are described exactly by a spinless fermion Hamiltonian. There is no such exact mapping in 2D. However, one expects that the charge degrees of freedom are qualitatively described by a similar spinless model. This way one simulates the "Coulomb hole" that accompanies a particle in the limit of infinite on-site repulsion by a "exchange hole". Such an approximation has been adopted by Balseiro et. al.[13] in numerical simulations providing qualitatively similar results as given by simulations of Hirsch et. al.[12], studying the original model for large on-site Coulomb repulsion. Both calculations indicate on pairing of particles for moderate values of U_{pd}, the nearest neighbour Coulomb repulsion. Such a charge-transfer pairing mechanism can be analyzed in the narrow band limit along the lines of Ref. [9] by doing perturbation in hopping. When a single particle is added to the system it generates charge fluctuations around it (the polaron effect). When two particles are put close to each other, low energy charge fluctuations are allowed that lower the energy and produce pairing. At the mean field level such charge fluctuations manifest themselves as permanent distortions of the mean field order parameter around the added particles. Here we prefer to carry out the calculations in the spinless model because it is simpler and it allows us to illustrate the effect of the charge degrees of freedom in action alone. We can remark that the perturbative calculations of Ref. [9] give similar results for both models with large on-site Coulomb repulsion and one has to go to higher order in perturbation to find any difference. The spinless Hamiltonian in 2D reads as

$$H = \sum_i E_i n_i + \sum_{i \neq j} E_{ij} c_i^\dagger c_j + \sum_{\langle i,j \rangle} U_{pd} n_i n_j \,. \tag{4.1}$$

where $n_i = c_i^\dagger c_i$, $c_i^\dagger$ creates a spinless fermion associated with charge degrees of freedom of a hole, on site i, $E_i = \epsilon_d$ (ϵ_p) for a Cu (O) site. The nearest-neighbour matrix elements are $E_{ij} = t_{pd}$ and the direct O-O hopping is $E_{ij} = -t_{pp}$.$\langle i,j \rangle$ indicates summation over nearest neighbours. As usual we define $\Delta = (\epsilon_p - \epsilon_d)/2$ and use units with $t = 1$. Details of the calculation are given in Appendix A. In Fig. 4.1 we show the chemical potential of this model as a function of doping in the uniform Hartree-Fock approximation. Since the same instability appears as in the 1D case, we expect important polaronic effects to be present. In Fig. 4.2 we show the polaron solution in the 2D case. There is a depletion in

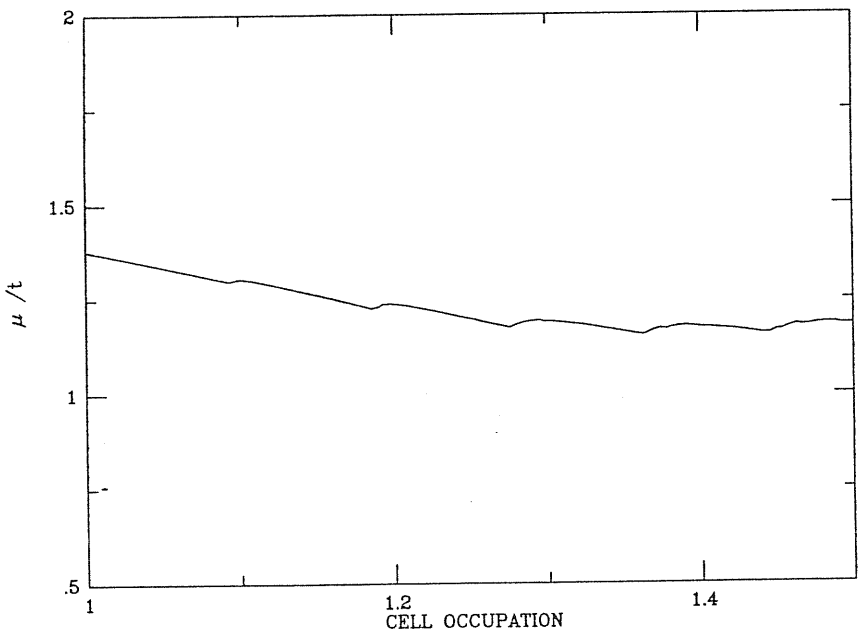

Figure 4.1: Chemical potential as a function of cell occupation for 2D, $\Delta = .25$, $t_{pp} = .2$, $U_{pd} = 1$. The ripple is due to the discreteness of the mesh.

the Cu charge due to the transfer to O and a bump in the O charge due to the localization of the added particle and the charge transfer from Cu. We note that as the system is

doped the gap is filled in with states.

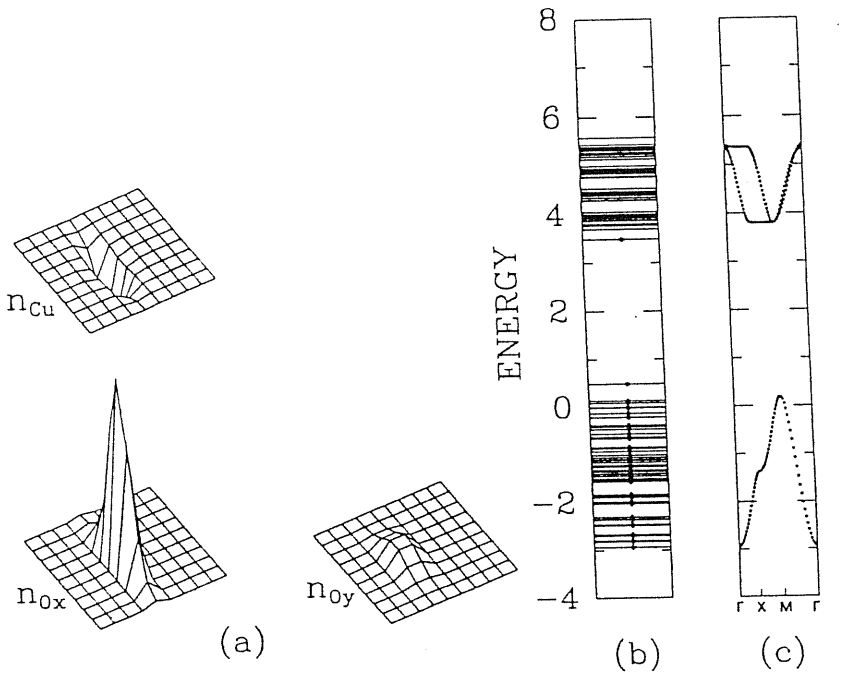

Figure 4.2: One particle added to the half filling case for $\Delta = .8$, $t_{pp} = .4$, $U_{pd} = 2$ and a 300-atom lattice. We show the site occupation for the three atoms in the unit cell (a) and the one particle energy levels (b). A dot represents an occupied level. We also sketch the band structure in the uniform case.

There is a tendency to form a cigar-like structure. This is related to the band structure of the Hamiltonian (4.1) for $U_{pd} = 0$. There are one lower Cu-like band and two higher O-like bands. One of the latter is dispersionless along the boundary of the Brillouin zone. By forming a linear combination of Bloch states with $k_y = \pi$ and k_x varying, where $k_{x,y}$ are the components of the wave vector in units of the inverse lattice constant, we can construct an eigenstate of the Hamiltonian in which the charge is localized in the x direction and is propagating like a 1D Bloch wave in the y direction with momentum $k_y = \pi$. By turning on U_{pd} the single particle wave function also gets localized in the y direction but still keeps

the cigar-like shape. The charge is mainly on one of the two O atoms in the unit cell. The 1D character of the band structure can be eliminated by adding next nearest neighbours O hopping matrix elements not included in (4.1). We have checked that these matrix elements do not change qualitatively the result if they are less than U_{pd}. In the results presented here we have set them equal to zero for the sake of simplicity.

We have also considered exciton states (Fig. 4.3).

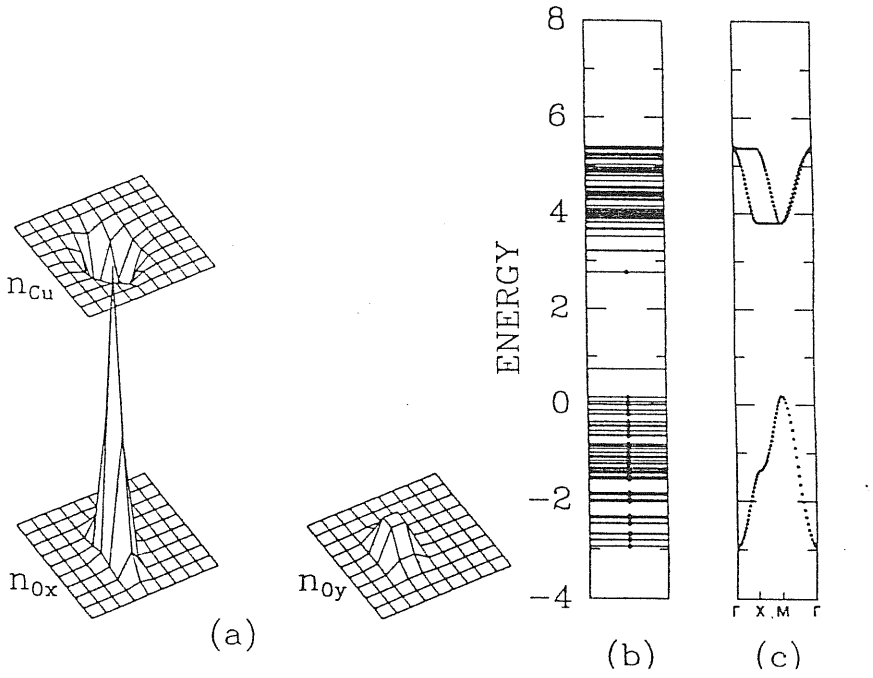

Figure 4.3: Exciton state for $\Delta = .8$, $t_{pp} = .4$, $U_{pd} = 2$ and a 300-atom lattice. We show the site occupation for the three atoms in the unit cell (a) and the one particle energy levels (b). A dot represents an occupied level. We also sketch the band structure in the uniform case.

Related states were considered in the past in 1D by exact diagonalization[23] and in 2D by solving realistic models[16] in the limit of zero band-width. Experimental evidence for such states has been found[41] although this point is still controversial. The gap for

such localized excitations is smaller than the charge transfer gap. For example, for the parameter values of Fig. 4.3 the charge transfer gap is 3.62 whereas the excitonic gap ($E_{exciton} - E_{uniform}$) is 3.08. As we noted in 1D, the exciton is more localized than the polaron.

If we add two particles to the system, in contrast with what happens in 1D, they do not repel each other. We define $E_n = E(N+n) - E(N)$ and the binding energy $E_b = E_2 - 2E_1$. In Fig. 4.4 we compare the exact diagonalization results of Ref.[13] with ours on a cluster of the same size. There is always binding of holes ($E_b < 0$). By varying

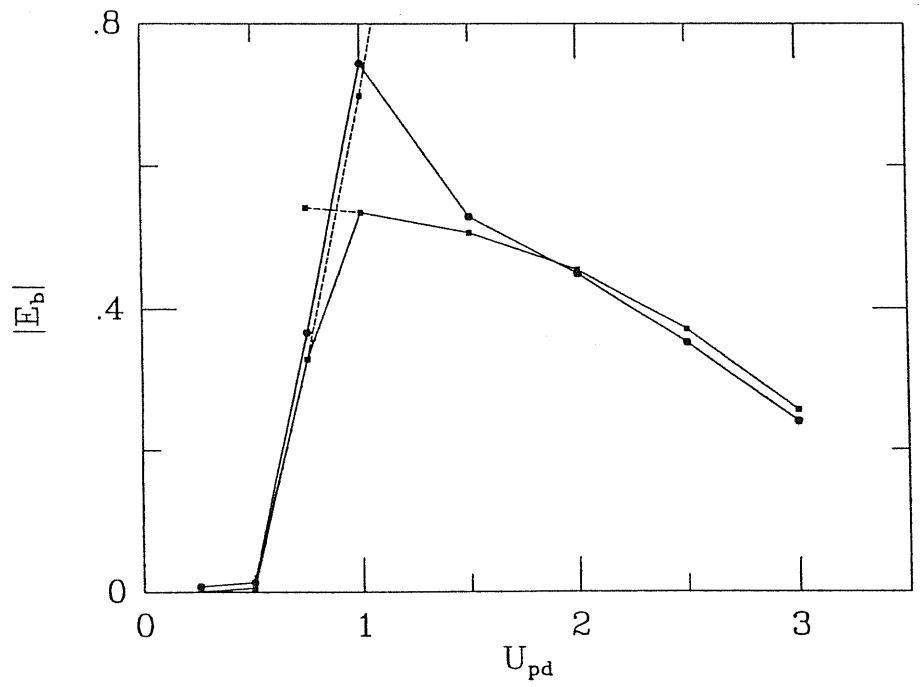

Figure 4.4: Absolute value of the binding energy for two holes as a function of U_{pd} for $\Delta = .25$, $t_{pp} = 0$ in a 12 atom lattice. Dots are exact diagonalization results from Ref.[13] and squares are from this work. The dashed line indicates the metastable Hartree-Fock solution.

U_{pd} there is a transition from one Hartree-Fock solution to another corresponding to the

fact that for large U_{pd} the system prefers to transfer all the charge to O in order to avoid the nearest neighbour repulsion. We indicated with a full line the lower energy solution and with a dashed line the higher energy solution. Except for one point which is near the crossing of the two solutions there is a good agreement between the Hartree-Fock results and those of exact diagonalization. This shows remarkably that the attractive interaction between particles can be captured at the mean field level. This serves also as a cross-check for our procedure. However, we expect the finite size effect to be important for such a small cluster. By doing the same calculation in bigger clusters we see that there is a bipolaron formation (Fig. 4.5). Due to the strong attractive forces the bipolaron is more compact than the polaron. Note that the charge distribution and the Hartree-Fock potential it generates have C_4 symmetry around the central Cu. Due to this symmetry the highest occupied energy level which is mainly of O character is twofold degenerate and it accommodates the two added particles. For smaller values of U_{pd} it has a cross-like shape resembling two cigar-like polarons intersecting each other. For n particles added we can define a cluster energy per added particle as $\varepsilon_n = E_n/n$. For $N \longrightarrow \infty$, ε_n should have a minimum in the most stable configuration. For large values of U_{pd} (Fig. 4.6) ε_n decreases monotonically with n indicating that the added particles prefer to form a big cluster and the system is separated into a hole rich region and a region without holes. In this case the starting Hamiltonian is not adequate and longer range Coulomb repulsion should be included. However, as U_{pd} decreases to more physical values, ε_n flattens more and more. At the same time the finite size effects become more severe. There seems to be a minimum at $n = 3$ for $U_{pd} = 1$. However, it is very shallow, within the error-bar of a finite size analysis. Anyway for such a flat curve a mean field value of the minimum should not be

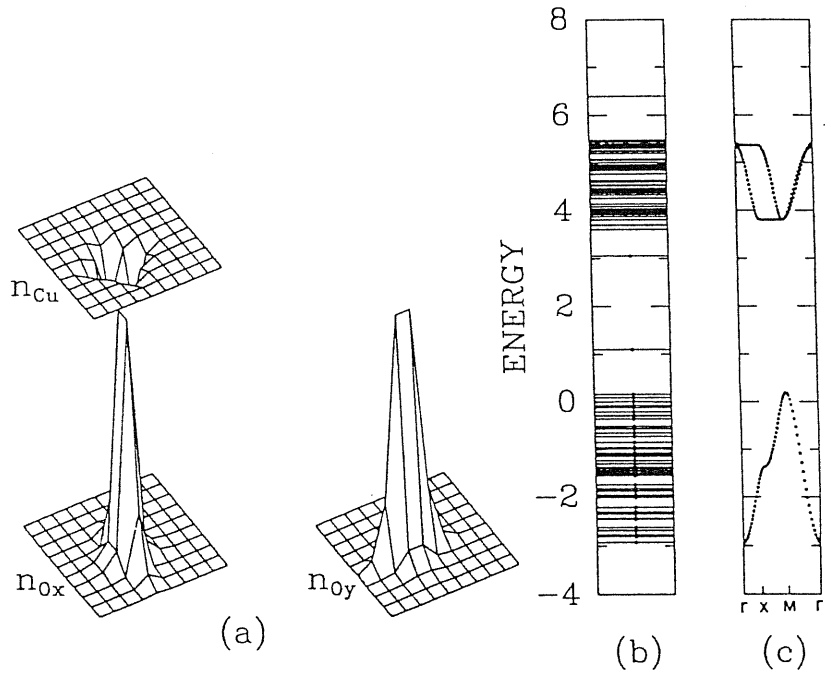

Figure 4.5: Two particles added to the half filling case for $\Delta = .8$, $t_{pp} = .4$, $U_{pd} = 2$ on a 300-atom lattice. We show the site occupation for the three atoms in the unit cell (a) and the one particle energy levels (b). A dot represents an occupied level. The upper level in the gap has double degeneracy, whereas the lower level is not degenerate. We also sketch the band structure in the uniform case.

taken too seriously. There are important corrections to the energy not considered here that can strongly depend on n. In the limit of a very localized cluster we can consider the tunneling amplitude from one site to the neighboring sites. If we construct a Bloch state the energy should be lowered by a quantity equal to the tunneling amplitude. This must scale as $1/nm^*$ where nm^* is some effective mass of a cluster of n holes and gives a correction to ε_n that scales as $1/n^2m^*$. Even without moving the polarons there should be important corrections coming from the RPA fluctuations around the mean field solutions. These are the internal modes of the cluster like those found for kinks and polarons in

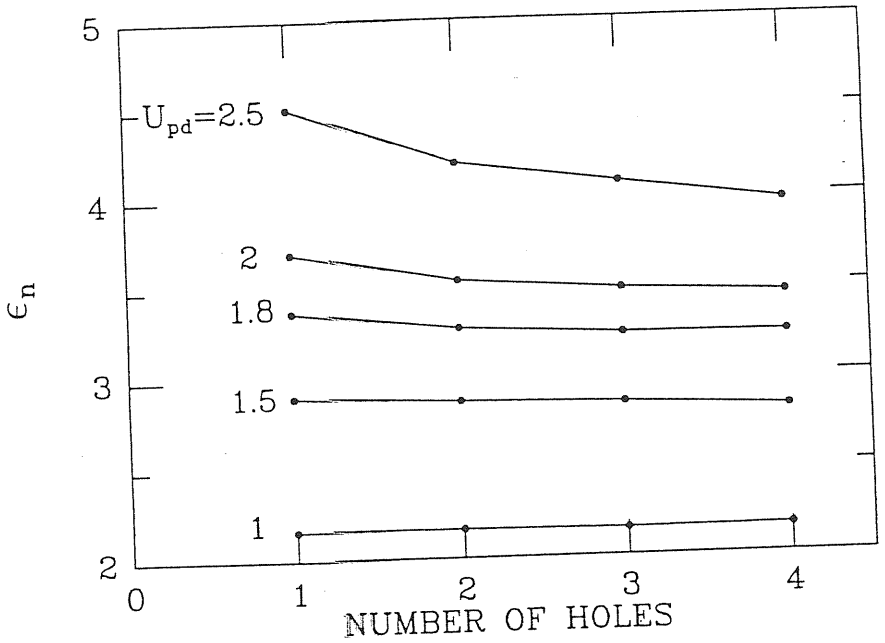

Figure 4.6: Binding energy per particle in a cluster as a function of the number of holes clamping for $\Delta = .8$, $t_{pp} = .4$.

polyacetylene[31] or the RPA modes studied in the previous and following chapters and they should also depend strongly on n. The electron-phonon and magnetic interactions can stabilize one of these configurations. In fact one expects the lattice to relax around the localized excitations as is seen in the experiments[4, 2]. All these effects will be considered in the more realistic calculations of the following chapters. A very plausible scenario is that the system fluctuates between quasi-degenerate configurations.

In summary we have shown that charge transfer polarons can be realized in 2D as well. We found excitonic states which are possibly related to optical measurements[41]. Moreover, other excitations like bipolarons, relevant for superconductivity, are also found. For large values of U_{pd} there is a tendency for phase separation, but as U_{pd} is lowered,

different configurations become quasi-degenerate and our present analysis is insufficient to determine the true ground state. Nevertheless, the charge-transfer excitations are shown to provide a strong gluonic force between holes as was discussed in the literature for weak[11, 42, 43] and strong couplings[13, 9, 12]. In the present scheme we can study the non-perturbative intermediate coupling regime.

Our calculation suggests a possible appealing scenario for the Cu oxides. As the system is doped, the gap is filled in with bipolaronic or polaronic bands with attractive correlations responsible for superconductivity. Eventually for high enough doping the Pauli exclusion principle prevents true polaron formation and it becomes a resonant state. For even higher doping levels the polaronic behavior disappears completely. We will show in the next chapter that when the realistic p-d model is used this scenario is consistent with our present understanding of these materials and is supported by various experiments.

Chapter 5

Doping states in the p-d model

In this chapter we study the p-d model. We try to be more realistic in order to make a detailed comparison with experiments. Doping states are investigated with inhomogeneous Hartree-Fock and random phase approximations. For parameter values relevant to cuprate superconductors, a small electronic polaron is found. The polaron can be thought of as an approximate solution to an ideal state which is in an intermediate regime between a Zhang-Rice singlet and a covalent molecular singlet. The former case corresponds to large U_d with respect to Cu-O covalency whereas the later corresponds to small U_d with respect to Cu-O covalency. The last case is favored if covalency is increased. One way of doing that, as we will see in the next chapter, is by relaxing the lattice. The other way is by increasing the doping. Both effects favor the quenching of the magnetic moment at the central Cu of the polaron. When the doping is high enough and the polarons overlap strongly the system becomes metallic and it looks more like a conventional Fermi liquid.

We have used the Hartree-Fock (HF) technique of the previous chapters, totally unrestricted in both spin *and* direct spaces. For our problems this is very much superior to the traditional homogeneous HF approaches. On top of the generally inhomogeneous HF con-

figurations, we have added a similarly inhomogeneous RPA analysis of linear fluctuations to calculate infrared optical absorption.

The general model Hamiltonian we consider is (see Chapter 2):

$$\begin{aligned} H &= \sum_{i\neq j,\sigma} t_{ij}^{0} c_{i\sigma}^{\dagger} c_{j\sigma} + \sum_{i,\sigma} e_{i}^{0} c_{i\sigma}^{\dagger} c_{i\sigma} + \sum_{i} U_{i} c_{i\uparrow}^{\dagger} c_{i\downarrow}^{\dagger} c_{i\downarrow} c_{i\uparrow} \\ &+ \sum_{\langle i\neq j\rangle,\sigma,\sigma'} U_{ij} c_{i\sigma}^{\dagger} c_{j\sigma'}^{\dagger} c_{j\sigma'} c_{i\sigma} \quad . \end{aligned} \tag{5.1}$$

We consider the nearest-neighbor Cu-O (t_{pd}) and O-O ($-t_{pp}$) hoppings for t_{ij}^{0}, Cu-site (ϵ_d) and O-site (ϵ_p) energies for e_i^0, with $2\Delta = \epsilon_p - \epsilon_d$, Cu-site ($U_d$) and O-site ($U_p$) repulsions for U_i, and the nearest-neighbor Cu-O repulsion (U_{pd}) for U_{ij}. The parameter set we use is $t_{pd} = 1$, $t_{pp} = 0.4$, $2\Delta = 2.2$, $U_d = 5$, $U_p = 2.1$, and $U_{pd} = .4$, which are almost in proportion to the values $t_{pd} = 1.47$eV, $t_{pp} = 0.61$eV, $2\Delta = 3.29$eV, $U_d = 7.42$eV, $U_p = 3.09$eV, and $U_{pd} = .41$eV derived from the constrained-density-functional approach for La_2CuO_4[18, 17]. We use this parameter set because it was successfully used by the same group that derived it, in homogeneous HF calculations[18] and because we intend to compare our results with $La_{2-x}Sr_xCuO_4$ for which abundant and good quality optical data are available.

Mean-field states were obtained by solving the unrestricted HF Hamiltonian with self-consistency conditions for on-site and nearest-neighbor, charge and spin densities without assumption on the form of these quantities. The self-consistency equations are obtained by minimizing the total energy with respect to these quantities which are treated as classical numbers. On a second step we perform an RPA analysis (see Appendix A)[38, 44, 45]. Here we take advantage of the fact that in the small doping regime the IHF Hamiltonian conserves the z component of the spin to reduce the large RPA matrix. In the heavily doped region where our results are more qualitative than quantitative we restrict ourselves

to the configurations that meet the above condition. We have not investigated restoration of translational symmetry. This is necessary for polaron band formation and transport but beyond the present RPA scope. Calculations were made on systems of 6×6 unit cells with periodic boundary condition.

5.1 Small doping regime

In Fig. 5.1(a) we show the density of states (DOS) in the HF approximation without doping. The one particle energy levels are broaden with a very narrow Lorentzian in order to resolve each single particle level. The arrows indicate the position of the highest occupied energy level for each spin orientation. The whole band structure can be understand by doing a "back of the envelop" calculation. We take a CuO_4 cluster. The Hamiltonian is:

$$\begin{aligned} H &= \sum_{j=1,\sigma}^{4} t_{pd}(d_\sigma^\dagger p_{j\sigma} + h.c.) \\ &\quad - \sum_{j=0,\sigma}^{4} t_{pp}(p_{j\sigma}^\dagger p_{j+1\sigma} + h.c.) \\ &\quad + \sum_\sigma \epsilon_d d_{i\sigma}^\dagger d_{i\sigma} + \sum_{j=1,\sigma}^{4} \epsilon_p p_{j\sigma}^\dagger p_{j\sigma} \\ &\quad + U_d d_\uparrow^\dagger d_\downarrow^\dagger d_\downarrow d_\uparrow + \sum_{j=1}^{4} U_p p_{j\uparrow}^\dagger p_{j\downarrow}^\dagger p_{j\downarrow} p_{j\uparrow} \\ &\quad + \sum_{j=1,\sigma,\sigma'}^{4} U_{pd} p_{j\sigma}^\dagger d_{\sigma'}^\dagger d_{\sigma'} p_{j\sigma} \quad . \end{aligned} \tag{5.2}$$

We decouple the many body terms in Hartree-Fock approximation and obtain the single particle Hamiltonians for up and down spin in the cluster respectively. We assume that the majority spin in the cluster is up. The single particle Hamiltonian can be easily diagonalized by defining the operators that create a particle as a linear combination of the

four O orbitals,

$$p_{m\sigma} = \frac{1}{2}\sum_{j=1}^{4} e^{imj\frac{\pi}{2}} p_{j\sigma}. \tag{5.3}$$

Here m can take the values $m = 0, \pm 1, 2$. The t_{pp} term splits the energy levels with

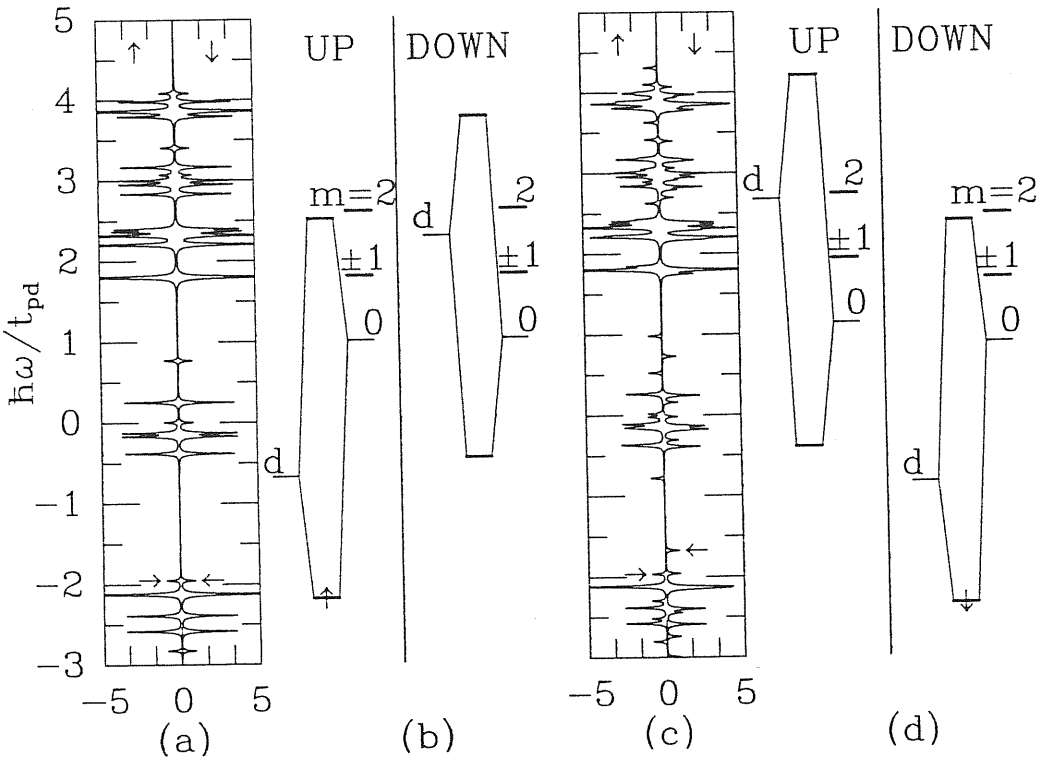

Figure 5.1: HF density of states and single particle energy levels of a CuO_4 cluster as explained in the text, for $x = 0$. The d labels the Cu energy levels whereas the O energy levels are labelled by the quantum number m. The horizontal arrows indicate the position of the highest occupied energy level for each spin orientation. (a) and (b) HF ground state, (c) and (d) spin flip state.

different $|m|$. The distance between levels is $2t_{pp}$. Only the state with $m = 0$ mixes with the Cu resulting in a 2×2 matrix. The energy levels for up and down spins are shown in Fig. 5.1(b). In practice we had inserted in the single particle Hamiltonians the energy levels of the 6×6 cluster rather than to solve again the HF equations. Each eigenstate of the CuO_4 single particle Hamiltonian corresponds to a band in the bulk. The bonding

state for ↑ spin corresponds to the lower Hubbard band. The antibonding state for ↓ spin corresponds to the upper Hubbard band. The antibonding state for ↑ spin lies very close to the $m = 2$ O level, so they repel each other a bit, and give rise to two bands of mainly O character. The $m = \pm 1$ levels give a large peak in the DOS corresponding to a purely O band. The lowest available energy level in the cluster has spin ↓ *opposite* to the spin of the central Cu. The important thing to notice is that the splitting between the two Hubbard bands is not the distance between the Cu levels (d in Fig. 5.1) i.e. $U_d\langle n_{d\uparrow} - n_{d\downarrow}\rangle$ with $n_{d\sigma}$ the Cu occupancy, but is much larger than that due to covalency. This effect is missing in a large U_d calculation and we believe it is of paramount importance in determining the doping states.

When a hole is added it forms a small polaron. In the above parameter set, each added hole is localized primarily on a single Cu site and four surrounding O sites (Fig. 5.2). The spin density at the central Cu site is in the opposite direction of the undoped case. Two HF eigenstates appear deeply inside the charge-transfer gap [Fig. 5.3(a)] per added hole. These states are occupied by holes and their associated HF wave functions are spatially localized. The higher one corresponds to an oxygen state formed by the four O that surround a Cu ($m = 0$) and has smaller weight on Cu. The lower one corresponds mainly to the central Cu, has opposite spin to the previous one, consistent with the cluster analysis, and has smaller weight on O. In a Zhang-Rice picture this many-body state mixes with a similar state in which the directions of the spins on Cu and O are reversed. Because such a correlated state cannot be constructed with a single Slater determinant, HF fails to describe it properly. However, we expect much of the energetics of the state to be captured at the unrestricted mean-field level.

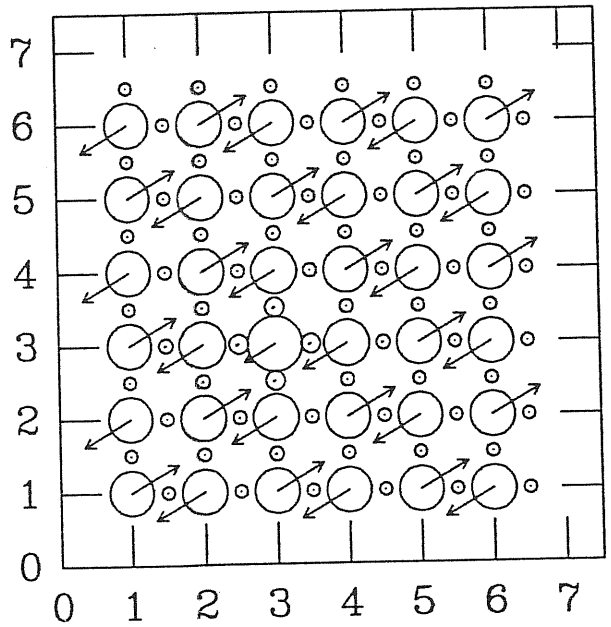

Figure 5.2: Hole charge (radius of the circles) and spin densities (arrows) for $x = 1/36$, with parameters[18, 17] appropriate for $La_{2-x}Sr_xCuO_4$. Big (small) circles correspond to Cu (O).

The formation of the polaron can be thought as a two step process. At the first step a spin is reversed without doping. We can obtain a metastable HF solution realizing such state (Fig. 5.4). The corresponding DOS is shown in Fig. 5.1(c). In Fig. 5.1(d) we show the energy levels obtained by replacing in the HF Hamiltonian of the small cluster the energy levels of the large system *on the site corresponding to the spin flip*. We see that there is little variation of the cluster energy levels with respect to the undoped case (apart from the trivial exchange of up levels with down levels). In particular it fails to explain the gap levels generated with the spin flip. The reason is that the appearance of these gap levels is a magnetic effect involving sites beyond the CuO_4 cluster. The highest occupied down level in Fig. 5.3 (c) corresponds to the flipped Cu spin. Since the orientation is parallel to the surrounding spins the removal energy in HF increases by a quantity of order $8J$

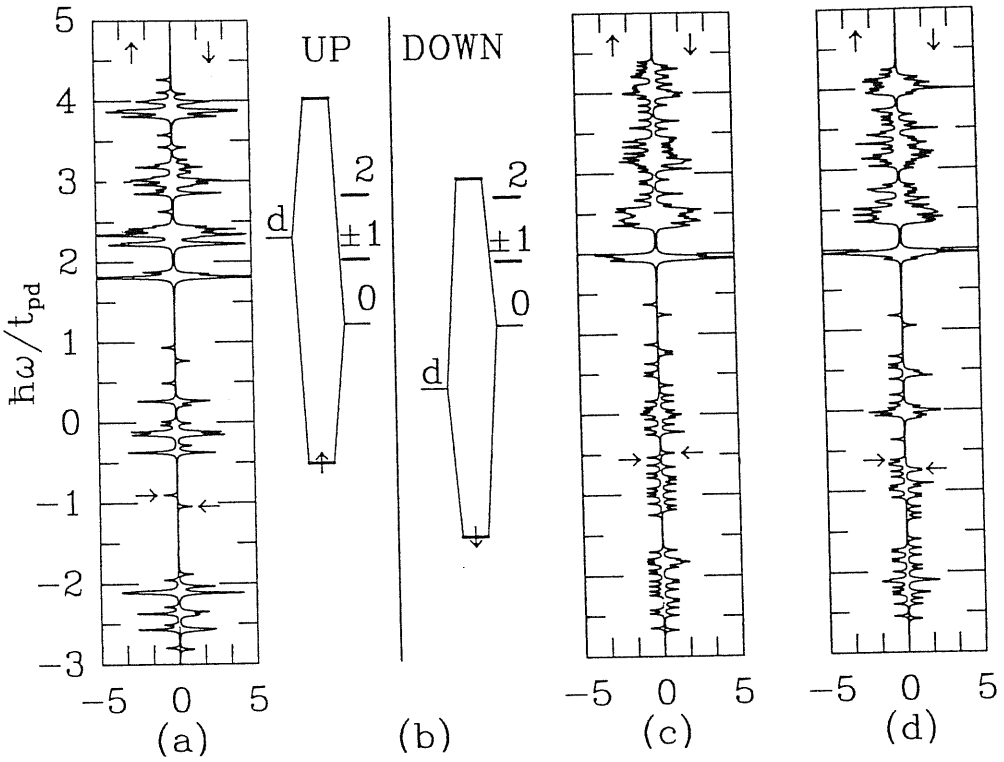

Figure 5.3: HF density of states and single particle energy levels of a CuO_4 cluster as explained in the text. The d labels the Cu energy levels whereas the O energy levels are labelled by the quantum number m. The horizontal arrows indicate the position of the highest occupied energy level for each spin orientation. (a) and (b) $x = 1/36$, (c) $x = 1/4$ (d) $x = 1/4$ (higher energy state).

with respect to the more favorable antiparallel orientation. Here J is the effective Cu-Cu superexchange interaction. This explains the shift of the level form the lower Hubbard band into the gap. On the other hand to add a particle on O in between two parallel Cu (without any further relaxation) is more favorable in energy by a quantity $2J_{CuO}$ provided the spin is antiparallel to the one on Cu. This explain the shift downward of the unoccupied level in the gap.

At the second step a particle is added to the first available level. If no further relaxation of charges were to occur, this would be a conventional small ferromagnetic polaron. In

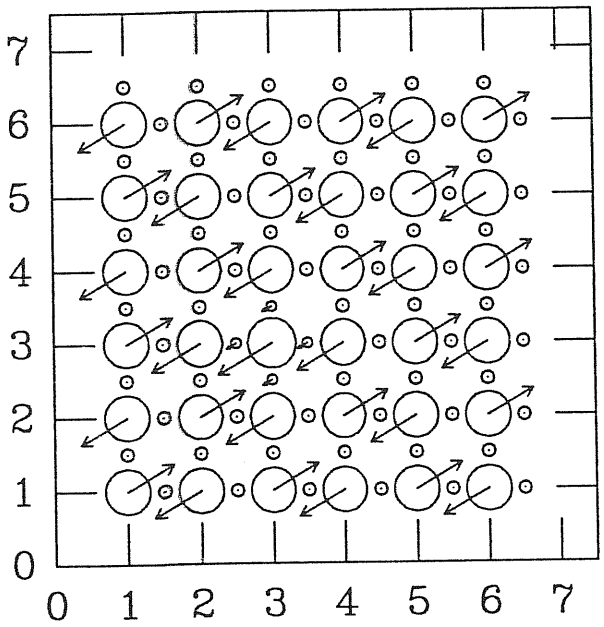

Figure 5.4: Hole charge (radius of the circles) and spin densities (arrows) for the spin flip metastable state at $x = 0$, with parameters[18, 17] appropriate for $La_{2-x}Sr_xCuO_4$. Big (small) circles correspond to Cu (O).

fact this is what one expects in the large U_d limit (in practice this does not happen since other, more extended states, with canting of the spins, began to compete[38]). However, when the strong mixing between Cu and O is taken into account, a different effect takes place. In Fig. 5.2 we show the resulting state. The first available level, due to the strong mixing has weight on the $\uparrow$ Cu spin state. Part of the added charge goes to the $\uparrow$ Cu spin state and this trough the renormalization of the $\downarrow$ Cu spin level ($U_d < n_{d\uparrow} >$) pushes up the corresponding $\downarrow$ state from the lower Hubbard band which becomes more mixed with O. As a result of this mixing the charge on the $\downarrow$ Cu site decreases, and the Cu $\uparrow$ spin level goes down due to the $U_d < n_{d\downarrow} >$ term and the added particle actually sits in the gap state resulting of the hybridization of the Cu$\uparrow$ spin and the $m = 0$ O state. This shifting of levels is illustrated in Fig. 5.3(b) where, as above, the local HF energy levels have been

inserted in the single particle Hamiltonian of the CuO_4 cluster. The actual shift of levels in Fig. 5.3(a) can be rationalized as a combined magnetic and covalent effect. In fact the total shift corresponds roughly to the sum of the shift observed in Fig. 5.1(c) for the spin flip plus the shift of the energy levels in the CuO_4 cluster. As we will show in the next section this movement of levels is fundamental to understand the optical conductivity of this material. In next chapter we will discuss how this effect, reinforced by the relaxation of the lattice and as a consequence, increase of hybridization, can produce a transition to a non magnetic state in the Cu signaled by both levels in the gap becoming degenerate. The closeness of the two higher occupied levels in Fig. 5.3(a) indicates that the system is close to that transition.

If the system is doped with an electron a small polaron is also formed: an interesting feature of these states is that the large shifts in the single particle energy levels toward the center of the gap result in similar levels positions for both the hole- and electron-doped cases, as found in spectroscopic experiments[46].

5.2 Optical conductivity of $La_{2-x}Sr_xCuO_4$ and soft electronic modes.

It is believed that the understanding of the normal state properties of the high temperature superconductors is a prerequisite to a description of the superconducting mechanism. Among these properties a striking one is the optical conductivity which has received recently theoretical[47]-[50] and experimental[4, 5, 6, 51] attention. At half filling the system is a charge transfer (CT) insulator with an onset of in-plane optical absorption[6, 52] at $\sim 2eV$ for $La_2Sr_xCuO_4$ corresponding to CT transitions between Cu and O in the plane. As the system is doped, spectral weight from the CT band is transferred to a mid infrared

(MIR) band initially at $\sim .5eV$. As doping increases the spectral weight transfer proceeds further and at the same time the MIR band merges with the Drude component. For doping $x > x_c \sim 1/4$ the electronic ground state seems to change and both the optical conductivity and other normal state properties like the Hall effect show a sudden change. The integrated optical conductivity also shows a peculiar behaviour. For $x < x_c$ all the curves cross in one point at $\sim 3eV$ indicating that all the spectral weight shifts occurs below this energy. In this section we calculate the optical conductivity in the inhomogeneous Hartree-Fock (IHF) plus RPA approach applied to the p-d model[21, 38, 44, 53]. Positions of the bands and relative intensities are obtained without free parameters in our calculations since the Hamiltonian is completely determined by constrained local density approximation (LDA) calculations[18, 17]. For the sake of simplicity we associate x, the concentration of Sr with the number of added holes in the Cu-O planes.

The following picture emerges. At half filling we obtain an onset of in-plane absorption in close agreement with experiments [Fig. 5.5] due to in plane Cu-O CT transitions. When a particle is added to our 6×6 unit cell system (extreme dilute limit) a polaron forms (see Fig. 5.2). As explained in the previous section the energy levels locally renormalize for $\uparrow$ and $\downarrow$ spins [Fig. 5.3(a)]. Then a level from the lower Hubbard band shifts into the gap. As a consequence, the corresponding Cu-O CT transition becomes a transition from the localized level in the gap, corresponding to the mixture of the central spin with the surrounding O, to an extended state above the gap and correspondingly an absorption band grows in the infrared as the CT band is eroded (Fig. 5.5). Its shape and position are quite similar to what is observed in photoinduced infrared absorption (inset of Fig. 5.5). The spectral weight will be discussed later. As the number of particles increases the polarons

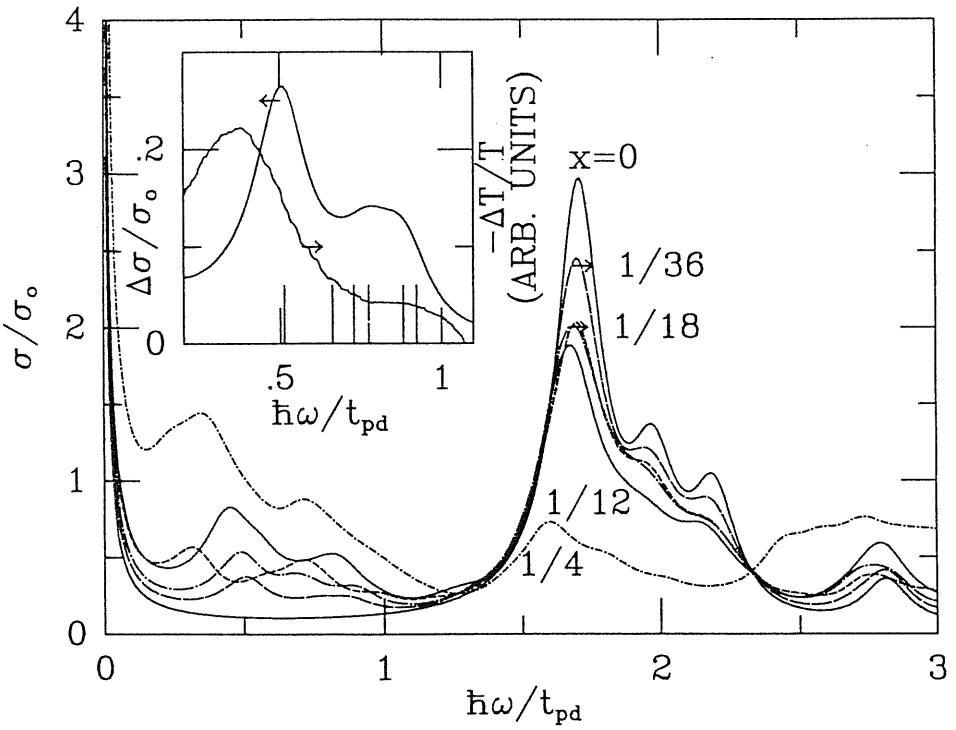

Figure 5.5: Optical conductivity of $La_{2-x}Sr_xCuO_4$ for different values of x. A Lorenzian broadening ($.1t_{pd}$) has been introduced. For the case of two polarons ($x = 1/18$) we show the case with one polaron siting in the second (fourth) neighbour Cu of the other with dash (dash doted) line. For $x = 1/4$ we show the curve corresponding to Fig. 5.7. The upturn at zero energy is due to the broadening. The actual position of the states can be deduced from Fig. 5.8. The inset shows the difference in the optical conductivity between the $x = 0$ case and the $x = 1/36$ case and the observed photoinduced change in transmission (T) (Adapted from Ref.[51]).

began to overlap and a region is reached in which many metastable HF configurations compete, with the polarons sitting in different relative positions. This is indicative of a strongly fluctuating regime where our approach is expected to be only qualitative. When the concentration of particles reaches $\sim x_c \sim 1/4$ the polarons overlap more strongly and the Fermi level is not any more at a single particle mean field localized level but it reaches an extended state. At the same time the magnetic moment in the Cu's belonging to the

polarons tend locally to collapse. We associate this with a sudden metallization of the system. In fact the Drude weight calculated in the HF approximation (D_{HF}) increases around that point (Fig. 5.9) indicating that the effective number of charge carriers has grown. In a calculation where the strongly fluctuation region is properly taken into account we expect the MIR precursor mode, which is connected with the delocalization of the Cu holes, to become a soft electronic mode and to merge with the Drude peak as in the experiments[6]. In Fig. 5.3(c) and (d) we show the HF DOS for $x = 1/4$ for the two studied configurations. Comparison with Fig. 5.3(a) shows the evolution from the dilute polaronic case to the nearly metallic case.

The method has already been described (see Appendix A). Here we take advantage of the fact that in the small doping regime the IHF Hamiltonian conserves the z component of the spin to reduce the large RPA matrix. In the heavily doped region where our results are more qualitative than quantitative we restrict ourselves to the configurations that meet the above condition.

At half filing HF has been shown to work quite well for magnetic insulators like La_2CuO_4 by Grant and McMahan[18]. We use the same parameters as theirs but we only keep the O in plane p_x, p_y orbitals pointing toward the Cu and the $d_{x^2-y^2}$ orbital. Since we are calculating the in-plane optical conductivity, we do not expect that out of plane orbitals change our results significantly. Our uniform HF band structure for $x = 0$ closely resembles theirs for the in-plane polarizations.

Our units of conductivity and spectral weight are determined by (see Appendix B),

$$\sigma_o = \frac{e^2}{4d_\perp \hbar \epsilon_b}, \tag{5.4}$$

$$N_o = \frac{2t_{pd} m_o a_{pd}}{\hbar^2 \epsilon_b}, \tag{5.5}$$

where $d_\perp$ is the distance between adjacent Cu-O planes, and a_{pd} and t_{pd} are the in-plane Cu-O distance and hopping integral, respectively. A screening constant (ϵ_b) related to all bound electrons not included in the Hamiltonian is introduced. It is the only unknown parameter. In principle it can be calculated from the LDA band structure. It only affects the overall intensity. We fix it by matching the experimental crossing point of the integrated optical conductivity[6] with our calculated result. We get $\epsilon_b = 1.3$. With this value and $d_\perp = 12.465$ bohrs, $a_{pd} = 3.606$ bohrs, we get $\sigma_o = 7.13 \times 10^2 (\Omega cm)^{-1}$, $N_o = 1.08$. For the rest of this section we set $\hbar = c = e = a_{pd} = 1$. In analogy with the exact result[48, 54], the real part of the optical conductivity at the RPA level is given by the sum of a regular (σ_{reg}) and a non-regular part (see Appendix B):

$$\sigma(\omega) = 2\pi D_{HF}\delta(\omega) + \sigma_{reg}, \tag{5.6}$$

$$\sigma_{reg} = \sigma_o \frac{\pi}{N} \sum_{\lambda \neq 0} \frac{|<0|j|\lambda>|^2}{E_\lambda - E_o} \delta[|\omega| - (E_\lambda - E_o)], \tag{5.7}$$

where the Hartree-Fock Drude weight (D_{HF}) is given by the quadratic change in the Hartree-Fock total energy due to a twist in the boundary conditions parameterized by a vector potential A[54, 48]

$$D_{HF} = \frac{N_o}{2N} \frac{\partial^2 E_{HF}}{\partial A^2} \tag{5.8}$$

and can be calculated in terms of the RPA matrix elements of the paramagnetic current operator ($<0|j|\lambda>$), the RPA excitation energies (E_λ) and the expectation values in the HF ground state ($|HF>$):

$$D_{HF} = \frac{N_o}{N}[-\frac{1}{2}\sum_s t_s x_s^2 <HF|\frac{\partial H}{\partial t_s}|HF> - \sum_{\lambda \neq 0} \frac{|<0|j|\lambda>|^2}{E_\lambda - E_o}]. \tag{5.9}$$

Here N is the number of unit cells in the Cu-O plane. s labels all different kinds of bonds. t_s and x_s are the hopping matrix elements of the bond and the difference of the

x coordinates of atoms in the bond, respectively. Bonds with t_s different from zero are Cu-O nearest neighbours ($t_s = t_{pd}$) and O-O nearest neighbours ($t_s = -t_{pp}$). Within the present approximation the f-sum rule[48, 54] is exactly satisfied[55].

In Fig. 5.2 we showed the one particle IHF doped case ($x = 1/36$). Its feature has already been described in the previous section. Here we stress again the local reduction of magnetic moment on Cu due to the enhanced covalency not found in large onsite U_d calculations. It will be shown[38] in the next chapter that this enhanced covalency couples strongly with the Cu-O phonon stretching mode (among others) and gives rise to doping induced side phonon bands in infrared spectra (IR). Here for simplicity we do not include such lattice effects. The IR absorption due to phonons is not expected at the energies we are interested, however small changes in the electronic bands can be found due to relaxation of the lattice.

Fig. 5.5 shows the optical conductivity. At half filling the CT band peaks at $1.7t_{pd}$ (2.5eV) whereas recent measurements[52] show a peak at 2.25 eV. The sharp decrease at higher energy is also in agreement with the lower temperature measurements of Ref.[52]. They also observe a small shoulder at lower energies. We have also some modes in that energy region but they are not IR active.

In the inset of Fig. 5.5 we show the difference between the optical conductivity at half filling and that for the one particle doped case in the MIR region. For comparison we also show the experimental photoinduced optical absorption[51] spectra. Given the uncertainty in the Hamiltonian parameters[17], the agreement for shape and position is quite good. The main peak is due to the transition from the $\downarrow$ level in the gap to the first available level with the same spin (extended state) above the Fermi level. The tail, also observed

in experiments is due to transitions to higher excited levels all renormailzed by RPA.

For two added holes we find a strong dependence of the MIR structure on the distance between the self-trapped states in the HF solution. For the weakly overlapped case (one polaron sitting on the second nearest neighbour Cu of the other) we find lower IR modes than for longer distances (Fig 5.5). The lowest-energy two-polaron HF state correspond to one polaron sitting on the fourth neighbour Cu of the other. Since the total energy depends weakly on the distance of the particle (except for strong overlap), in a calculation that takes into account the mixing between the different HF configurations we expect a substantial broadening of the structure. As the number of particles increases, the number of metastable HF configurations increases as well. In such conditions our approach is not expected to work well since RPA is a theory of small amplitude oscillations around some IHF state but the metastable states are indicative of the presence of many Slater determinants in the ground states that can not be connected by small displacements (i.e. a few particle-hole excitations). Furthermore, the Hartree-Fock ground state for each filling tend to be a polaron lattice commensurate with our system size Fig. 5.6. This makes the Hartree-Fock state for one particular configuration (the commensurate one) to be pinned more than the others and hence lower in energy, but this is clearly a finite size effect since different sizes have different periodic configurations and all of them should be important in the true ground state (except, perhaps, for the mysterious $x = 1/8$ T_c dip[56]). We believe this effect underestimates the softening of the state and makes the lower RPA modes to produce a narrow peak and lay at a higher energy than what we expect on physical grounds. Instead, if quantum fluctuation were fully taken into account, we expect that the above discussed "configurational" broadening will distribute that intensity over a much wider

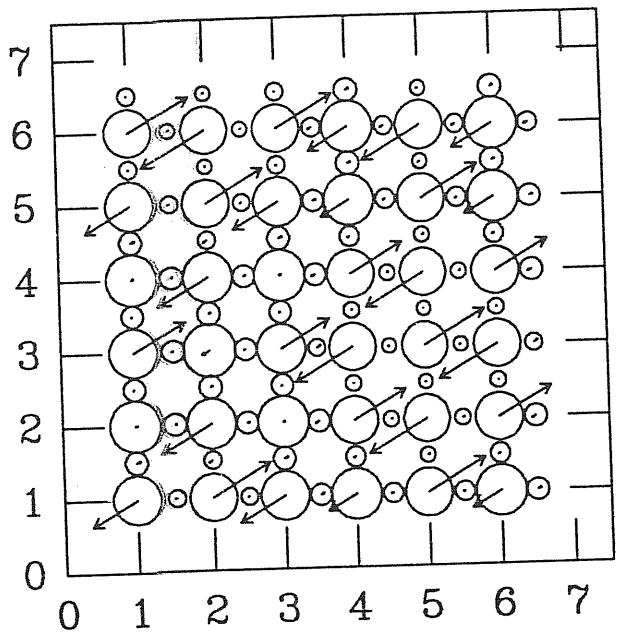

Figure 5.6: Hole charge (radius of the circles) and spin densities (arrows) for $x = 1/4$ (lower energy state), with parameters[18, 17] appropriate for $La_{2-x}Sr_xCuO_4$. Big (small) circles correspond to Cu (O).

range of frequency. We expect, the higher the doping, the broader is the structure in the MIR. For nine holes ($x = 1/4$) we show the optical conductivity (Fig.5.5) corresponding to a "disordered" configuration [Fig. 5.7] which tend to have lower energy modes in the MIR than the slightly more stable ordered one [Fig. 5.6] and a much broaded spectra.

Since for energies higher than the MIR and $x < x_c$ the results are not so much configurationally dependent we believe that some qualitative understanding can be gained from our calculations in that strongly fluctuating region and in fact we still found some agreement with experiments for the optical conductivity and the integrated optical conductivity (N_{eff}) at energies higher than the MIR. Note that all curves cross at $\sim \omega_{iso} = 1.25t_{pd}$ ($\sim 1.8eV$) in Fig. 5.5. A similar isosbestic point is observed[6] at ($\sim 1.5eV$). Another peculiar point is located at $\sim 2.3t_{pd}$ ($\sim 3.4eV$) where all the integrated conductivity curves

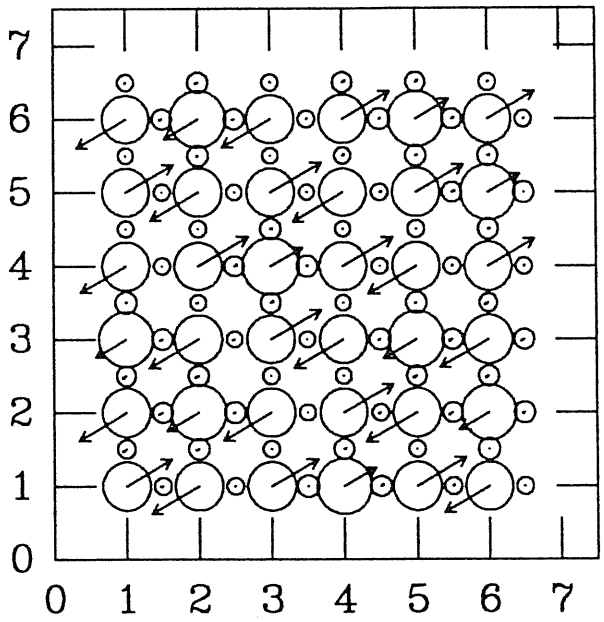

Figure 5.7: Hole charge (radius of the circles) and spin densities (arrows) for $x = 1/4$ (higher energy state), with parameters[18, 17] appropriate for $La_{2-x}Sr_xCuO_4$. Big (small) circles correspond to Cu (O).

(Fig. 5.8) with $x < x_c$ tend to converge in agreement with the analogous experimental point mentioned in the introduction. For $x > x_c$ the curves pass above the crossing point instead of below like in experiments. This is probably because the spectral weight transferred to the MIR becomes so broad in the experiment that the range of frequencies over which it is distributed reaches $\sim 2.3t_{pd}$ and it does not make any more sense to distinguish low energy and high energy features. Since we are not considering such strong damping of the modes, which should come from the explained configurational broadering, we probably overestimated the weight at low frequencies and give a too big integrated spectral weight at the crossing point.

Due to the depletion of the optical conductivity at ω_{iso} the integrated optical conductivity for theory and experiment show a plateau in that region for small doping. In Fig. 5.9

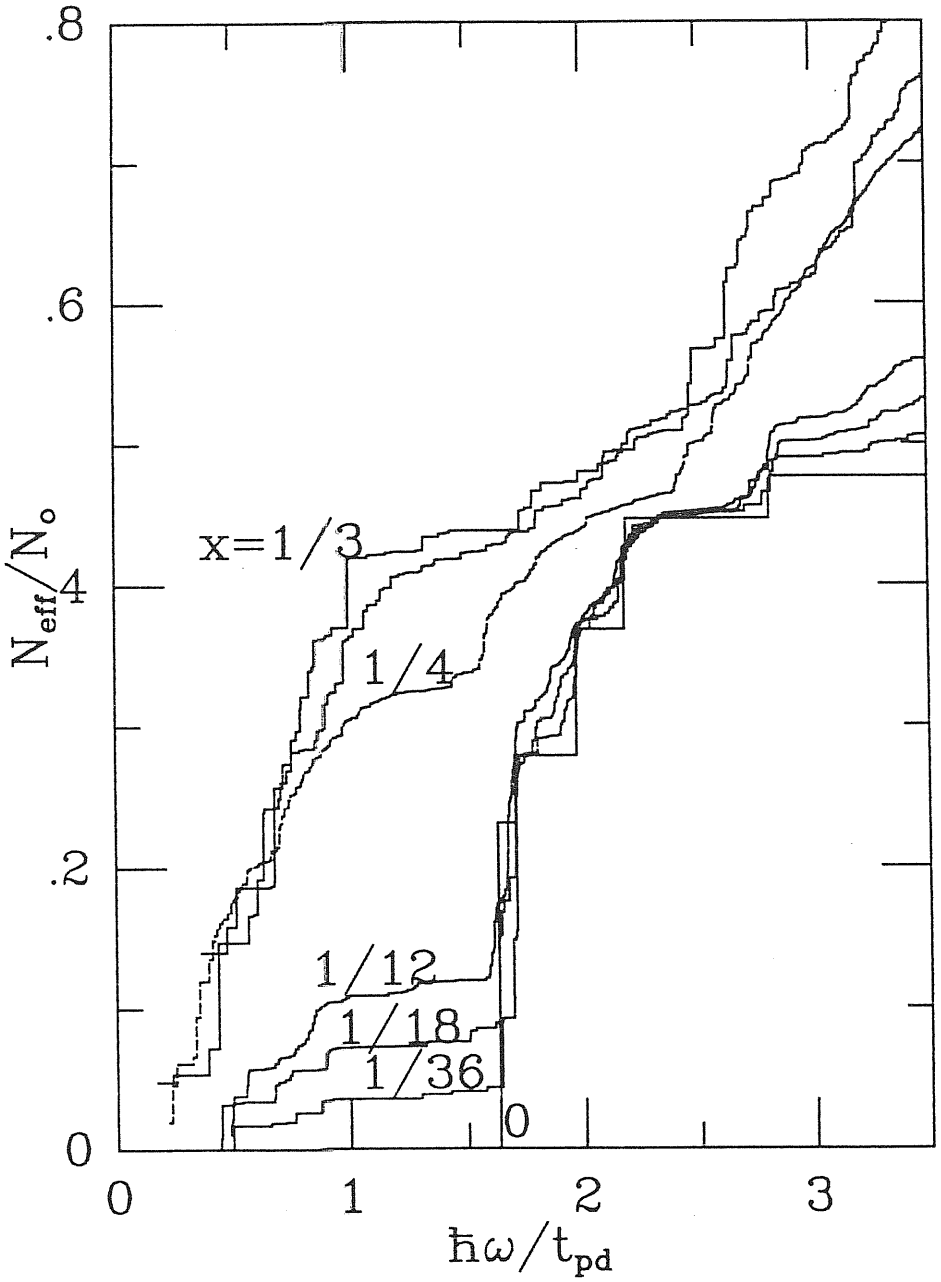

Figure 5.8: Integrated optical conductivity of $La_{2-x}Sr_xCuO_4$ for different values of x. For $x = 1/4$ we show the case corresponding to Fig. 3.3(c) with dashed line. Open symbols correspond to metastable states.

we show the integrated conductivity (N_{eff}) up to ω_{iso} as a function of x. This measures the spectral weight transferred to the MIR upon doping (Lorentzian broadening is not included here). For $x < .1$ the curve is nearly parallel to the experimental one. At $x = 0$ the experiments extrapolate to a non-zero value. This is because a long tail from the CT band, reaches the MIR region and can be assigned to disorder since the tail is very much suppressed in Ref.[52]. If the experimental curve is shifted down by that amount then the two curves lay on top of each other for small x. This shows that the spectral weight of the MIR band is obtained in agreement with the experiments without free parameters. For $x > .1$ probably the same configurational broadering effect occur, that is, the structure in the MIR becomes so broad that it's tail reaches ω_{iso}. This explains the deviation from linearity of the experimental curve as opposed to the theoretical one. When the polarons began to overlap around x_c there is a saturation of the theoretical curve qualitatively consistent with the saturation observed in experiments.

We also show in Fig. 5.9 D_{HF} as function of x. For $x = 0$ the value is very small. It should go to zero as $\sim exp(-\sqrt{N}/\xi_{HF})$ in the thermodynamic limit in analogy with the discussion of Ref. [49]. ξ_{HF} is a localization length in the HF approximation. When a particle is added ξ_{HF} remains finite since the added particle is self-trapped and due to that D_{HF} is still expected to be zero in the thermodynamic limit. The non zero values of D_{HF} for small x are clearly a finite size effect. The fact that ξ_{HF} remains finite does not mean that the system is really an insulator since there exist many HF solutions with polarons sitting in different cells with the same HF energy. Tunneling between the different solutions should recover translational invariance in the ground state. Unfortunately, such processes are beyond RPA since this approximation can only explore the immediate positive curved

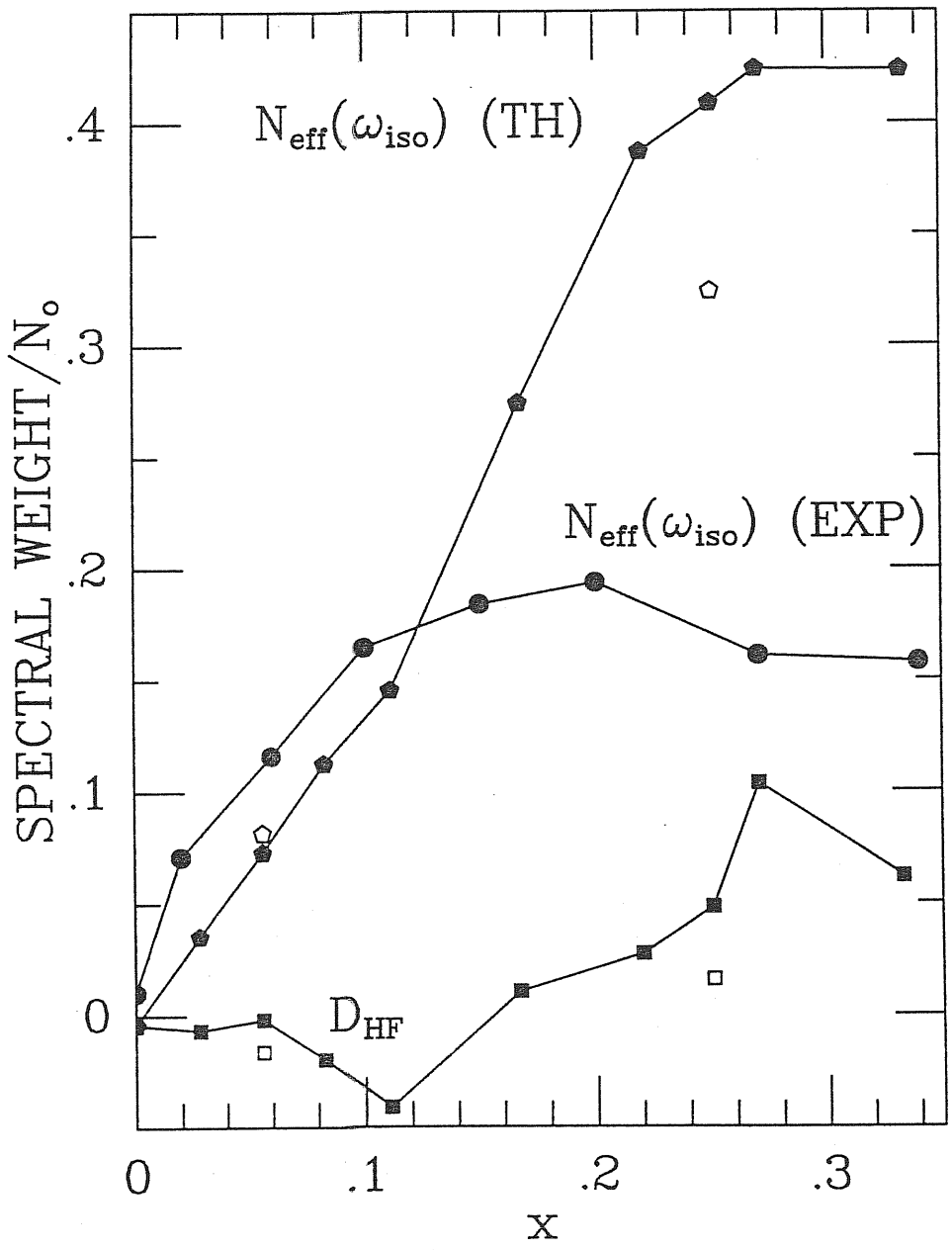

Figure 5.9: Experimental[6] (EXP) and theoretical (TH) integrated conductivity up to the isosbestic point $[N_{eff}(\omega_{iso})]$ and D_{HF} as a function of x.

vicinity of one solution and not the barrier between them. Such tunneling process should give a small Drude weight in the thermodynamic limit as seen in experiments. When x_c is reached the Fermi level reaches an extended state and D_{HF} increases. At the same time the HF solutions tend to show collapsed magnetic moments. (However, magnetic spatial "fluctuations" are found well above x_c, and mobile holes are expected to screen them at low energies). Qualitatively we associate that with a metallization of the system and a sudden increase of the number of charge carriers. This indicates that the Cu holes delocalize and began to participate in the transport. Since the frequency of the MIR precursor in the extreme dilute limit is determined by the excitation energy to delocalize the original Cu hole we expect it to become a soft electronic mode near x_c and merge with the Drude component. Such low energy excitations are completely unconventional in a Fermi liquid and we postulate that they are responsible of the possible non-Fermi liquid behaviour. How in detail, our MIR band precursor evolves into an object of the kind of the marginal Fermi liquid phenomenology[57], deserves more theoretical work. However, we expect the configurational broadening effects discussed here will give some clues.

It is interesting to compare our results with what was found in a simplified model[45] showing self-trapping. There, as one parameter was varied it was possible to continuously reach a pseudo phase transition at the HF level in which a polaronic solution becomes uniform (see Chapter 3). The transition was signaled by an RPA mode going to zero frequency.

Our results restrict to the in-plane conductivity. However, we speculate that the out of plane DC conductivity should be strongly suppressed by large Huang-Rhys factors[58] for $x < x_c$. This will result in a partial "confinement" for $x < x_c$ disappearing for $x > x_c$

where the polaronic character is lost.

Another interesting possibility is that this soft electronic modes are the ghost bosons that particles interchange to produce Cooper pairs. We expect that as x_c is approached fluctuations to the metallic phase make the number of effective carriers increase and at the same time the characteristic frequency of the boson to go down. This is what one needs to get a strong dependence of T_c on x.

To conclude we have calculated the optical conductivity of $La_{2-x}Sr_xCuO_4$ for different values of x. For low and zero x we found good agreement with experiments for band positions and relatives intensities *without* free parameters. We identified the precursor of the MIR band and found a transition at the mean field level from a polaronic phase to a metallic phase near the point where a sudden change in transport and optical properties is observed. We argue that near the transition the MIR precursor modes should become soft electronic modes and probably can be related to the breakdown of Fermi liquid behaviour. Our results show also that the method, at least in the small doping regime is an appropriate bridge between first principle calculations and experiments.

Chapter 6

Lattice effects

In this chapter we consider the effects of relaxing the lattice around the polarons. Polaronic effects of the kind considered in the previous chapter and here have been invoked[59, 60, 61, 62, 63] to explain experimental results like optical spectroscopy[64, 65], photoinduced optical absorption[3, 4], transport[66] and photoemission[67, 68], among others. For a complete review on polaron and bipolaron theory see Refs.[69, 70]. The photoinduced optical absorption experiments by Kim et al.[4] and Taliani et al.[2] show the importance of localized states in the gap combined with lattice effects. The latter shows that they are common features in both Cu and non-magnetic Bi-based high temperature superconductors.

Considerable modeling of high-temperature superconductors has focused on the identification of hole doping states (spin bags, polarons, excitons) defined with respect to stoichiometric antiferromagnetic (AF) two-dimensional (2-d) Cu-O ground states. Here, we demonstrate that the nature of doping states and their interactions can indeed go beyond a pure 2-d, 1-band Hubbard model. Doping states in a two-dimensional three-band Peierls-Hubbard model are investigated with inhomogeneous Hartree-Fock[38]. We repro-

duce adiabatic random phase approximations (ARPA) calculations performed by Kenji Yonemitsu[38]. Unlike the calculation of the previous section these results are valid only in the phonon frequency range. We find that a moderate intersite electron-lattice coupling strength triggers a rapid cross-over from a small polaron with well formed moment on Cu to a local collapse of the Cu magnetic moment and strong local lattice distortion in the AF background[see Fig.6.1(a)]. This can be viewed as a transition from a Zhang-Rice singlet[71] to a covalent molecular state. For sufficiently strong electron-lattice coupling the ground state changes completely to a nonmagnetic bond-order or charge-density-wave state. Large Cu-O Coulomb nearest neighbor repulsion drives phase separation. The various doping states produce distinct infrared optical absorption spectra, relevant to chemical[5] and photodoping experiments[4, 2].

We have used a Hartree-Fock (HF) technique for the electronic part, totally unrestricted in both spin *and* direct space[21, 37, 38] and a classical treatment for the lattice part. Infrared-active (IR) phonon modes were calculated by adding a similarly inhomogeneous RPA analysis of linear fluctuations.

The general model Hamiltonian we consider is:

$$\begin{aligned} H &= \sum_{i\neq j,\sigma} t_{ij}(\{u_k\})c^\dagger_{i\sigma}c_{j\sigma} + \sum_{i,\sigma} e_i(\{u_k\})c^\dagger_{i\sigma}c_{i\sigma} \\ &\quad + \sum_i U_i c^\dagger_{i\uparrow}c^\dagger_{i\downarrow}c_{i\downarrow}c_{i\uparrow} + \sum_{\langle i\neq j\rangle,\sigma,\sigma'} U_{ij}c^\dagger_{i\sigma}c^\dagger_{j\sigma'}c_{j\sigma'}c_{i\sigma} \\ &\quad + \sum_l \frac{1}{2M_l}p_l^2 + \sum_{k,l}\frac{1}{2}K_{kl}u_k u_l \quad . \end{aligned} \tag{6.1}$$

Here, $c^\dagger_{i\sigma}$ creates a *hole* with spin σ at site i in the Cu $d_{x^2-y^2}$ or the O $p_{x,y}$ orbital. For the lattice part, we study only the motion of O ions along the Cu-O bonds and assume that only diagonal components of the spring-constant matrix are finite, $K_{kl} = \delta_{k,l}K$,

for simplicity. For electron-lattice coupling, we assume that the nearest-neighbor Cu-O hopping is modified by the O-ion displacement u_k as $t_{ij} = t_{pd} \pm \alpha u_k$, where the + (−) applies if the bond shrinks (stretches) with positive u_k. The Cu-site energy is assumed to be modulated by the displacements of the O ions u_k linearly as $e_i = \epsilon_d + \beta \sum_k' \pm u_k$, where the sum extends over the four surrounding O ions; here the sign takes + (−) if the bond becomes longer (shorter) with positive u_k. The other electronic matrix elements are: O-O hopping $(-t_{pp})$ for t_{ij}, O-site energy (ϵ_p) for e_i, with $2\Delta = \epsilon_p - \epsilon_d$, Cu-site (U_d) and O-site (U_p) repulsions for U_i, and the nearest-neighbor Cu-O repulsion (U_{pd}) for U_{ij}. Parameter values are used in regimes relevant to oxide superconductors. We have taken $t_{pd} = 1$, $t_{pp} = 0.5$, $2\Delta = 3$, $U_d = 8$, $U_p = 3$, $U_{pd} = 1$. (This parameter set is taken from constrained LDA calculations[16]). The above defined parameters and $\lambda_\alpha = \lambda_\beta = 0$ are hereafter termed the reference parameter set: $\lambda_\alpha = \alpha^2/(Kt_{pd})$, $\lambda_\beta = \beta^2/(Kt_{pd})$. We vary λ_α and λ_β. Comparison of our results for local lattice distortion and Cu reduced magnetic moments accompanied by added holes with generalized, inhomogeneous LDA calculations[19] is consistent, e.g., with values of $\lambda_\alpha = 0.28$, $\lambda_\beta = 0$ and $K = 32t_{pd}/\mathring{A}^2$.

Mean-field states were obtained by solving the unrestricted HF Hamiltonian with self-consistency conditions for on-site and nearest-neighbor, charge and spin densities as well as lattice displacements, without assumption on the form of these quantities. The self-consistency equations are obtained by minimizing the total energy with respect to these quantities which are treated as classical numbers. The kinetic part of the lattice is incorporated with particle-hole excitations later into the ARPA analysis. We have not investigated restoration of translational symmetry. This is necessary for polaron band formation and transport but beyond the present ARPA scope. Calculations were made on systems of

6×6 unit cells with periodic boundary condition.

6.1 Transition from a Zhang-Rice singlet state to a covalent molecular singlet state

For the reference parameter set, each added hole forms a small polaron like in the previous chapter. The spin density at the central Cu site is in a direction opposite to the undoped case. The spin densities at the four O sites are small and have an opposite direction to that at the central Cu site. As λ_α is turned on, the Cu magnetic moment is reduced and the O ions displace toward the central Cu. From the HF single particle levels two are located deeply inside the gap [Fig. 6.1 (b)] and are well localized: the higher one corresponds to an oxygen state formed by the four O that surround a Cu and has smaller weight on Cu. The lower one corresponds mainly to the central Cu, has opposite spin to the previous one, and has smaller weight on O.

Once the added hole is localized around a Cu with a reversed spin, the mechanism of the previous chapter is set up. The lower level in the gap [dashed line in Fig.6.1 (b)] results from the mixing of the $\downarrow$ level and the O, $m = 0$, $\downarrow$ level of the previous chapter. The higher the Cu $\downarrow$ level shifts, the bigger the mixing. This reduces the amount of charge in the Cu $\downarrow$ orbital pulling down the state originally at $\sim \epsilon_d + U_d\langle n_{d\downarrow}\rangle$. The upper level in the gap results from the mixing of this state with the O $\uparrow$ level [solid line in Fig.6.1 (b)]. Clearly this process feeds back positively. The $\uparrow$ level on the O mixes more and more with the $\uparrow$ level on the Cu, generating even more double occupancy and the two levels on the Cu approach each other as do the two levels in the gap.

The interplay with the lattice is also important. The strong mixing of the four surrounding O with the central Cu allows the state to gain energy if the O approach ($\lambda_\alpha \neq 0$)

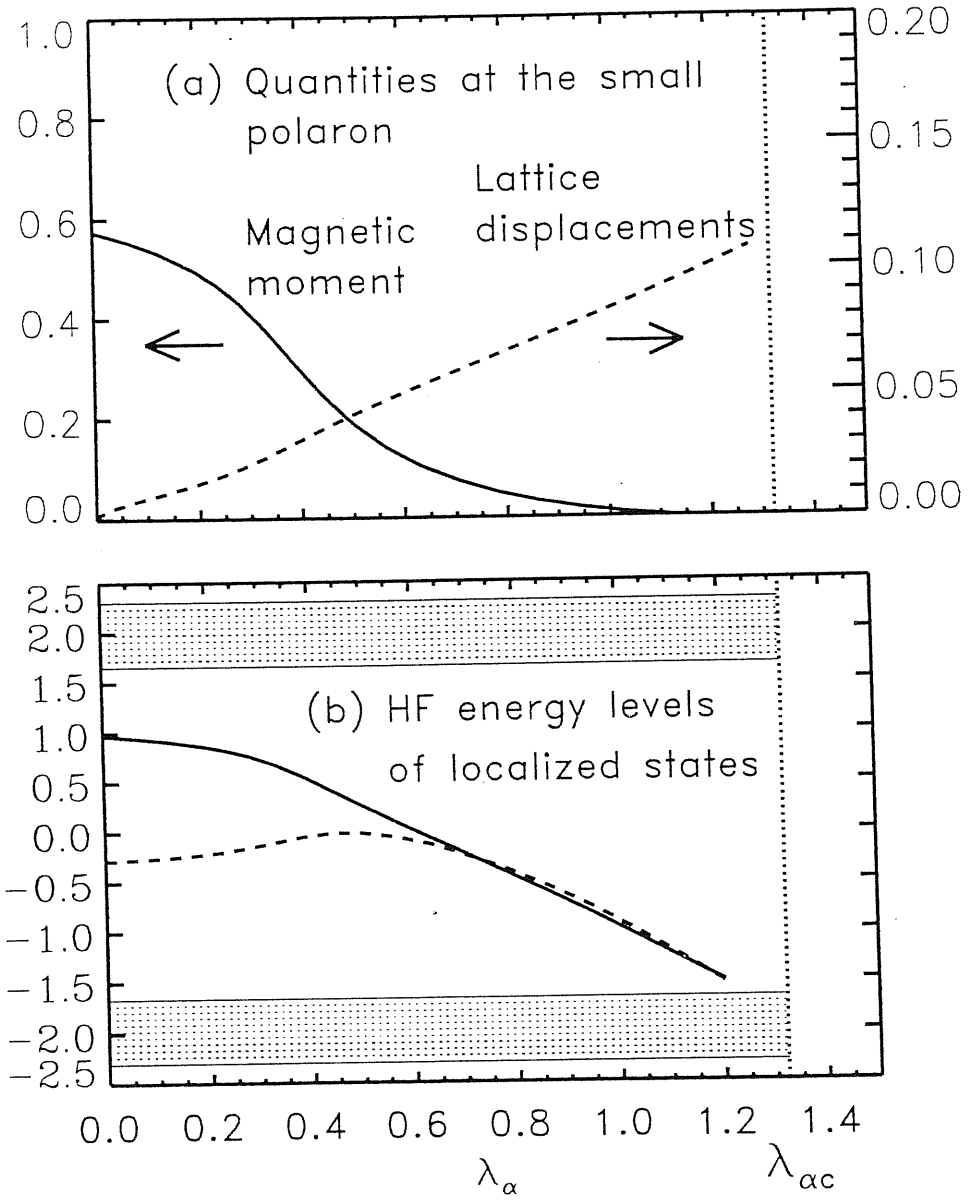

Figure 6.1: (a) Magnetic moment on the central Cu site and ratio of the displacement of the surrounding O atoms to the Cu-O distance (1.89Å), and (b) gap energy levels, for the small polaron state as functions of λ_α. Other energy levels in the gap close to the bands (shaded areas) are not shown. Parameters are $t_{pd} = 1$, $t_{pp} = 0.5$, $2\Delta = 3$, $U_d = 8$, $U_p = 3$, $U_{pd} = 1$, $\lambda_\beta = 0$, and $K = 32t_{pd}/\mathring{A}^2$.

experiments[46].

If λ_α is increased even more, covalency is locally enhanced and correspondingly the two levels in the gap go down. Above a critical value $\lambda_{\alpha c}$ the *undoped* ground state is replaced by a nonmagnetic bond-order-wave state.

Note that the strong local effects of intersite electron-lattice coupling upon doping occur in a regime extending significantly below $\lambda_{\alpha c}$ (see Fig.6.1).

The effect of finite λ_β is very weak up to a certain critical value ($\lambda_{\beta c} \simeq 1.0$) at which the ground state changes to a charge-density-wave state (Fig. 6.3).

In contrast to Fig.6.1 the Cu magnetic moment remains almost constant for $\lambda_\beta < \lambda_{\beta c}$. If $(U_d, 2\Delta)$ is increased from (8,3) to (10,4) the $\lambda_{\alpha c}$, $\lambda_{\beta c}$ and the cross-over λ_α are rescaled towards higher values by a ratio of 10/8 showing that U_d fixes the energy scale for the different λ's.

Large values of U_{pd} produce phase separation as found in Chapter 4.

In Fig.6.4 we show IR optical absorption spectra obtained from the current-current correlation functions. To evaluate the IR optical absorption spectra, the adiabatic approximation in the RPA[72, 38] was used, where quadratic and higher order terms with respect to frequency are neglected in the RPA electronic bubble. In the phonon-frequency range, including the IR range, this approximation is expected to work well, as is supported by comparison with nonadiabatic inhomogeneous RPA results on small systems. With $K = 32t_{pd}/\mathring{A}^2$, bare phonons ($\lambda_\alpha = \lambda_\beta = 0$) oscillate with $\omega = 0.0914$. For $t_{pd} = 1.3eV$ this corresponds to $840cm^{-1}$ which is comparable with the in-plane stretching IR active mode found in La_2CuO_4 ($706cm^{-1}$)[4, 2]. As the electron-lattice coupling λ_α increases, phonons are further softened and the theoretical peak approaches the experimental one.

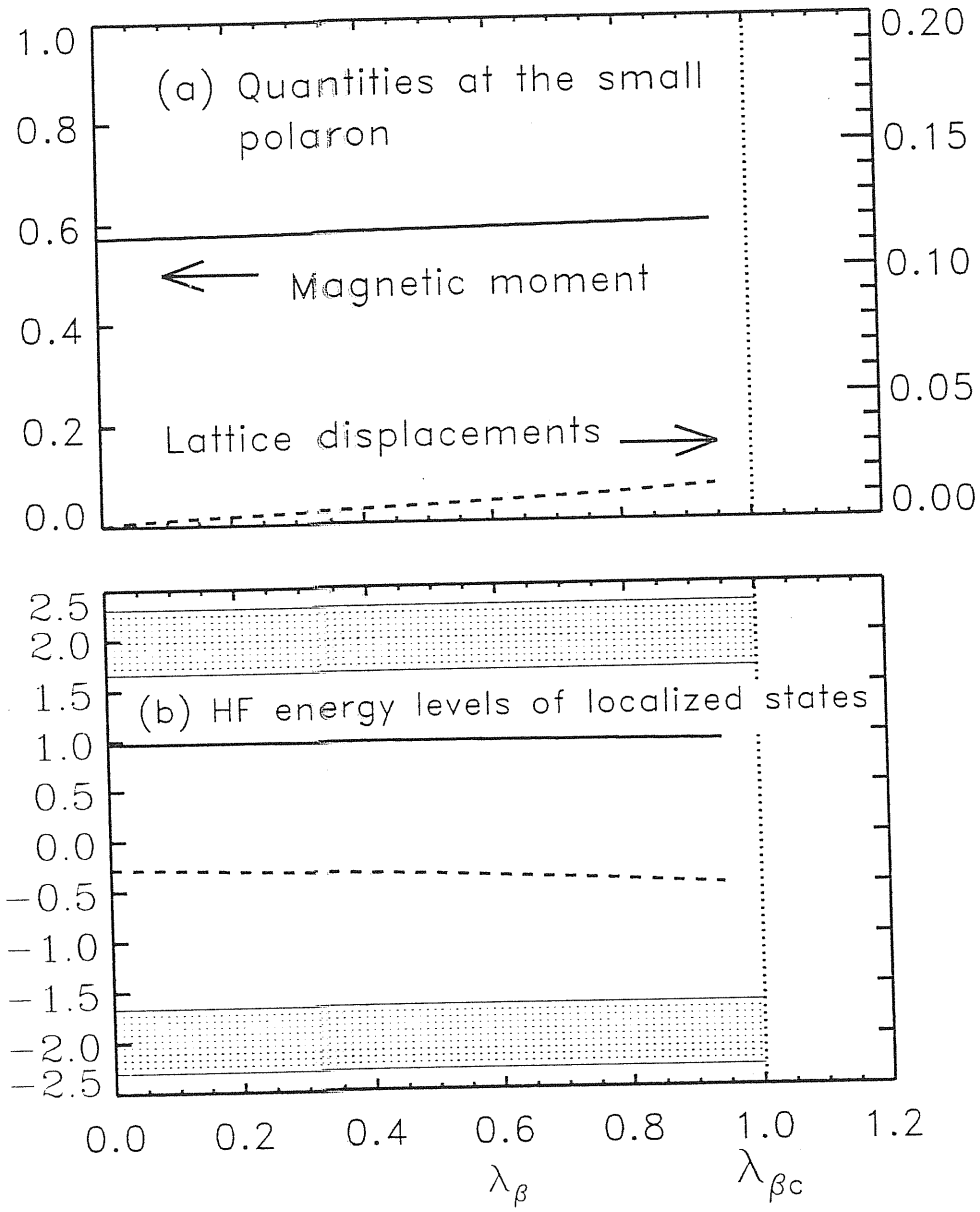

Figure 6.3: (a) Magnetic moment on the central Cu site and ratio of the displacement of the surrounding O atoms to the Cu-O distance (1.89Å), and (b) gap energy levels, for the small polaron state as functions of λ_β. The symbols and the parameters are the same as in Fig. 6.1 except for finite λ_β and $\lambda_\alpha = 0$.

The delta peaks have been broadened with Lorentzians of width 10^{-3}.

For $\lambda_\alpha = 0.125$, the peak ($\omega = 0.088$) is mainly due to extended modes which oscillate O atoms almost uniformly in the x or y direction but weakly around the small polaron (Fig. 6.4(a)). There are local IR active phonon modes ($\omega = 0.086$) corresponding to the antisymmetric oscillations of pairs of O atoms in the small polaron. There is another type of IR active phonon modes (also at $\omega = 0.088$) which are extended in the direction of oscillation and localized in the other direction so that we term them semilocal modes. But both the local and semilocal modes are indistinguishable in the IR absorption spectra, hidden by the broadening of the extended modes.

For $\lambda_\alpha = 0.500$, a doping-induced peak due to the local IR active phonon modes ($\omega = 0.071$) (652 cm^{-1}) is well split from the main peak due to the extended ones ($\omega = 0.076$) (698 cm^{-1}) and clearly visible (Fig. 6.4(b)). The semilocal modes ($\omega = 0.075$) are still indistinguishable in the spectrum from the extended modes.

This spectrum is consistent with the experimentally observed[4, 2] bleaching of phonon modes and intensity shift to lower frequencies following photoexcitation. Such "finger-print" of the polarons are clearly seen in the present compound by photoinduced IR absorption[4] as a bleaching of the $710cm^{-1}$ mode and growth of a side band at $640cm^{-1}$ and have received recent experimental attention in the chemically doped case[5], where a one-to-one correspondence of this effect with the photoinduced doping can be seen. Also observed in the same experiments is a bleaching of the interband electronic absorption and the corresponding activation of an electronic absorption in the gap, which we can associate with the results of the previous chapter as shown in the inset of Fig. 5.5.

For $\lambda_\alpha = 1.125$, both peaks due to the local modes ($\omega = 0.045$) and the semilocal

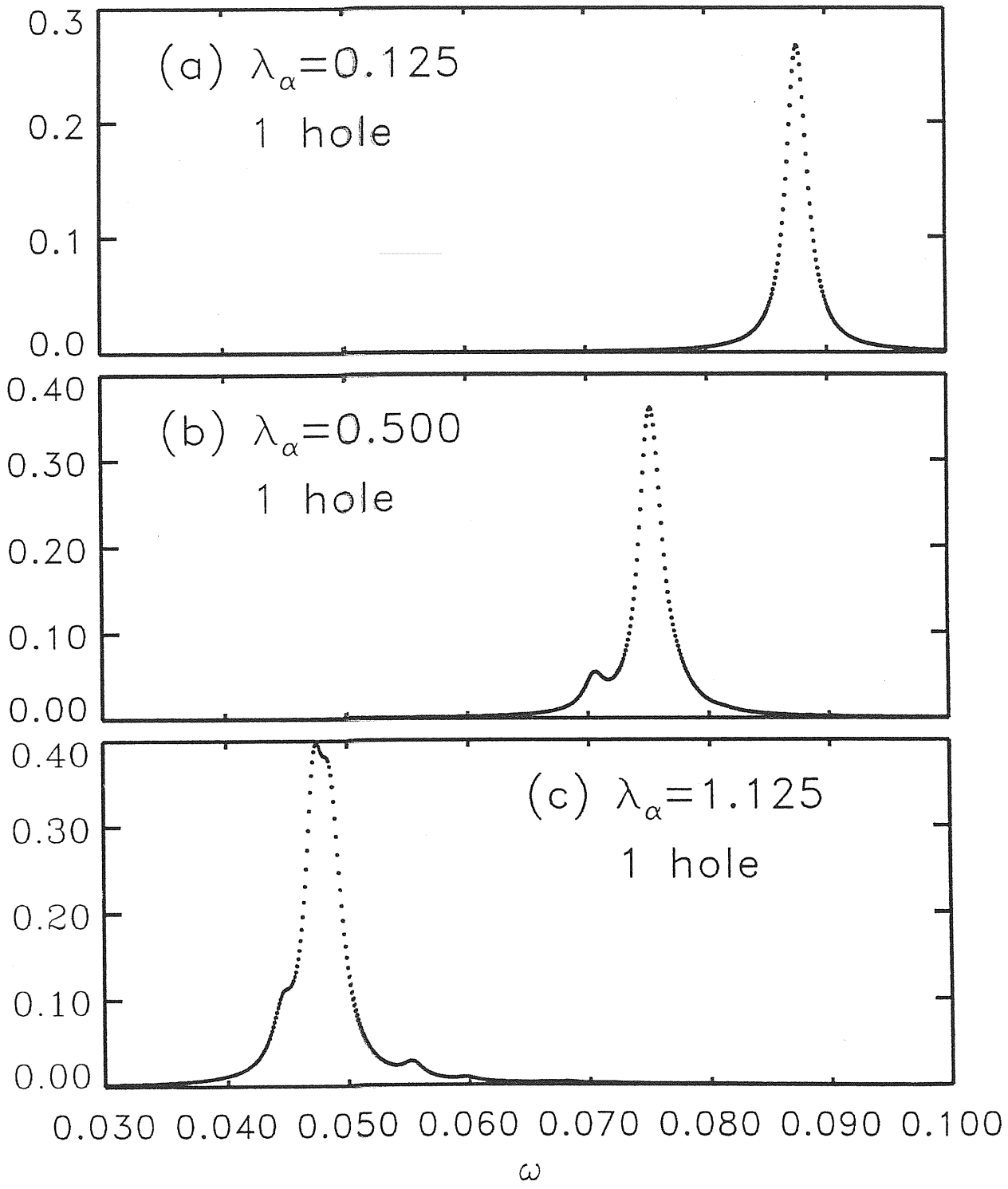

Figure 6.4: IR absorption spectra for the one-hole doped systems with a small polaron. (a) $\lambda_\alpha = 0.125$; (b) $\lambda_\alpha = 0.500$; and (c) $\lambda_\alpha = 1.125$. The other parameters are as in Fig. 6.1.

modes ($\omega = 0.047$) are split from the peak coming from the extended modes ($\omega = 0.049$) (Fig. 6.4(c)). Here the oscillator strength of the semilocal modes is the largest and those of the local and extended modes are seen as shoulders on the low- and high-frequency sides, respectively. Furthermore, extended modes which do *not* uniformly oscillate O atoms develop IR activity at $\omega = 0.055$ and $\omega = 0.060$.

In conclusion, we have used a convenient inhomogeneous HF-RPA approach to study hole doping states in the 2-d 3-band Peierls-Hubbard model. We find that the competition of broken-symmetry ground states in this model is extremely sensitive to parameter values. Nonlinear feedback effects produce a rapid cross-over from a Zhang-Rice regime to a molecular singlet state with local quenching of the Cu moment and large local lattice distortion, induced by intersite-electron-lattice coupling values in a regime extending substantially below the critical value for destruction of the AF state in the undoped system. The doping states are characterized by distinct high energy (electronic optical absorption) and low energy (IR) signatures relevant to chemical and photodoping experiments.

Chapter 7

Conclusions

There has been a lot of controversy[71]-[77] about which is the simplest model, one or two bands, that can capture the essential physics of the high temperature superconductors. The problem is not trivial because by simple arguments[71] one could draw the conclusion that it is possible, in some limit, to map the p-d model into a one-band model. However, one must be sure that no important piece of physics is lost in this process. This is not an easy task because, firstly, one has to be sure to understand the p-d model. Secondly even if one is confident of a simple effective model at some point theory needs feedback from experiment to progress and this is very hard to obtain from oversimplified models. Where as the ultimate objective is to understand the behaviour at very low energies, the basic idea in this work is that understanding of the behaviour at not so low energy can be of great help. For example, for some of the effects discused here, common assumptions of oversimplified models - like very large Coulomb repulsion - can prove to be too drastic. The approach used here is *complementary* to other low energy approaches like renormalization group or mapping to low energy effective models. In fact one has to keep in mind that the techniques used here break down at very low energies and one has to switch to more

refined formalism.

We have shown that one particle added to the half-filling case distorts the background and forms a polaron with different effects contributing to the self-trapping. As we could see in the previous chapters, this idea give a qualitative and sometimes quantitative explanation to many experiments like optical measurements[64, 78, 6], photoinduced absorption[79, 4, 2], photoemission spectroscopy[80, 81] and X-Ray absorption[81]. Because of that we believe our results are on a firm ground and should give further insight to the main unresolved mysteries of these materials: the strange normal state properties[57] and the superconducting mechanism.

Appendix A

Inhomogeneous Hartree-Fock plus RPA Formalism

Here we sketch the formalism we are using. A more detailed discussion can be found in many nuclear physics text books[32, 55]. We describe the RPA fluctuations in terms of a quasi-boson approach because of its intuitive appeal. However, great care must be taken in interpreting the quasi-boson expressions because of frequent double counting issues, as in one-body correlation functions[82, 83] and the ground state energy[32]. From now on we call quasi-boson (QB) approach the naive interpretation of the QB expressions, and RPA those results that can be derived by solving a Bethe-Salpeter equation for the particle-hole Green function including ladder and bubble diagrams. The difference will become clear when we examine the correlation energy in these two approaches [Eqs. (A.20) and (A.21)].

A general many body Hamiltonian is,

$$H = \sum_{kl} \langle k \mid T \mid l \rangle c_k^\dagger c_l + \frac{1}{2} \sum_{klpq} \langle kl \mid V \mid qp \rangle c_k^\dagger c_l^\dagger c_p c_q \tag{A.1}$$

where $c_l^\dagger$ crates a particle in a member of an arbitrary orthogonal basis set (generally the

Wannier orbitals). We introduce a canonical transformation to the Hartree-Fock basis set,

$$a_\nu^\dagger = \sum_l \psi_{\nu l} c_l^\dagger, \tag{A.2}$$

where $\psi_{\nu l}$ will be found self-consistently. In the new basis set the Hamiltonian reads,

$$H = \sum_{\mu\nu} \langle \mu \mid T \mid \nu \rangle a_\mu^\dagger a_\nu + \frac{1}{2} \sum_{\mu\nu\rho\tau} \langle \mu\nu \mid V \mid \tau\rho \rangle a_\mu^\dagger a_\nu^\dagger a_\rho a_\tau. \tag{A.3}$$

The new matrix elements are easily found to be,

$$\langle \mu \mid T \mid \nu \rangle = \sum_{kl} \langle k \mid T \mid l \rangle \psi_{\mu k}^* \psi_{\nu l}, \tag{A.4}$$

$$\langle \mu\nu \mid V \mid \tau\rho \rangle = \sum_{klqp} \langle kl \mid V \mid qp \rangle \psi_{\mu k}^* \psi_{\nu l}^* \psi_{\rho p} \psi_{\tau q}. \tag{A.5}$$

(A.6)

By means of the Wick's theorem the original Hamiltonian [Eq. (A.3)] can be exactly rewritten as

$$H = E_{HF} + : H_{HF} : + V_{res}. \tag{A.7}$$

The HF Hamiltonian is then given by

$$H_{HF} = \sum_{\mu\nu} [\langle \mu \mid T \mid \nu \rangle + \sum_i (\langle i\mu \mid V \mid i\nu \rangle - \langle i\mu \mid V \mid \nu i \rangle)] a_\mu^\dagger a_\nu \tag{A.8}$$

Here ":" denotes normal product with respect to the HF vacuum:

$$|HF\rangle = \prod_{\nu \langle F} a_\nu^\dagger |0\rangle \tag{A.9}$$

and we use m, n to label states above the Fermi level F; i, j for states below and μ, ν, τ, ρ in general. The Hartree-Fock energy is $E_{HF} = \langle HF|H|HF\rangle$. We choose $\psi_{\nu l}$ in such a way that H_{HF} is diagonal,

$$\langle \mu \mid T \mid \nu \rangle + \sum_i (\langle i\mu \mid V \mid i\nu \rangle - \langle i\mu \mid V \mid \nu i \rangle) = \delta_{\mu\nu} \epsilon_\mu. \tag{A.10}$$

Here ϵ_μ are the single-particle HF energies. The HF equations can be obtained by substituting Eq. (A.4) in Eq. (A.10). The same equations can be obtained by decoupling the four fermion terms in the standard way as done below.

The last term in Eq. (A.7) represents the residual interaction between particles,

$$V_{res} = \frac{1}{2} \sum_{\mu\nu\rho\tau} \langle \mu\nu \mid V \mid \tau\rho \rangle : a^\dagger_\mu a^\dagger_\nu a_\rho a_\tau : \ . \tag{A.11}$$

The main effect of V_{res} is to create electron-hole excitations over $|HF\rangle$ and to produce scattering among them. The effect of $: H_{HF} :$ is to limit the electron-hole pair production, because of the energy cost $\epsilon_m - \epsilon_i$. After normal ordering the residual interaction shows a number of terms representing different scattering processes, as well as particle hole production and annihilation. Now, assuming that the number of particles above F (or equivalently holes below F) will be small in the true ground state, we keep only those terms in the residual interaction that represent creation or destruction of particle hole pairs, or scattering among themselves. We expect the above condition to be satisfied if we start from a "good" HF state even in strong coupling. Identifying sufficiently "good" states requires searching for the lower energy, truly relaxed mean field states.

We would like to find a new correlated vacuum $|RPA\rangle$ and a new set of operators Q_λ that diagonalize the Hamiltonian in this subspace. However, even with the above simplifications this can not be done exactly.

We define the particle hole creation operators,

$$b^\dagger_{mi} = a^\dagger_m a_i, \tag{A.12}$$

and their hermitian conjugate b_{mi}. The next approximation is to treat b_{mi} as bosons.

Boson commutation relations are obtained if one takes the expectation value of the commutators in the $|HF\rangle$ state. The fact that one uses the HF vacuum and not the new vacuum $|RPA\rangle$ implies an internal inconsistency of the QB approximation[82]. This is not a big problem if, as expected, $|RPA\rangle$ is not too far from $|HF\rangle$. Now we proceed to construct a boson Hamiltonian (H_{QB}) in such a way that, with the above approximations, it reproduces the commutation relations of the original Hamiltonian. The result is

$$H_{QB} = E_{HF} + \sum_{mi,nj} (A_{mi,nj} b^{\dagger}_{mi} b_{nj} + \frac{1}{2} B_{mi,nj} b^{\dagger}_{mi} b^{\dagger}_{nj} + \frac{1}{2} B^{*}_{mi,nj} b_{nj} b_{mi}), \tag{A.13}$$

where the RPA matrices[32] are given by

$$\begin{aligned} A_{mi,nj} &= (\epsilon_m - \epsilon_i)\delta_{mn}\delta_{ji} + \langle jm|V|ni\rangle - \langle jm|V|in\rangle, \\ B_{mi,nj} &= \langle mn|V|ij\rangle - \langle mn|V|ji\rangle. \end{aligned} \tag{A.14}$$

The constant term in Eq. (A.13) can be obtained by taking the expectation value in the $|HF\rangle$ state and using the fact that it is the vacuum of the b_{mi} operators. H_{QB} is diagonalized by the following Bogoliubov transformation:

$$Q^{\dagger}_{\lambda} = \sum_{mi} (X^{\lambda}_{mi} b^{\dagger}_{mi} - Y^{\lambda}_{mi} b_{mi}). \tag{A.15}$$

$Q^{\dagger}_{\lambda}$ creates an excitation of frequency $\omega_{\lambda} > 0$ over the new vacuum $|RPA\rangle$ and its hermitian conjugate destroys it. $\lambda > 0$ ($\lambda < 0$) labels amplitudes and frequencies related to creation (destruction) operators. X^{λ}, Y^{λ} and ω_{λ} are obtained from the RPA eigenvalue problem:

$$\begin{pmatrix} A & B \\ B^{*} & A^{*} \end{pmatrix} \begin{pmatrix} X^{\lambda} \\ Y^{\lambda} \end{pmatrix} = \omega_{\lambda} \begin{pmatrix} X^{\lambda} \\ -Y^{\lambda} \end{pmatrix}. \tag{A.16}$$

Positive (negative) eigenvalues correspond to creation (destruction) operators in Eq. (A.15) and obey the normalization condition:

$$\left(X^{\lambda\dagger},\, Y^{\lambda\dagger}\right)\begin{pmatrix} X^{\lambda'} \\ -Y^{\lambda'} \end{pmatrix} = \delta_{\lambda,\lambda'} sgn(\omega_\lambda). \tag{A.17}$$

With this transformation the Hamiltonian can be put in the canonical form:

$$H_{QB} = E_{HF} + E_{QB} + \sum_{\lambda>0} \omega_\lambda Q^\dagger_\lambda Q_\lambda. \tag{A.18}$$

Matrix elements of operators can be calculated using the relations,

$$\begin{aligned} \langle RPA|b_{mi}|\lambda\rangle &= X^\lambda_{mi} \\ \langle RPA|b^\dagger_{mi}|\lambda\rangle &= Y^\lambda_{mi}, \end{aligned} \tag{A.19}$$

with $|\lambda\rangle = Q^\dagger_\lambda|RPA\rangle$.

The constant term can be obtained as before by taking the expectation value in the $|HF\rangle$ state and is given by[32]

$$E_{QB} = \frac{1}{2}(\sum_\lambda \omega_\lambda - trA). \tag{A.20}$$

Unfortunately, E_{QB} is not the same expression that one would obtain diagrammatically for the RPA correction to the Hartree-Fock ground state energy. The problem is that, as compared with diagram expansions, the above expression double-counts the second order term[32] in the residual interaction. We believe the problem is related to the internal inconsistency of the QB approximation mentioned above and should be cured in a fully self-consistent[82, 84] approach. The correct RPA expression is obtained by subtracting the overcounted part:

$$E_{RPA} = E_{QB} - (-\frac{1}{4}\sum_{mi,nj}\frac{|\langle ij|V|mn\rangle|^2}{\epsilon_m + \epsilon_n - \epsilon_i - \epsilon_j}). \tag{A.21}$$

Note that the subtracted perturbation in the above expression is not due to the bare interaction but the residual interaction, which is small whenever the true ground state is close to the HF state. For example, for $t \to 0$ limit the Hamiltonian is diagonal in real space; the eigenstates can be written as Slater determinants and the off-diagonal matrix elements of the interaction, like the ones appearing in Eq. (A.21), vanish.

Note also that the eigenvalue problem is the same as that obtained with diagrammatic techniques. In this sense the two approximations are equivalent to each other.

A.1 One dimensional spinless model

We start with the spinless Hamiltonian Eq. (2.5). In the Hartree-Fock approximation the four-fermion terms $n_l n_{l+1}$ are decoupled by:

$$\begin{aligned} n_l n_{l+1} &= n_l\langle n_{l+1}\rangle + n_{l+1}\langle n_l\rangle - \langle n_l\rangle\langle n_{l+1}\rangle \\ &\quad + c_l^\dagger c_{l+1}\gamma_l + c_{l+1}^\dagger c_l\gamma_l - \gamma_l^2, \end{aligned} \tag{A.22}$$

where we have defined,

$$\gamma_l = \langle c_l c_{l+1}^\dagger\rangle. \tag{A.23}$$

The first three terms are the diagonal or Hartree part and the last three terms are the exchange or Fock part. The Hartree-Fock Hamiltonian in the original base reads as

$$H_{HF} = \sum_l [\tilde{\epsilon}_l c_l^\dagger c_l + \tilde{t}_l(c_l^\dagger c_{l+1} + c_{l+1}^\dagger c_l)] + , \tag{A.24}$$

where

$$\tilde{\epsilon}_l = (-1)^l\Delta + U_{pd}(\langle n_{l+1}\rangle + \langle n_{l-1}\rangle) ,$$

(A.25)

$$\tilde{t}_l = t + U_{pd}\gamma_l \, .$$

And the HF equations read

$$(\tilde{\epsilon}_l - \epsilon_\nu)\psi_{\nu l} + \tilde{t}_l\psi_{\nu l+1} + \tilde{t}_{l-1}\psi_{\nu l-1} = 0 \, . \tag{A.26}$$

With the self-consistency equations

$$\langle n_l \rangle = \sum_i \psi^*_{il}\psi_{il} \, , \tag{A.27}$$

and from Eq. (A.23)

$$\gamma_l = \sum_i \psi^*_{il+1}\psi_{il}, \tag{A.28}$$

where i label states bellow the Fermi level.

In order to solve these equations, we just diagonalize Eq. (A.26) with some initial value for the $\tilde{E}_l$, $\tilde{t}_l$ and then recalculate the renormalized matrix elements Eq. (A.26). We return to Eq. (A.26) and reiterate until convergence. We check that the energy decreases monotonically in order to be stabilized at some equilibrium value.

For the RPA part in this case the matrix elements of the interaction are,

$$\langle \mu\nu|V|\tau\rho\rangle = \sum_l U_{pd}(\psi^*_{\mu l}\psi^*_{\nu l+1}\psi_{\rho l+1}\psi_{\tau l} + \psi^*_{\mu l}\psi^*_{\nu l-1}\psi_{\rho l-1}\psi_{\tau l}). \tag{A.29}$$

A.2 Two dimensional spinless model

The spinless Hamiltonian in 2D reads as

$$H = \sum_i E_i n_i + \sum_{i\neq j} E_{ij}c^\dagger_i c_j + \sum_{\langle i,j\rangle} U_{pd}n_i n_j \, , \tag{A.30}$$

where $n_i = c_i^\dagger c_i$, $c_i^\dagger$ creates a spinless fermion associated with charge degrees of freedom of a hole, on site i (here i, j are spatial indices), $E_i = \epsilon_d$ (ϵ_p) for a Cu (O) site. The nearest-neighbour matrix elements are $E_{ij} = t_{pd}$ and the direct O-O hopping is $E_{ij} = -t_{pp}$.$\langle i, j\rangle$ indicates summation over nearest neighbours. As usual we define $\Delta = (\epsilon_p - \epsilon_d)/2$ and use units with $t = 1$.

As in the previous case, we decouple the many-body term in Eq. (A.30) as,

$$\begin{aligned} n_i n_j &\doteq n_i\langle n_j\rangle + \langle n_i\rangle n_j - \langle n_i\rangle\langle n_j\rangle \\ &\quad +(c_i^\dagger c_j \gamma_{i,j} + h.c.) + |\gamma_{i,j}|^2 , \\ \gamma_{i,j} &= \langle c_i c_j^\dagger\rangle , \end{aligned} \tag{A.31}$$

where i, j are the nearest neighbours.

This gives rise to the following Hartree-Fock hamiltonian

$$H_{HF} = \sum_i \tilde{E}_i n_i + \sum_{i\neq j} \tilde{E}_{ij} c_i^\dagger c_j + \sum_{\langle i,j\rangle} U_{pd}(-\langle n_i\rangle\langle n_j\rangle + |\gamma_{i,j}|^2) \tag{A.32}$$

where

$$\begin{aligned} \tilde{E}_i &= E_d + U_{pd}\sum_{\delta=1}^{4}\langle n_\delta\rangle \quad (i \in Cu) , \\ \tilde{E}_i &= E_p + U_{pd}\sum_{\delta=1}^{2}\langle n_\delta\rangle \quad (i \in O) , \\ \tilde{E}_{i,j} &= t + U_{pd}\gamma_{i,j} , \end{aligned} \tag{A.33}$$

with δ labeling the 4 (2) nearest neighbour O (Cu) of a Cu (O) site and i, j are the nearest neighbours. Direct O-O hopping is not renormalized ($\tilde{E}_{i,j} = -t_{pp}$).

A.3 The p-d model

Here we treat the case without electron-lattice coupling in Chapter 3.7. The RPA equations in the general case can be obtained by adding to the Hamiltonian (A.13) the bosonic

terms coming from the second quantaized phonons and the electron-phonon interaction. For the HF calculation of the p-d model one can proceed as before or by plugging the expressions for the matrix elements in Eq. (A.10). The matrix elements of the one- and two-body terms are given by

$$\langle \rho \mid T \mid \mu \rangle = \sum_{i \neq j, \sigma} t_{ij} \psi^*_\rho(i\sigma)\psi_\mu(j\sigma) + \sum_{i,\sigma} e_i \psi^*_\rho(i\tau)\psi_\mu(i\tau) \quad , \tag{A.34}$$

$$\begin{aligned}\langle \rho\mu \mid V \mid \nu\tau \rangle = \frac{1}{2}\sum_i U_i(\psi^*_\rho(i\uparrow)\psi^*_\mu(i\downarrow) - \psi^*_\rho(i\downarrow)\psi^*_\mu(i\uparrow))(\psi_\nu(i\uparrow)\psi_\tau(i\downarrow) - \psi_\nu(i\downarrow)\psi_\tau(i\uparrow)) \\ + \frac{1}{2}\sum_{\langle i \neq j\rangle,\sigma,\sigma'} U_{ij}(\psi^*_\rho(i\sigma)\psi^*_\mu(j\sigma') - \psi^*_\rho(j\sigma')\psi^*_\mu(i\sigma))(\psi_\nu(i\sigma)\psi_\tau(j\sigma') - \psi_\nu(j\sigma')\psi_\tau(i\sigma))\end{aligned} \tag{A.35}$$

Here $(i\sigma), (j\sigma)$ correspond to the orbital indices of Eq. (A.1).

Appendix B

Optical conductivity of lattice models

The results of this section follow the approach of Ref. [54, 48] We want to calculate the response of a strongly correlated system described by a lattice Hamiltonian to an uniform external electric field in the x direction. The electric field is given by $\vec{E} = E\hat{x}$ where,

$$E = -\frac{1}{c}\frac{\partial A}{\partial t}. \tag{B.1}$$

The kinetic energy is given by

$$T = \sum_{i \neq j} t_{ij} c_i^\dagger c_j. \tag{B.2}$$

The perturbed Hamiltonian is obtained by the Peierls substitution,

$$t_{ij} \rightarrow t_{ij} e^{i\phi_{ij}} = t_{ij}(1 + i\phi_{ij} - \frac{1}{2}\phi_{ij}^2 + ...), \tag{B.3}$$

$$\phi_{ij} = -\frac{e}{\hbar c}\int_{x_i}^{x_j} dx A = -\frac{eAx_{ij}}{\hbar c}, \tag{B.4}$$

where we define the difference in the x coordinates of sites i and j:

$$x_{ij} = x_j - x_i. \tag{B.5}$$

With this the total Hamiltonian can be put as,

$$H = H_o - \frac{A}{c} j - \frac{1}{2}\left(\frac{eA}{\hbar c}\right)^2 \sum_s t_s x_s^2 \frac{\partial H_o}{\partial t_s} \tag{B.6}$$

H_o is the fully interacting Hamiltonian without the external field. The second term in Eq. (B.6) contains the paramagnetic current operator in the x direction,

$$j = \frac{ie}{\hbar} \sum_{ij} t_{ij} x_{ij} c_i^\dagger c_j \tag{B.7}$$

The total current also has a diamagnetic contribution,

$$J = -c\frac{\partial H}{\partial A} = j + \left(\frac{e}{\hbar}\right)^2 \frac{A}{c} \sum_s t_s x_s^2 \frac{\partial H_o}{\partial t_s}. \tag{B.8}$$

The last term in Eq. (B.6) comes from the second order term in the Taylor expansion of Eq. (B.3) and Eq. (B.2) in the following way

$$-\frac{1}{2}\left(\frac{eA}{\hbar c}\right)^2 \sum_{i \neq j} t_{ij} x_{ij}^2 c_i^\dagger c_j = -\frac{1}{2}\left(\frac{eA}{\hbar c}\right)^2 \sum_s t_s x_s^2 \sum_i c_i^\dagger c_{i+s} = -\frac{1}{2}\left(\frac{eA}{\hbar c}\right)^2 \sum_s t_s x_s^2 \frac{\partial H_o}{\partial t_s}. \tag{B.9}$$

Here we use translational invariance to define

$$t_{ii+s} = t_s, \tag{B.10}$$

$$x_{ii+s} = x_s. \tag{B.11}$$

Now we use ordinary perturbation theory to calculate the change in the ground state energy in the particular case in which A is static

$$E(A) - E(0) = -\frac{1}{2}\left(\frac{eA}{\hbar c}\right)^2 \sum_s t_s x_s^2 < 0|\frac{\partial H_o}{\partial t_s}|0 > - \left(\frac{A}{c}\right)^2 \sum_\lambda \frac{| < 0|j|\lambda > |^2}{E_\lambda - E_0}. \tag{B.12}$$

The stiffness constant is defined as

$$D = \frac{c^2}{2V} \frac{\partial^2 E(A)}{\partial A^2}|_{A=0}, \tag{B.13}$$

with V as the total volume, and is given by

$$D = \left(\frac{ne^2}{2m^*} - \frac{1}{V} \sum_{\lambda} \frac{| < 0|j|\lambda > |^2}{E_\lambda - E_0} \right). \tag{B.14}$$

The number of particles is N_p and the density is

$$n = \frac{N_p}{V}. \tag{B.15}$$

The effective mass is defined as,

$$\frac{m_o}{m^*} = \frac{1}{N_p} \sum_{s} \frac{-t_s < 0| \left(\partial H_o / \partial t_s\right) |0 >}{\hbar^2 / m_o x_s^2}. \tag{B.16}$$

In the same way we can define a stiffness constant in the HF approximation. The change of the HF energy due to A is given by the static part of the RPA response function[55] so that the analogue of Eq. (B.12) is:

$$E_{HF}(A) - E_{HF}(0) = -\frac{1}{2} \left(\frac{eA}{\hbar c} \right)^2 \sum_{s} t_s x_s^2 < HF| \frac{\partial H_o}{\partial t_s} |HF > - \left(\frac{A}{c} \right)^2 \sum_{\lambda} \frac{| < 0|j|\lambda > |^2_{RPA}}{(E_\lambda - E_0)_{RPA}}. \tag{B.17}$$

Therefor,

$$D_{HF} = \left(\frac{ne^2}{2m^*_{HF}} - \frac{1}{V} \sum_{\lambda} \frac{| < 0|j|\lambda > |^2_{RPA}}{(E_\lambda - E_0)_{RPA}} \right) \tag{B.18}$$

and

$$\frac{m_o}{m^*_{HF}} = \frac{1}{N_p} \sum_{s} \frac{-t_s < HF| \left(\partial H_o / \partial t_s\right) |HF >}{\hbar^2 / m_o x_s^2}. \tag{B.19}$$

Now we want to calculate the linear response of the system to a time dependent field $A(t)$. In this case only the first term of the perturbation in Eq. (B.6) should be kept,

$$H = H_o - \frac{A}{c} j. \tag{B.20}$$

As usual the linear response of the paramagnetic current is given by,

$$< j > (t) = -\frac{i}{\hbar c} \int_{-\infty}^{t} dt' A(t') < 0|[j(t'), j(t)]|0 >, \tag{B.21}$$

where we have used that the unperturbed ground state has no currents and the <> denote expectation value in the time dependent solution of the Schrödinger equation with initial condition given by $|0>$. Defining a generalized susceptibility

$$\chi_{jj}(t-t') = -\frac{i}{\hbar} < 0|[j(t'), j(t)]|0 > \theta(t-t'), \tag{B.22}$$

we get for the total current response,

$$< J > (t) = \int_{-\infty}^{\infty} dt'[\chi_{jj}(t-t') - \frac{N_p e^2}{m^*}\delta(t-t')]\frac{A(t')}{c}. \tag{B.23}$$

Now we put

$$A(t) = A(\omega)e^{-i(\omega - i\eta)t}, \tag{B.24}$$

$$< J > (t) = J(\omega)e^{-i(\omega - i\eta)t}, \tag{B.25}$$

and we get for the Fourier component of the electric field [Eq. (B.1)],

$$E(\omega) = \frac{A(\omega)}{c} i(\omega - i\eta)e^{-i(\omega - i\eta)t}. \tag{B.26}$$

The limit of η going to zero is made at the end of the calculation. We define the optical conductivity from,

$$\frac{J(\omega)}{V} = \sigma(\omega)E(\omega) \tag{B.27}$$

and is given from Eq. (B.23) and Eq. (B.26) by

$$\sigma(\omega) = \frac{1}{i(\omega - i\eta)}\left(\frac{\chi_{jj}(\omega)}{V} - \frac{ne^2}{m^*}\right). \tag{B.28}$$

Defining

$$\omega_\lambda = \frac{E_\lambda - E_o}{\hbar} \tag{B.29}$$

the real and imaginary parts of the optical conductivity are given by,

$$Re\sigma(\omega) = 2\pi\delta(\omega)D + \frac{\pi}{V}\sum_{\lambda}\frac{|<0|j|\lambda>|^2}{E_\lambda - E_0}\delta(\omega_\lambda - |\omega|), \tag{B.30}$$

$$Im\sigma(\omega) = P\frac{1}{\omega}\left(\frac{ne^2}{m^*}\right) - \frac{1}{\hbar V}\sum_{\lambda}|<0|j|\lambda>|^2 P\frac{2\omega_\lambda}{\omega_\lambda^2 - \omega^2}, \tag{B.31}$$

respectively. Here we have used the Lehmann representation of χ_{jj} and

$$\frac{1}{\omega \mp i\eta} = P\frac{1}{\omega} \pm i\pi\delta(\omega) \tag{B.32}$$

For comparison with real experiment one has to take into account that not all the possible polarization processes are taken into account in H. In fact all bound electrons not included in H_o, which we call the background, will screen the external field $\vec{E}_{ext} = E_{ext}\hat{x}$. In other words, the total field felt by the electrons in H_o is

$$\vec{E} = \vec{E}_{ext} - 4\pi\vec{P}_b \tag{B.33}$$

here $\vec{P}_b$ is the polarization of the background. Since it is proportional to $\vec{E}_{ext}$, $\vec{E}$ and $\vec{E}_{ext}$ are also proportional so that

$$E = \frac{E_{ext}}{\epsilon_b}, \tag{B.34}$$

where ϵ_b is the dielectric constant due to this screening. Here we made two non-trivial assumptions. First that the process not included involve transitions at much higher energies than the process included in H_o. This means that they can be considered instantaneous in the time scale of H_o and that ϵ_b can be calculated as a static response. In practice sometimes H_o has low-energy process and high-energy process and the high-energy process can be close to other high-energy process not included. Clearly this has to be kept in mind when analysing the results at high energies. At least one should require that there are no real transitions of the background in the region of interest. The other assumption is that

the electrons in H_o feel the macroscopic P_b and not the microscopic one. This is probably not true in complicated structures but as a first approximation such inaccuracies can be incorporated in ϵ_b. With that we can define a screened (and measured) conductivity as,

$$\frac{J(\omega)}{V} = \sigma_{sc}(\omega)E_{ext}(\omega) = \frac{\sigma(\omega)}{\epsilon_b}E_{ext}(\omega), \tag{B.35}$$

where the last equality is a consequence of Eq. (B.27) In the case of layered systems we can reinterpret the above expressions as referring to the volume containing one layer

$$V = d_\perp a^2 N, \tag{B.36}$$

where $d_\perp$ is the distance between layers, a is the cell lattice constant in the layer and N the number of cells in the layer. For the Cu-O layers we put $a^2 = 4a_{pd}^2$ so that $|x_1| = a_{pd}$ is the Cu-O distance. With this the real part of the screened optical conductivity can be put as:

$$Re\frac{\sigma_{sc}(\omega)}{\sigma_0} = 2\pi\delta(\omega)\frac{D_{sc}}{\sigma_0} + \frac{\pi}{N}\sum_\lambda \frac{|<0|j/a_{pd}e|\lambda>|^2}{(E_\lambda - E_0)/\hbar}\delta(\omega_\lambda - |\omega|) \tag{B.37}$$

with

$$\frac{D_{sc}}{\sigma_0} = \frac{1}{N}\left[-\frac{1}{2}\sum_s \frac{t_s}{\hbar}\left(\frac{x_s}{a_{pd}}\right)^2 <0|\frac{\partial H_o}{\partial t_s}|0> - \sum_\lambda \frac{|<0|j/a_{pd}e|\lambda>|^2}{(E_\lambda - E_0)/\hbar}\right] \tag{B.38}$$

$$\sigma_0 = \frac{e^2}{4d_\perp \hbar \epsilon_b}. \tag{B.39}$$

The last two expressions are useful to check that the dimensions in Eq. (B.37) are correct.

Experimentalists usually define an effective number of particles per unit cell,

$$\begin{aligned} N_{eff}(\omega) &= \frac{2m_o V}{\pi e^2 N}\int_0^\omega d\omega' \sigma_{sc}(\omega') \\ &= \frac{t_{pd}}{\epsilon_b \hbar^2/2m_o a_{pd}^2}\frac{1}{N}\left[-\frac{1}{2}\sum_s \frac{t_s}{t_{pd}}\left(\frac{x_s}{a_{pd}}\right)^2 <0|\frac{\partial H_o}{\partial t_s}|0> - \sum_{\lambda,\omega_\lambda>\omega}\frac{|<0|j/a_{pd}e|\lambda>|^2}{t_{pd}(E_\lambda - E_0)/\hbar^2}\right]. \end{aligned} \tag{B.40}$$

The f-sum rule reads as,

$$\int_0^{\omega} d\omega' \sigma_{sc}(\omega') = \frac{\pi e^2 N_{eff}(\infty)}{2m_o V/N} = \frac{\pi e^2 n}{2m^* \epsilon_b} = \frac{\omega_p^{*2}}{8}, \tag{B.41}$$

where we have defined a screened plasma frequency,

$$\omega_p^{*2} = 4\pi \frac{e^2 n}{m^* \epsilon_b} \tag{B.42}$$

We see that m^* and N_{eff} are two alternative ways of include the effects of correlations and it is not consistent to use both at the same time.

Bibliography

[1] J. G. Bednorz and K. A. Müler. *Z. Phys. B*, 64:189, 1986.

[2] C. Taliani, A.J. Pal, G. Ruani, R. Zamboni, X. Wei, and Z.V. Vardeny. In H. Kuzmany, M. Mehring, and J. Fink, editors, *Electronic properties of High Tc Superconductors and Related Compounds, Vol. 99 of Springer Series of Solid State Sciences.* Springer-Verlag, Berlin, 1990.

[3] C. M. Foster, A. J. Heeger, Y.H. Kim, and G. Stucky. *Physica C*, 162-164:1107, 1989.

[4] Y. H. Kim, C. M. Foster, and A. J. Heeger. *Phys. Scr. T*, 27:19, 1989.

[5] G. A. Thomas, D. H. Rapkine, S-W. Cheong, and L. F. Schneemeyer, *Tempreature Dependence of Doping-Induced Modes in the Cu-O Planes* . Preprint.

[6] S. Uchida, T. Ido, H. Takagi, T. Arima, Y. Tokura, and S. Tajima. *Phys. Rev. B*, 43:7942, 1991.

[7] S. Lupi, P. Calvani, M. Capizzi, and P. Maselli, *Infrared Optical Conductivity of the Nd-Ce-Cu-O System.* Preprint.

[8] P. Calvani, S. Lupi, and G. Paleologo, *Mid-Infrarred Absorption and Critical Temperature in Superconducting Cuprates* . Preprint.

[9] M. D. Nuñez Regueiro and A.A. Aligia. *Phys. Rev. Lett.*, 61:1889, 1988.

[10] N. Nücker, J. Fink, B. Renker, D. Ewert, C. Politis, P. J. Weijs, and J. C. Fuggle. *Z. Phys. B*, 67:9, 1987.

[11] C.M. Varma, S. Schmitt-Rink, and E. Abrahams. *Solid State Commun.*, 62:681, 1987.

[12] J.E. Hirsch, S. Tang, Jr. E. Loh, and D.J. Scalapino. *Phys. Rev. Lett.*, 60:1668, 1988.

[13] C. A. Balseiro, A.G. Rojo, E.R. Gagliano, and B. Alascio. *Phys. Rev. B*, 38:9315, 1988.

[14] N. P. Ong, Z.Z. Wang, J. Clayhold, J. M. Tarascon, L.H. Green, and W.R. McKinnon. *Phys. Rev. B*, 35:8807, 1987.

[15] H. Eskes, G.A. Sawatzky, and L.F. Feiner. *Physica C*, 160:424, 1989.

[16] M.S. Hybertsen, M. Schlüter, and N.E. Christensen. *Phys. Rev. B*, 39:9028, 1989.

[17] A. K. McMahan, J. F. Annett, and R. M. Martin. *Phys. Rev. B*, 42:6268, 1990.

[18] J. B. Grant and A. K. McMahan. *Phys. Rev. Lett.*, 66:488, 1991.

[19] V. I. Anisimov, M. A. Korotin, J. A. Zaanen, and O. K. Andersen. *Phys. Rev. Lett.*, 68:345, 1992.

[20] V. J. Emery. *Phys. Rev. Lett.*, 65:1076, 1990.

[21] J. Lorenzana and L. Yu. *Phys. Rev. B*, 43:11474, 1991.

[22] R. Bruinsma, P. Bak, and J. B. Torrance. *Phys. Rev. B*, 27:456, 1983.

[23] E. R. Gagliano and C. A. Balseiro. *Phys. Rev. B*, 38:11766, 1988.

[24] C.N.R. Rao, G.R. Rao, M.K. Rajumon, and D.D. Sarma. *Phys. Rev. B*, 42:1026, 1990.

[25] K. Kamarás, C. D. Porter, M. G. Doss, S. L. Herr, and D. B. Tanner. *Phys. Rev. Lett.*, 59:919, 1987.

[26] J. Humlíček, M. Garriga, and M. Cardona. *Solid State Commun.*, 67:589, 1988.

[27] U. Venkateswaran, K. Syassen, Hj. Mattausch, and E. Schönherr. *Phys. Rev. B*, 38:7105, 1988.

[28] M. Garriga, J. Humlíček, M. Cardona, and E. Schönherr. *Solid State Commun.*, 66:1231, 1988.

[29] M. K. Kelly, P. Barboux, J. M. Tarascon, and D. E. Aspnes. *Phys. Rev. B*, 40:6797, 1989.

[30] E. Dagotto and A. Moreo. *Phys. Rev. D*, 31:865, 1985.

[31] L. Yu. *Solitons and Polarons in Conducting Polymers.* World Scientific, Singapore, 1988.

[32] J.-P. Blaizot and G. Ripka. *Quantum Theory of Finite Systems.* The MIT Press, Cambridge, Massachusetts, 1986.

[33] J. Hubbard. *Phys. Rev. B*, 17:494, 1978.

[34] M. Grilli, R. Raimondi, C. Castellani, C. Di Castro, and G. Kotliar. *Phys. Rev. Lett.*, 67:256, 1991.

[35] J. Lorenzana and C. A. Balseiro. *Phys. Rev. B*, 42:936, 1990.

[36] V. J. Emery. In J. T. De Vreese, R.P. Evrard, and V.E. Van Doren, editors, *Highly Conducting One-Dimensional Solids*, New York, 1987. Plenum.

[37] K. Yonemitsu, I. Batistić, and A.R. Bishop. *Phys. Rev. B*, 44:2652, 1991.

[38] K. Yonemitsu, A.R. Bishop, and J. Lorenzana. *Phys. Rev. Lett.*, 69:965, 1992.

[39] A. Auerbach and B. L. Larson. *Phys. Rev. B*, 43:7800, 1991.

[40] J.A. Vergés, E. Louis, P.S. Lomdahl, F. Guinea, and A.R. Bishop. *Phys. Rev. B*, 43:6099, 1991.

[41] Yun-Yu Wang and L. Ritter. *Phys. Rev. B*, 43:1241, 1991.

[42] Z. Tešanović, A.R. Bishop, R.L. Martin, and C. Harris. *Int. J. Mod. Phys. B*, 1:907, 1988.

[43] P.B. Littlewood, C.M. Varma, and E. Abrahams. *Phys. Rev. Lett.*, 63:2602, 1989.

[44] K. Yonemitsu and A.R. Bishop. *Phys. Rev. B*, 45:5530, 1992.

[45] J. Lorenzana, M. D. Grynberg, L. Yu, K. Yonemitsu, and A. R. Bishop. *Dynamic and Static Correlation Functions in the Inhomogeneous-Hartree-Fock-State Approach with Random-Phase-Approximation Fluctuations* . Submited to *Phys. Rev. B.*

[46] J. W. Allen, C. G. Olson, M. B. Maple, J.-S. Kang, L. Z. Liu, J.-H. Park, R. O. Anderson, W. P. Ellis, J. T. Markert, Y. Dalichaouch, and R. Liu. *Phys. Rev. Lett.*, 64:595, 1990.

[47] I. I. Mazin, E. G. Maksimov, S. N. Rashkeev, S. Y. Savrasov, and Y. A. Usppenskiĭ. *Pis'ma Zh. Eksp. Teor Fiz.*, 47:94, 1988. [JETP Lett,**47**, 113 (1988)].

[48] B. S. Shastry and B. Sutherland. *Phys. Rev. Lett.*, 65:243, 1990.

[49] J. Wagner, W. Hanke, and D. J. Scalapino. *Phys. Rev. B*, 43:10517, 1991.

[50] C.-X. Chen and H.-B. Schüttler. *Phys. Rev. B*, 43:3771, 1991.

[51] X. Wei, C. Chen, Z.V. Vardeny, C. Taliani, R. Zamboni, A.J. Pal, and G. Ruani. *Physica C*, 162-164:1109, 1989.

[52] J. P. Falck, A. Levy, M. A. Kastner, and R. J. Birgeneau. *Phys. Rev. Lett.*, 69:1109, 1992.

[53] J. Lorenzana and L. Yu. *Mod. Phys. Lett. B*, 5:1515, 1991.

[54] W. Kohn. *Phys. Rev.*, 133:A171, 1964.

[55] P. Ring and P. Schuck. *The nuclear many-body problem.* Springer-Verlag, New York, 1980.

[56] M. K. Crawford, W. E. Farneth, E. M. McCarron III, R. L. Harlew, and A. H. Moudden. *Science*, 250:1390, 1989.

[57] C.M. Varma, P.B. Littlewood, S. Schmitt-Rink, E. Abrahams, and A. E. Ruckenstein. *Phys. Rev. Lett.*, 63:1996, 1990. (E) 64:497, 1990.

[58] K. Huang and A. Rhys. *Proc. Roy. Soc.*, A204:406, 1950.

[59] B. R. Alascio, R. Allub, C. R. Proetto, and C. I. Ventura. *Solid State Commun.*, 77:949, 1991.

[60] B. J. Scalapino, R. T. Scalettar, and N. E. Bickers. In S. E. Wolf and V. Z. Kresin, editors, *Proceedings of the International Conference on Novel Mechanisms of Superconductivity*, New York, 1987. Plenum.

[61] D. Emin. *Phys. Rev. Lett.*, 62:1544, 1989.

[62] G. Wendin. *Phys. Scr. T*, 27:31, 1989.

[63] J. Ranninger and U. Thibblin. *Phys. Rev. B*, 45:7730, 1992.

[64] I. Bozovic. *Phys. Rev. B*, 42:1969, 1990.

[65] I. Bozovic. *Physica C*, 162-164:1239, 1989.

[66] N. F. Mott. *Adv. in Phys.*, 39:55, 1990.

[67] A. S. Alexandrov and J. Ranninger. *Phys. Rev. B*, 45:13109, 1992.

[68] A. S. Alexandrov and J. Ranninger. *Physica C*, 198:360, 1992.

[69] A. S. Alexandrov. *Polaron Theory of High-Tc Strong-Coupling Superconductors.* In A. V. Narlikar, editor, *Studies of High Temperature Superconductors*, Vol. 6, 195. 1990.

[70] R. Micnas, J. Ranninger, and S. Robaszewicz. *Rev. Mod. Phys.*, 62:113, 1990.

[71] F. C. Zhang and T.M. Rice. *Phys. Rev. B*, 37:3759, 1988.

[72] I. Batistić and A.R. Bishop. *Phys. Rev. B*, 45:5282, 1992.

[73] F. C. Zhang and T.M. Rice. *Phys. Rev. B*, 41:2560, 1990.

[74] F. C. Zhang and T.M. Rice. *Phys. Rev. B*, 41:7243, 1990.

[75] V. J. Emery and G. Reiter. *Phys. Rev. B*, 38:4547, 1988.

[76] V. J. Emery and G. Reiter. *Phys. Rev. B*, 38:11938, 1988.

[77] V. J. Emery and G. Reiter. *Phys. Rev. B*, 41:7247, 1990.

[78] Minoru Suzuki. *Phys. Rev. B*, 39:2312, 1989.

[79] J. M. Ginder, M. G. Roe, Y. Song, R. P. McCall, J. R. Gaines, and E. Ehrenfreund. *Phys. Rev. B*, 37:7506, 1988.

[80] A. Fujimori, Y. Tokura, H. Eisaki, H. Takagi, S. Uchida, and M. Sato. *Phys. Rev. B*, 40:7303, 1989.

[81] H. Matsuyama, T. Takahashi, H. Katayama-Yosida, T. Kashiwakura, Y. Okabe, and S. Sato. *Physica C*, 160:567, 1989.

[82] D. J. Rowe. *Phys. Rev.*, 175:1283, 1968.

[83] R.E. Johnson, R. M. Dreizler, and A. Klein. *Phys. Rev.*, 186:1289, 1969.

[84] N. Meshkov, A. J. Glick, and H. J. Lipkin. *Nuc. Phys.*, 62:199, 1965.